Reprinted from

Volume 32, Number Chapter 11 **1995**

REVIEWS in
MINERALOGY &
GEOCHEMISTRY

Pressure Effects on Silicate Melt Structure and Properties

G. H. Wolf and Paul F. McMillan

Chapter 11

PRESSURE EFFECTS ON SILICATE MELT STRUCTURE AND PROPERTIES

George H. Wolf and Paul F. McMillan

Department of Chemistry and Biochemistry
Arizona State University
Tempe, Arizona 85287 U.S.A.

INTRODUCTION

The high-pressure properties of silicate melts are likely to have played the single most important role in shaping the physical and chemical evolution of the earth and other terrestrial planets. Magma ascent and emplacement, as well as crystal nucleation, growth and segregation, are all principally controlled by the pressure-dependent densities and transport properties of silicate melts. In the pressure range of the Earth's mantle, silicate melts display high compressibilities relative to their crystalline counterparts, as a result of the great diversity in structural compression mechanisms that occur in these molten systems. Magmatic buoyancy forces, which are determined by the density contrast between the melt and surrounding rock matrix, can strongly decrease as a function of depth and can even invert in the deep interior of a planet (Stolper et al., 1981). Thus, gravitationally stable magma oceans can exist at depth within a planet, profoundly influencing its thermal and chemical evolution (Nisbet and Walker, 1982; Ohtani, 1984; Rigden et al., 1984; Ohtani et al., 1986; Takahashi, 1986; Ohtani and Sawamoto, 1987; Ryan, 1987; Agee and Walker, 1988, 1993; Miller et al., 1991a,b). Pressure can also have an equally large, and sometimes surprising (see below), effect on the viscosities and other transport properties of magmatic liquids. In turn, these effects can significantly influence the segregation dynamics and crystal fractionation pathways in magmas.

There is currently much interest in understanding the microscopic atomistic processes that control the bulk physical properties of magmatic liquids. Experimental and theoretical investigations of aluminosilicate and related liquids and glasses over the last few decades, together with a growing body of data from fundamental studies on the viscoelastic behavior and structural properties of network forming liquids, have led to the emergence of a more complete understanding of the interrelations between the thermodynamic and transport properties of magmatic liquids and their microscopic structure and dynamical processes. This chapter will focus on the pressure variable, both as a critical thermodynamic variable that affects the physical properties of silicate melts and hence magmatic processes within the earth, and as a powerful experimental and theoretical variable that has yielded new fundamental insights into the microscopic origin of silicate melt properties.

It is well known that the effects of volatiles on melt properties is dramatic. Moreover, pressure has a profound influence on the physical properties of hydrous and other volatile-bearing magmas, as underscored by the strong increase in solubility of CO_2 and H_2O that occurs in silicate melts with increasing pressure (see Burnham, 1979; Spera and Bergman, 1980; Stolper and Holloway, 1988; Lange and Carmichael, 1990).

However, the discussion in this chapter is limited to *anhydrous* melts and glasses. A more complete discussion on the properties of volatile-bearing silicate melts was the topic of a recent Mineralogical Society of America short course (Carroll and Holloway, 1994).

GENERAL HIGHLIGHTS

One of the most intriguing aspects of aluminosilicate liquids is the rich diversity in phenomenology which they display. Lower-silica, highly depolymerized aluminosilicate melts behave like normal ionic liquids in their response to pressure. These liquids undergo a gradual, continuous densification with increasing pressure, and display a gradual decrease in their fluidity and atomic diffusivities. However, higher-silica liquids, with compositions near those of crystalline tektosilicates, display more unusual behavior in their physical properties. Most significantly, the viscosity of many of these liquids *decreases* with increasing pressure (Fig. 1) (Kushiro, 1976, 1977, 1978a,b, 1980, 1986; Kushiro et al., 1976; Fujii and Kushiro, 1977; Scarfe et al., 1979, 1987). This is contrary to the behavior expected from free-volume theory, and that observed for most "normal" liquids, where applied pressure leads to an increase in viscosity (see chapters by Richet and Dingwell in this volume). A similar anomaly in the pressure effect on viscosity occurs in water at low temperatures. The microscopic structural and energetic factors which are responsible for the anomalous transport properties in water may also be connected to its well known density maximum at low temperatures. This unusual behavior has been rationalized in terms of the free energy competition between the high energetic stability and low configurational entropy of an open ice-like tetrahedral framework structure in water. Similar explanations have been presented for silica, which itself displays a density maximum in its supercooled liquid state (Bruckner, 1970).

High-silica liquids also display anomalous pressure-dependent behavior in their atomic diffusivities. Experiments reveal that, while the diffusivities of network-modifying ions generally decrease with increasing pressure for aluminosilicate liquids, the diffusivities of the network ions (i.e., Si, Ge, Ga, Al, O) actually *increase* with pressure in many highly polymerized liquids near tektosilicate compositions (see Fig. 2a) (Watson, 1979; Fujii, 1981; Kushiro, 1983; Shimizu and Kushiro, 1984; Dunn and Scarfe, 1986; Rubie et al., 1993; Poe et al., 1994, 1995). These observations were first predicted, and are generally supported, by theoretical molecular dynamics simulations (see Fig. 2b) (Woodcock et al., 1976; Angell et al., 1982, 1987; Kubicki and Lasaga, 1988, 1990, 1991).

The general inverse relation between oxygen diffusion and viscosity suggests that oxygen exchange is the rate limiting step in the viscous flow mechanism of aluminosilicate melts (Scarfe et al., 1987). Results from molecular dynamics simulations on aluminosilicate, and related, liquids have been used to propose that five-coordinated silicon ($^{[5]}$Si) and aluminum ($^{[5]}$Al) species are important reactive intermediate states in transport mechanisms and act to facilitate ion exchange (Brawer, 1981; Angell et al., 1982, 1983; Kubicki and Lasaga, 1988, 1991). In the simulations, there is a strong correlation between the network ion diffusivities and the abundance of five-coordinatedd Si and Al species in the melt (Angell et al., 1982, 1983; Kubicki and Lasaga, 1988). The existence of significant abundances of $^{[5]}$Si (Stebbins and McMillan, 1989; Xue et al., 1991) and $^{[5]}$Al (Yarger et al., 1995) species in partially depolymerized silicate and aluminosilicate melts has now been confirmed experimentally from MAS NMR studies of glasses quenched from high-pressure.

Although moderately high abundances of high-coordinated Si and Al species can occur in depolymerized composition alkali silicate and aluminosilicate glasses quenched

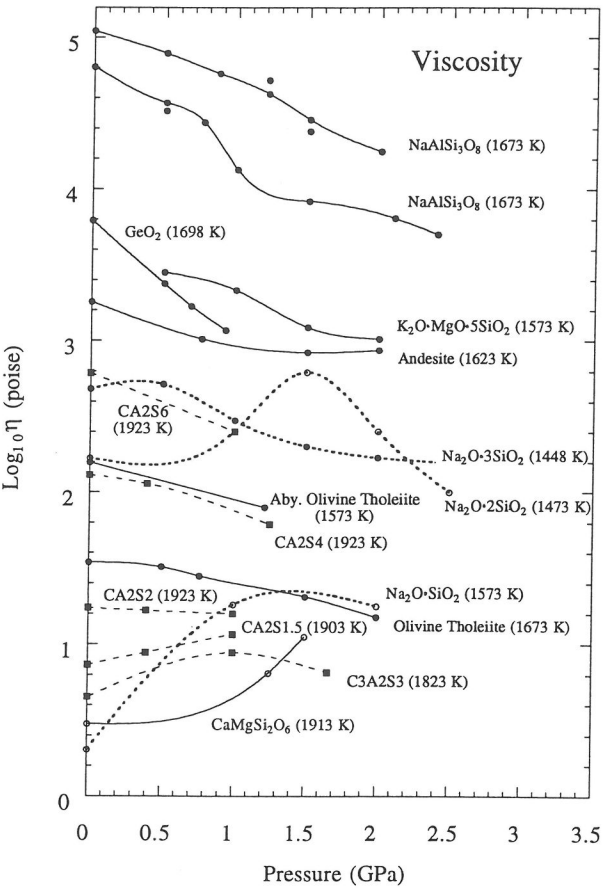

Figure. 1. Viscosity of silicate and aluminosilicate melts as a function of pressure. Temperatures of the measurements are given in parentheses. Data for the calcium aluminosilicate system along the charge-balanced $CaAl_2O_4$-SiO_2 join: CA2S6, CA2S4, Anorthite (CA2S2), and CA2S1.5 taken from Kushiro (1981) and for the depolymerized $Ca_3Al_2Si_3O_{12}$ (Gross) composition melt from Mysen et al. (1983). Viscosity data for sodium disilicate ($Na_2O{\cdot}2SiO_2$), sodium metasilicate ($Na_2O{\cdot}SiO_2$), and diopside ($CaMgSi_2O_6$) composition melts taken from Scarfe et al. (1979). Data for GeO_2, $K_2O{\cdot}MgO{\cdot}5SiO_2$, $Na_2O{\cdot}3SiO_2$, $NaAlSi_3O_8$, and $NaAlSi_2O_6$ taken from Kushiro (1976, 1977; 1978a,b). Viscosity data for natural systems from Kushiro et al. (1976) and Fujii and Kushiro (1977).

from high-pressure melts, the experimental evidence for the retention of high-coordinated species in fully polymerized tektosilicate composition glasses quenched from high-pressure melts is much less definitive. However, there is compelling in situ spectroscopic evidence that pressure-induced coordination changes do occur in the fully polymerized silicate and aluminosilicate glasses and melts. High-pressure infrared absorption studies on anorthite composition glass (Williams and Jeanloz, 1988) and spectroscopic studies of silica glass (Hemley et al., 1986) and germania glass (Itie et al., 1989; Durben and Wolf, 1991), a structural analog to silica, indicate that network forming cations of fully polymerized glasses form high-coordinated species at elevated pressures. However, for these fully polymerized systems the high-coordinated species revert to tetrahedral states

on decompression. Perhaps the most definitive documentation of this behavior is the in situ high-pressure X-ray absorption edge study of germania glass by Itie et al (Itie et al., 1989, 1990). The data indicate that germanium undergoes a four- to six-fold coordination change between 4 and 12 GPa, and, on decompression the high-coordinated species revert entirely to tetrahedral species over a very narrow pressure range below 4 GPa.

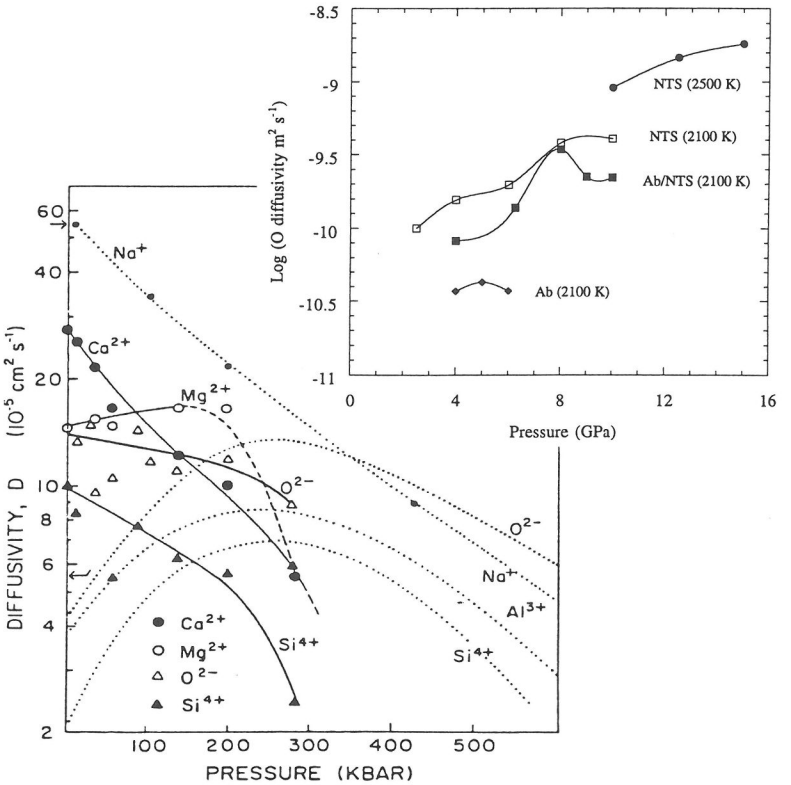

Figure 2. (a) Experimental values for the pressure dependence of oxygen diffusivity in sodium tetrasilicate (NTS) and albite (Ab) system melts as a function of pressure. Data for NTS at 2100 K taken from Rubie et al. (1993). Data for NTS at 2500 K, for Ab at 2100 K and for an equimolar Ab/NTS mixture at 2100 K were taken from Poe et al. (1995). (b) Molecular dynamics simulation results for the pressure dependence of ion diffusivities in diopside ($CaMgSiO_4$, solid lines) and jadeite ($NaAlSi_2O_6$, dotted lines) at 6000 K taken from Angell et al. (1987). [Used by permission of the editor of *Chemical Geology*, from Angell et al. (1987), Fig. 4, p. 89.]

In silica glass, analyses of the pressure-dependent Raman (Hemley et al., 1986; Sugiura and Yamadaya, 1992), infrared (Williams and Jeanloz, 1988; Williams et al., 1993) and X-ray diffraction (Meade et al., 1992) spectra suggest that the pressure-induced increase in the silicon coordination takes place above about 15 GPa at room temperature. However, in partially depolymerized alkali silicate glasses, an increase in the silicon coordination takes place at much lower pressures (Stebbins and McMillan, 1989; Xue et al., 1989; Wolf et al., 1990; Xue et al., 1991; Durben, 1993). In these systems, high-coordinated silicon species can be retained in samples quenched from high-pressure melts.

On the basis of the above studies, it has been suggested that there exist two distinct

mechanisms for coordination changes in silicate liquids, involving either the bridging or non-bridging oxygen atoms (Wolf et al., 1990; Xue et al., 1991). In the slightly depolymerized, high-silica systems, these mechanisms have very different activation energies and operate over separate pressure ranges. At low pressures, tetrahedral silicon (or aluminum) can be readily attacked by the non-bridging oxygen atoms to form high-coordinated $^{[5]}$Si and $^{[6]}$Si species. It is only at much higher pressures that the network bridging oxygens become involved in the formation of high-coordinated species. The differing energetics and reversibility of these two mechanisms can be rationalized by an inspection of the cation arrangement around the oxygen anion. The higher pressure mechanism, involving bridging oxygens, requires the energetically costly formation of oxygen anions bonded to three silicon atoms. However, the lower pressure mechanism involves non-bridging oxygens and requires formation of oxygen anions bonded to only two silicon atoms. The relative energetics of these two mechanisms appears to be strongly affected by the degree of depolymerization of the network structure (Xue et al., 1991; Durben, 1993). With increasing alkali or akaline earth oxide component, the pressure range for the coordination reaction involving non-bridging oxygen atoms is shifted to higher pressures, apparently due to the increasing steric restrictions imposed by the basic metal cations.

The in situ spectroscopic studies unequivocally demonstrate that significant local structural relaxations can occur in the glassy state on decompression from high pressure. It remains unclear as to whether these structural relaxations are equally significant in glasses that are formed from high-pressure melts. The room-pressure structural properties of glasses that have been pressure-cycled at 300 K can be quite different from that of samples which, in addition to pressure cycling, were also annealed or melted at high pressures (Mackenzie, 1963a,b; McMillan et al., 1984; Sugiura and Yamadaya, 1992; Yarger et al., 1995). For this reason, there is a growing emphasis on the development and application of in situ methods to investigate the structural properties of aluminosilicate liquids as a function of pressure and temperature. Although experimental investigations on the high-pressure structure of aluminosilicate melts have to date been limited either to ambient pressure studies on glasses quenched from high-pressure melts or to in situ high-pressure studies of glasses at room temperature, a few pioneering vibrational spectroscopic studies on the combined pressure and temperature effects have been made on alakli germanate (Farber and Williams, 1992) and alkali silicate systems (see chapter by McMillan and Wolf in this volume).

Although in situ spectrocopic investigations of the combined high-pressure and high-temperature effects on silicate melt structure are just beginning, measurements on the physical properties of silicate melts at high pressure have been made for some time and continue to be extended to higher pressures. A number of viscosity (Kushiro, 1976, 1977, 1978a,b, 1980, 1986; Kushiro et al., 1976; Fujii and Kushiro, 1977; Scarfe et al., 1979, 1987) and diffusivity (Watson, 1979; Fujii, 1981; Kushiro, 1983; Shimizu and Kushiro, 1984; Dunn and Scarfe, 1986) measurements have now been made on natural and synthetic composition aluminosilicate melts to pressures up to 2.5 GPa. Most recently, diffusion measurements on aluminosilicates melts have been extended to 15 GPa (Rubie et al., 1993; Poe et al., 1994 , 1995). The electrical conductivity of basaltic and andesitic melts has been examined to 2.5 GPa (Tyburczy and Waff, 1983; Tyburczy and Waff, 1985). Shock wave experiments have provided important fundamental information on the pressure-density equations of state of model aluminosilicate and magmatic liquids to pressures in excess of 30 GPa (Rigden et al., 1984, 1988, 1989; Schmitt and Ahrens, 1989; Miller et al., 1991a,b). Crystal flotation experiments have provided further constraints on the densities of silicate melts at high pressures and have

been used to directly test petrogenesis models of crystal segregation in mantle magmas (Agee and Walker, 1988, 1993; Suzuki et al., 1995).

PHYSICAL PROPERTIES

Density is perhaps the most fundamental physical property of a silicate melt or glass. In addition to the critical role that melt densities play in igneous petrogenesis and planetary evolution, the compositional and pressure dependences of silicate melt and glass densities can yield insights into their microscopic structure and deformational mechanisms (Bottinga and Weill, 1970). Equations for estimating densities of multicomponent magmas from acoustic velocity data (Manghnani et al., 1986; Rivers and Carmichael, 1987; Kress et al., 1988) at ambient pressure have recently been summarized by Lange and Carmichael (1990). Since these equations are based on ambient compressibilities, estimates of the high-pressure densities of silicate melts are valid only if there is no significant change in the compression mechanisms at high pressures.

Some of the first investigations of the pressure-dependent structural properties of glasses were directed toward understanding Birch and Dow's (1936) observation that silica glass can undergo a permanent densification under some conditions of pressure cycling. Subsequent studies established that this densification occurs for a number of highly polymerized tetrahedral network glasses and that the magnitude of this effect depends on the precise history of sample stress conditions and temperature (Bridgman and Simon, 1953; Boyd and England, 1963; Mackenzie, 1963a,b; Cohen and Roy, 1965; Uhlmann, 1973; Primak, 1975; Kushiro, 1976; Arndt, 1983; McMillan et al., 1984; Grimsditch, 1986; Hemley et al., 1986; Walrafen and Hokmabadi, 1986; Meade and Jeanloz, 1987; Grimsditch et al., 1988).

An understanding of the mechanisms responsible for the permanent densification and the volume relaxation of densified silicate glasses, and their possible relationship to mechanisms of viscous flow in the liquid near the glass transition temperature, has been of longstanding interest. Early studies identified two or more distinct structural mechanisms for the densification of silica glass (Mackenzie, 1963a; Kimmel and Uhlmann, 1969). Under non-hydrostatic compression, Mackenzie proposed that silica can suffer permanent densification without bond breaking via a polymer entanglement mechanism with a low activation energy (<30 kJ/mol). The second mechanism, involving bond breaking and rearrangement, occurs with much higher activation energies (>300 kJ/mol) and can even occur under completely hydrostatic conditions. Studies by Hsich et al. (1971) suggested that volume relaxation in densified silica glass is characterized by a very broad range of relaxation times, all with approximately the same activation enthalpy (~300 kJ/mol). Although, this value approaches that of the activation energy for viscous flow in silica liquid (400 to 600 kJ/mol), Hsich concluded that the molecular processes associated with viscous flow and volume relaxation were different since the width of the relaxation time distribution for volume relaxation in the glass is enormously broader than that of viscous flow.

Some of the earliest attempts at measurement of the pressure-density equations-of-state of anhydrous aluminosilicate melts were based on the falling-sphere method of Fujii and Kushiro (1977; Scarfe et al., 1979). These early experiments, carried out in a piston-cylinder apparatus, were limited to pressures below 2.5 GPa and were subject to large uncertainties. Using a finite strain expression for the equation of state, and employing the available room-pressure ultrasonic compressibility data on silicate liquids, Stolper et al. (1981) estimated the densities of basaltic liquids to high pressures. Despite the uncertainties in these extrapolations (i.e., without knowledge of the pressure derivatives

of compressibilities) they came to the conclusion that because of the high compressibility of liquid silicates relative to that of mantle minerals, ultrabasic liquids may actually be denser than the principal residual crystals in mantle source regions at high pressure. Consequently, magmatic liquids may become neutrally buoyant deep within the terrestrial planets, hence limiting the depths at which magmas will segregate from their source and the degrees of partial melting that can be achieved in these source regions before melt segregation occurs (Stolper et al., 1981).

Using a different approach based on a thermodynamic analysis of melting curve data, Ohtani et al. (1983, 1984) were also able to estimate the equations-of-state of basic to ultrabasic magmatic liquids throughout the pressure range of the upper mantle. From these estimates, they concluded that picritic silicate liquids generated by partial melting of the upper mantle become denser than olivine and pyroxenes at pressures higher than 7 GPa. The density estimates further support the idea that in the early Archaean, when extensive partial melting of Earth's upper mantle was likely, melt segregation could lead to the development of chemically stratified upper mantle composed of an upper residual layer rich in olivine underlain by a garnet-rich layer.

Shock wave experiments have confirmed that the compressibilities of many basaltic composition melts remain high, relative to their crystalline counterparts, throughout the pressure range of the upper mantle (Rigden et al., 1984, 1988, 1989; Boslough et al., 1986; Schmitt and Ahrens, 1989; Miller et al., 1991a,b). Moreover, the shock experiments, and the high-pressure olivine flotation experiments of Agee and Walker (1988; 1993) (see Fig. 3a), generally support earlier speculations on melt segregation in the upper mantle and the possibility for gravitationally stable deep magma source regions. These ideas have been further refined by Miller et al. (1991a,b) from shock experiments on a molten komatiite. The komatiite melt data indicate that olivine and clinopyroxene become neutrally buoyant in a komatiite melt near 8 GPa while garnet-majorite becomes buoyant in ultrabasic melts in the 20 to 24 GPa interval (Fig. 3b). From an extrapolation of their shock data to higher pressures, Miller et al. (1991a) reach the same conclusion made earlier by Ohtani (1983), that liquidus perovskite crystals may become buoyant in lower mantle ultrabasic liquids below 70 GPa. Consequently, a downward migration of a partial melt, with incompatible elements, could occur in the lower mantle at depths below ~1000 km.

The high compressibilities of aluminosilicate melts relative to those of their low pressure crystalline phases, indirectly support earlier speculations (Waff, 1975) and computer simulation results (Matsui and Kawamura, 1980; Angell et al., 1982, 1983, 1987; Matsui et al., 1982; Matsui and Kawamura, 1984) that the framework cations in aluminosilicate melts undergo pressure-induced coordination changes with increasing pressure. Waff (1975) first suggested, by analogy with the high-pressure behavior of crystalline aluminosilicates, that the tetrahedral network cations in aluminosilicate melts will also undergo transformations to six-coordinated species at high pressures. He further speculated that these coordination reactions would take place over a narrow pressure range and thus produce dramatic changes in the densities and viscosities of aluminosilicate melts at mantle conditions. However, shock wave estimates of the equations of state of aluminosilicate liquids reveal more gradual changes in density with increasing pressure, a result more in line with the computer simulations.

There is some indirect evidence that the compressibilities of several fully polymerized (tektosilicate composition) aluminosilicate liquids exhibit anomalous behavior at very low pressures, which is not likely to be resolvable in shock experiments. By employing a thermodynamic analysis of high-pressure melting data, Bottinga et al.

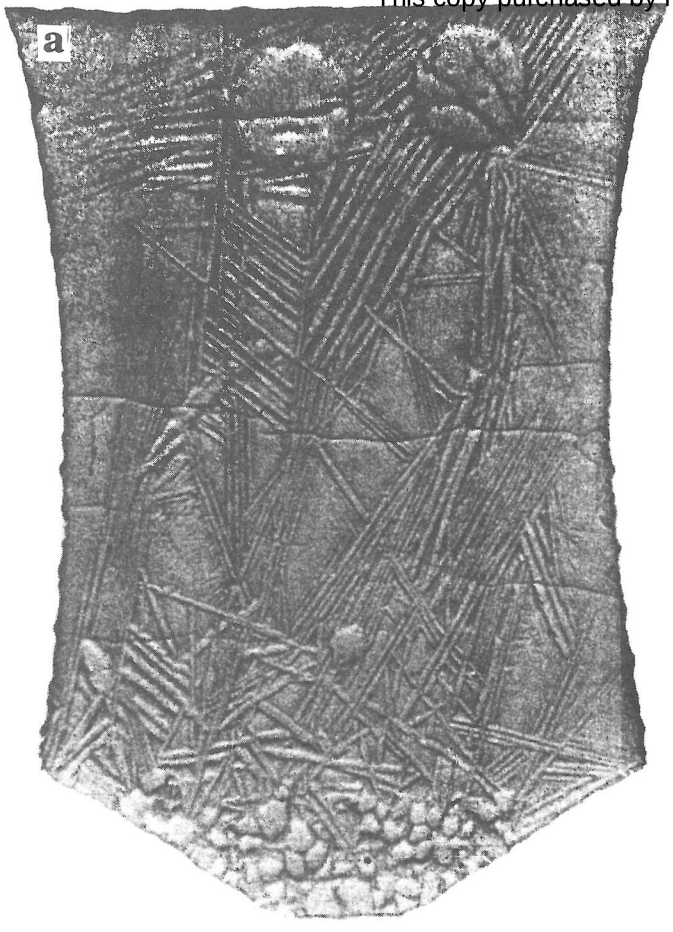

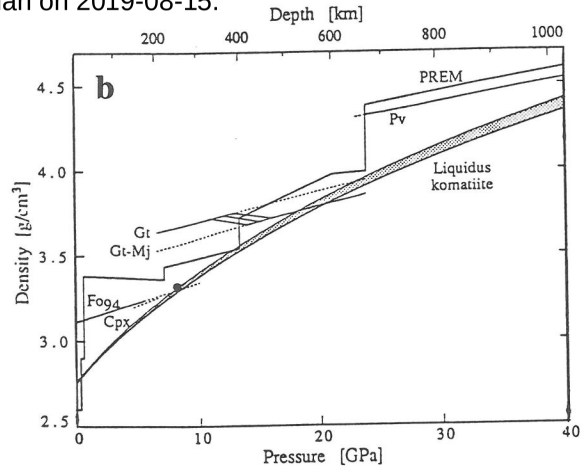

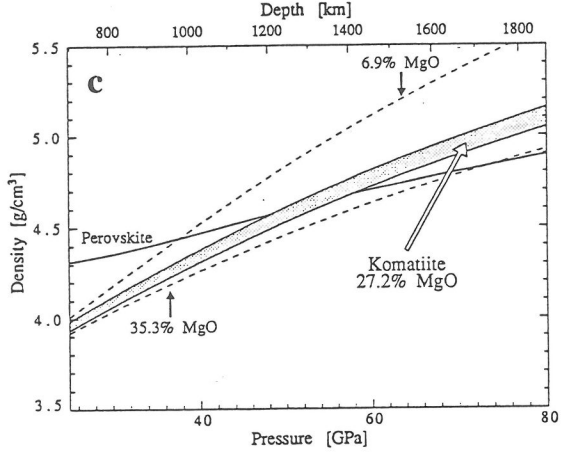

Figure 3 (opposite page). (a) Photomicrograph documenting the flotation of olivine spherules in a fayalite-enriched komatiite liquid (65% komatiite/35% fayalite) at 1.4 GPa and 1525°C. Denser Fe-rich equilibrium olivine crystals have segregated to the bottom of the capsule (taken from Agee and Walker, 1988). These and subsequent flotation results (Agee and Walker, 1993) indicate that equilibrium olivine crystals become buoyant at about 8 GPa in komatiite liguids along their liquidi. (b) The pressure-density relationships of komatiite liquid (27.2% MgO) and its liquidus phases (Fo_{94}, olivine; Cpx, clinopyroxene; Gt, garnet; Gt-Mj, garnet-majorite; Pv, perovskite) along the high-pressure liquidus. Estimate for the bulk mantle (PREM model) is also shown. The data suggests that olivine would be neutrally buoyant near 8.2 GPa (252 km). Figure taken from Miller et al. (1991a). (c) Extrapolation of the pressure-density relationships to lower mantle conditions. Shaded curve is the liquidus for komatiite liquid with 27.2% MgO and dotted lines represent komatiite liquids with 6.9% and 35.3% MgO. These results suggest that komatiite melts ranging from basic to ultrabasic compositions would become denser than perovskite at depths greater than 1000 to 1700 km, respectively. Figure taken from Miller et al. (1991a).

(1985) found that the compressibilities of jadeite and pyrope composition melts show a divergent increase in their compressibilities on decreasing pressure below 5 GPa (Fig. 4). (Compressibility estimates could not be derived at pressures below the termini of their respective congruent melting lines at 2.9 and 3.7 GPa.) Since the magnitude and correlation length of density fluctuations must also diverge as the compressibility diverges, this suggests that there may exist an underlying instability in the network structures of both of these liquids approaching ambient pressure on decompression.

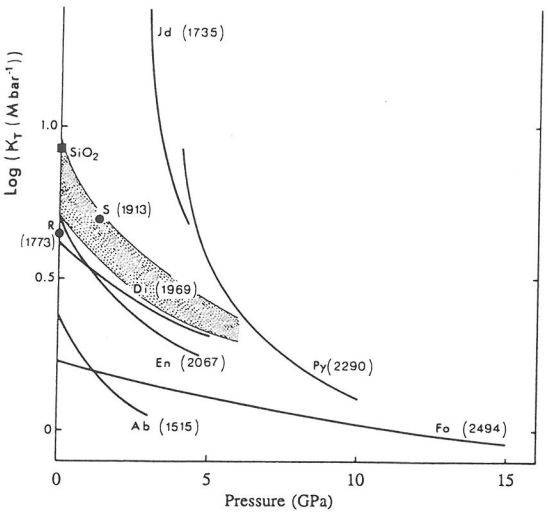

Figure 4. Logarithmic isothermal compressibilities of liquid jadeite (Jd), pyrope (Py), albite (Ab), forsterite (Fo), enstatite (En), and diopside (Di) derived by Bottinga et al. (1985) from a thermodynamic analysis of high-pressure melting data. Also plotted are data for liquid diopside, (S) and (R), from Scarfe et al. (1979) and Rivers and Carmichael (1987), respectively. Temperatures, in Kelvins, are given in parenthesis. The shaded area represents the range of compressibility values of liquid basalt proposed by Stolper et al. (1981). Data and Figure taken from Bottinga et al. (1985). [Used by permission of the editor of *Earth and Planetary Science Letters* from Bottinga (1985), Fig. 2, p. 354.]

Although the physical origin of this instability is not yet known, Bottinga et al. (1985) speculated that an aluminum coordination change could cause the anomalous compressibility and thermodynamic behavior. At first glance this argument appears compelling, since the anomalous behavior of the liquids occurs at about the same pressure as the aluminum coordination change in the stable crystalline phases of these same compositions. However, there is not yet any definitive structural data which supports this assertion. Furthermore, the pressure range of the aluminum coordination change is completely different to that which has been obtained from computer simulations (Angell et al., 1987). Nearly all ion dynamic simulations find that the coordination changes of the framework cations in aluminosilicate liquids take place over

a large pressure range. In fact, the pressure ranges are sufficiently large that the volume changes accompanying the coordination change are effectively smeared out. Angell et al. (1987) proposed an alternative origin for the anomalous low pressure compressibility behavior in jadeite melts. They suggested that the diverging compressibility resulted from an impending mechanical instability or "spinodal" which occurs in the tetrahedral network at slightly negative (i.e., tensile) pressures.

In the remaining sections, we focus more specifically on spectroscopic and structural investigations of the pressure-induced deformational mechanisms in simplified aluminosilicate and analog liquid and glass systems. The discussion is separated into classes of materials starting from the most polymerized systems (i.e., silica and germania) and progressing through to the most depolymerized systems (orthosilicates).

STRUCTURAL PROPERTIES

Fully polymerized systems

Silica. Silica is an important compositional component of essentially all magmatic liquids, and represents the reference structural archetype in the description of aluminosilicate glass and melt structures. At room pressure silica liquid and glass exist in a fully polymerized three-dimensional framework of corner-linked silica tetrahedra. The short range structure of the glass is characterized by highly regular SiO_4 tetrahedra with an average Si-O bond length of about 1.61 Å. At ambient pressure, the spread in the distribution of Si-O-Si inter-tetrahedral angles is large (from 120° to 180°) and the average value is near 144° (Mozzi and Warren, 1969; Dupree and Pettifer, 1984). In spite of the prominence of SiO_2 as a component in both technological glasses and magmatic liquids, fundamental details in the description of the intermediate and long range structure of silica glass remain controversial. Models ranging from those based on a continuous random network (Zachariasen, 1932; Warren 1933) to those based on microcrystallite building units (Lebedev, 1921; Valenkov and Porai-Koshits, 1936) have been proposed (see 1988 review by Galeener and chapter by Brown et al. in this volume).

It is well recognized that the extreme flexibility in the inter-tetrahedral angle of Si-O-Si can accommodate an enormous diversity of structures in response to chemical, temperature and pressure changes (Tossell and Gibbs, 1978; Navrotsky et al., 1985; Hemley et al., 1994). For example, the molar volumes of stable and metastable silica phases that are based on a tetrahedral framework structure range from 20.64 and 22.69 cm^3/mol in coesite and quartz to greater than 47 cm^3/mol in some zeolites. Over this enormous range in density the formation enthalpy varies by only 13.6 kJ/mol (Navrotsky, 1994). Room-temperature investigations of the high-pressure metastable behavior of quartz and other silica polymorphs (Hemley et al., 1988; Hazen et al., 1989; Halvorson and Wolf, 1990; Kingma et al., 1993a,b) suggest that the compressional deformation limit for the tetrahedral silica network is very near 17 cm^3/mol, roughly corresponding to the volume where the oxygen anions are in a cubic body-centered packing (Sowa, 1988; Hazen et al., 1989; Chelikowsky et al., 1990) and where the Si-O-Si intertetrahedral angle is close to 120° and the Si atoms are in non-bonded contact. Approaching this density, the SiO_4 tetrahedra become severely distorted (Hazen et al., 1989). Compression beyond this limit leads to bond rearrangement with a disruption of the tetrahedral framework and an increase in the silicon coordination (Verhelst-Voorhees et al., 1994). A mechanical instability of the tetrahedral network has been proposed to underlie the pressure-induced crystal-to-amorphous transition observed in many tetrahedral framework silicate and related phases (Hemley et al., 1988; Tse and Klug, 1991; Binggeli and Chelikowsky, 1992; Wolf et al., 1992; Chaplot and Sikka, 1993; Binggeli et al.,

1994). Chelikowsky et al. (1990) have suggested, on the basis of theoretical investigations, that this instability is driven by strong interpolyhedral oxygen-oxygen repulsions which occur in the superpressed tetrahedral framework at high pressure.

Studies on pressure compacted silica glass have found that residual irreversible densifications of up to 20% can be realized (Bridgman and Simon, 1953; Mackenzie, 1963a,b; Walrafen and Hokmabadi, 1986; Devine et al., 1987; Susman et al., 1990, 1991; Xue et al., 1991). The highest degree of compaction was obtained in glass samples pressure cycled up to 20 GPa and heated above 1600 K. In none of these samples was there evidence for the retention of high-coordinated silicon species. Diffraction and spectroscopic studies on compacted silica samples indicate that the major structural change is the shift in distribution of Si-O-Si intertetrahedral angles to smaller values with a decrease in the overall width of this distribution (Couty and Sabatier, 1978; Grimsditch, 1984; McMillan et al., 1984; Hemley et al., 1986; Devine and Arndt, 1987; Devine et al., 1987; Susman et al., 1990, 1991; Xue et al., 1991; Davoli et al., 1992). Furthermore, high-temperature annealing at high pressures tends to increase this effect. A slight increase in the average Si-O bond length can also be inferred from X-ray diffraction studies of compacted samples (Devine and Arndt, 1987).

In situ Raman (Hemley et al., 1986; Suguira and Yamadaya, 1992), infrared (Williams and Jeanloz, 1988; Williams et al., 1993), ultrasonic (Kondo et al., 1981; Sasakura et al., 1989), Brillouin (Zha et al., 1994; Rau, 1995) and X-ray diffraction (Meade et al., 1992) studies of silica glass have provided important information on the basic structural response of the SiO_2 network to changes in pressure. These studies have served to identify several primary deformation modes in silica glass that dominate over different but overlapping pressure regimes. Up to about 8 GPa, most of the compression of the tetrahedral network is taken up by a concerted rotational motion of the highly regular SiO_4 tetrahedra resulting in a gradual and reversible decrease in the Si-O-Si intertetrahedral angle. Above 8 GPa, increasing distortions of the SiO_4 tetrahedra become an important deformation mechanism. At higher pressures, possibly starting at pressures as low as 14 to 15 GPa, there is a gradual increase in the average silicon coordination number. Silicon is likely distributed over a range of four-, five-, and six-coordinated sites above 15 GPa with the most probable species progressing from four to five and to six with increasing pressure. Most of the four-coordinated silicon species appear to be consumed by about 30 GPa and have reacted to form either five- or six-coordinated species. However, some small concentration of four-coordinated species likely persists in the glass to 40 GPa. The completion of the coordination transformation to octahedral silicon likely occurs at much higher pressures, perhaps even above 50 GPa.

In situ infrared absorption studies (Williams and Jeanloz, 1988; Williams et al., 1993) provide compelling evidence for a pressure-induced coordination change in silica glass above 20 GPa (see Fig. 5b). A similar coordination change is also inferred to occur in metastable crystalline quartz and coesite under compression to pressures well above their thermodynamic stability fields (Williams et al., 1993; Verhelst-Voorhees et al., 1994). The primary spectroscopic signature for the loss of SiO_4 species is the reduction in intensity of the infrared tetrahedral stretching peak near 1100 cm^{-1} relative to absorption in the 600 to 900 cm^{-1} region. This progression is observed for silica glass at high pressures and is most evident in the spectra above 17 GPa (Williams and Jeanloz, 1988; Williams et al., 1993). At 39 GPa only a weak relatively diffuse absorption band is observed in the spectral region near 1100 cm^{-1} for silica glass. A similar loss of a distinct tetrahedral stretching band is also observed for metastable quartz at 39 GPa and for coesite above 47 GPa (see Fig. 6). The infrared absorption spectrum of silica glass at 39

GPa is qualitatively similar to that of stishovite at the same pressure (Williams et al., 1993).

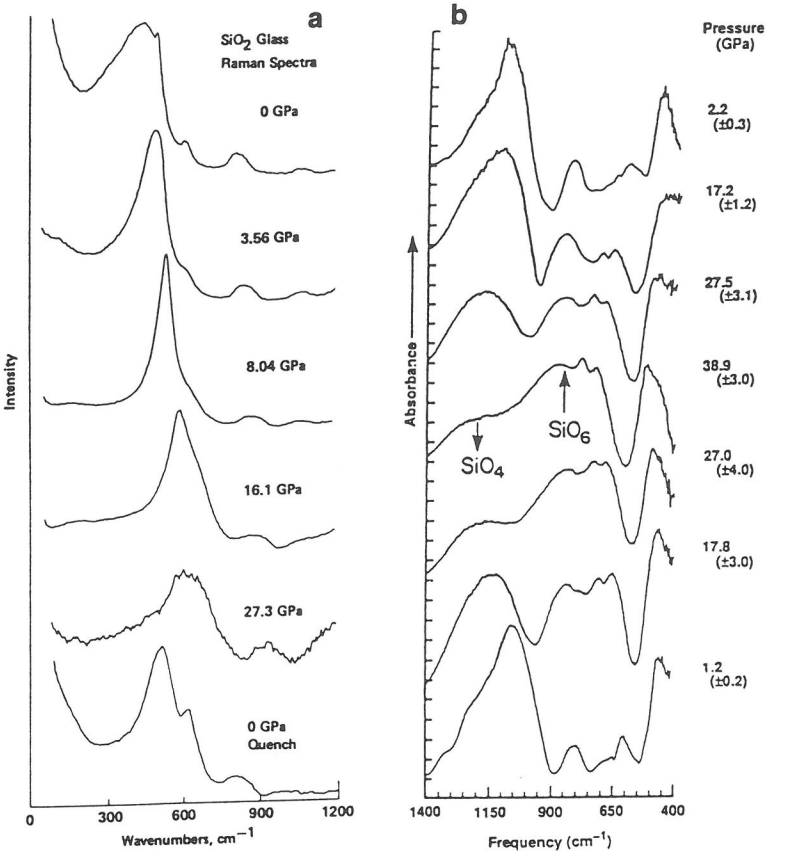

Figure 5 (above). Pressure dependence of the vibrational spectrum of silica glass. (a) Raman spectrum on increasing pressure and on recovered, pressure-cycled sample (Hemley et al., 1986). (b) Infrared absorbance spectrum on increasing and decreasing pressure (Williams and Jeanloz, 1988). Figure taken from spectra redrawn by Hemley et al. (1994).

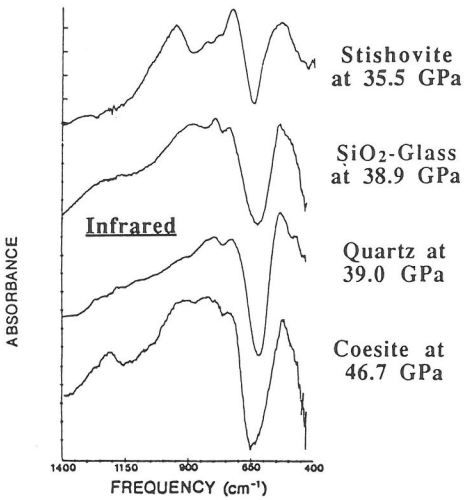

Figure 6 (right). Comparison of the high-pressure infra-red absorbance spectra of silica glass and several crystalline silica polymorphs (Williams et al., 1993).

Further details of the compressional behavior in silica glass can be obtained from the pressure-dependent changes in the Raman spectrum. At ambient pressure, the Raman spectrum of silica glass in the low frequency region is characterized by a strongly polarized, diffuse band centered near 430 cm^{-1} with two relatively sharp bands on the high frequency shoulder at 492 and 606 cm^{-1} (see Fig. 5a) The diffuse band is typically associated with a symmetric bending motion of the Si-O-Si linkages largely involving the motion of oxygen atoms in the plane bisecting the Si...Si line. The frequency of this mode is very sensitive to the value of the intertetrahedral angle and increases with decreasing SiOSi angles. The broad, diffuse nature of the scattering in this region is consistent with the broad distribution of intertetrahedral angles and high intermediate range disorder in silica glass. The sharp polarized bands at 492 and 606 cm^{-1} have been denoted as "defect" bands and are thought to represent symmetric oxygen breathing motions from, respectively, four- and three-membered siloxane rings which are vibrationally decoupled from the rest of the network (for a more complete description of the Raman bands in silica and other aluminosilicate glasses see McMillan and Wolf's chapter on vibrational spectroscopy in this volume).

Hemley et al. (1994) have measured the in situ Raman spectrum of silica glass to 30 GPa (Fig. 5a). Detailed measurements of the Raman spectra of silica glass have recently been obtained in the 0-20 GPa region by Sugiura and Yamadaya (1992). At pressures up to about 8 GPa, the primary effect of compression on the Raman spectrum is the gradual shift of the main symmetric stretching band to higher frequencies with a strong decrease in width and increase in absolute intensity. These spectral changes are consistent with a significant decrease in the Si-O-Si intertetrahedral angle and a gradual increase in the intermediate range order (Hemley et al., 1994). At pressures near 1 to 15 GPa there begins a marked decrease in intensity and apparent broadening of the main symmetric stretching band with increasing pressure (Sugiura and Yamadaya, 1992). Spectral intensity in the region near the 606 cm^{-1} defect band does not appear to decrease. At 27 GPa, the absolute intensity of the Raman scattering is very low and the spectrum is characterized by a weak, very diffuse band centered near 600 cm^{-1}.

Previous interpretations of the Raman scattering data have concluded that the onset of the silicon coordination change in SiO_2 glass occurs above 20 GPa (Williams et al., 1993; Hemley et al., 1994). We suggest, however, that the strong reduction in the intensity of the main symmetric stretching band in the Raman spectrum that begins near 14 to 15 GPa may be an indication of the onset of this transition. Although the precise pressure of the onset of the silicon coordination change is difficult to unambiguously constrain from the vibrational spectroscopic data, this interpretation is generally consistent with the in situ X-ray diffraction and Brillouin data on silica glass, discussed below, and is also consistent with interpretations of similar pressure-induced spectral changes observed in GeO_2 glass which we discuss in a latter section.

Meade et al. (1992) have measured, in situ, the X-ray diffraction spectrum of silica glass as a function of pressure to 42 GPa (Fig. 7). Their analysis of the diffraction data is generally consistent with conclusions based on the vibrational spectroscopic data. The derived pair correlation functions indicate that at 8 GPa the average Si-O bond length is consistent with complete tetrahedral coordination of silicon. At 28 GPa the average Si-O bond length is about halfway between those expected for tetrahedral and octahedral silicon at the same pressure, and implies that the average silicon coordination is approximately five. No data points between 8 and 28 GPa were reported; thus, the onset pressure of the silicon coordination change could not be more tightly constrained. At 42 GPa, the average Si-O bond length is about 0.03 Å smaller than that of stishovite at this same pressure, consistent with an average silicon coordination in the glass of about 5.5.

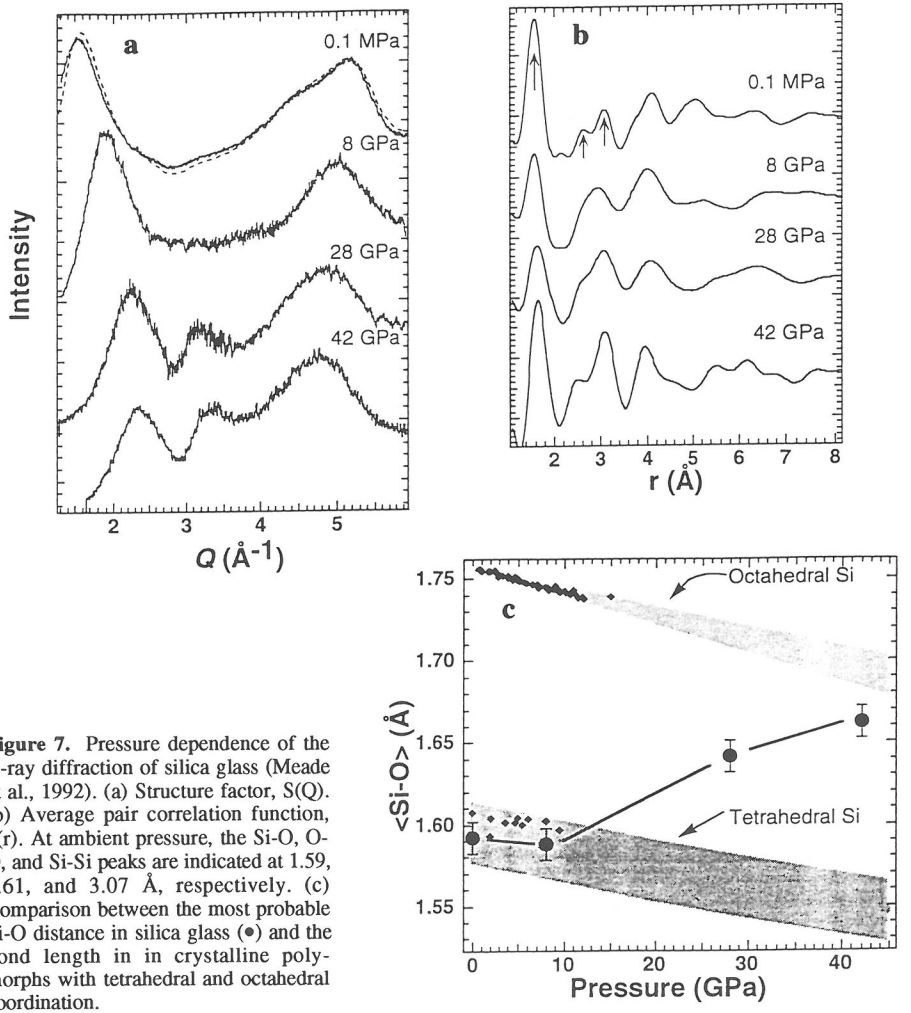

Figure 7. Pressure dependence of the X-ray diffraction of silica glass (Meade et al., 1992). (a) Structure factor, S(Q). (b) Average pair correlation function, g(r). At ambient pressure, the Si-O, O-O, and Si-Si peaks are indicated at 1.59, 2.61, and 3.07 Å, respectively. (c) Comparison between the most probable Si-O distance in silica glass (•) and the bond length in in crystalline polymorphs with tetrahedral and octahedral coordination.

A critical evaluation of deformational models inferred from the spectroscopic data can be obtained from an analysis of data on the high-pressure compressibility (Kondo et al., 1981; Schroeder et al., 1982; Grimsditch, 1984, 1986; Sasakura et al., 1989; Suito et al., 1992; Polian and Grimsditch, 1993; Zha et al., 1994; Rau, 1995) and equation of state (Bridgman, 1948; Meade and Jeanloz, 1987) of silica glass. Kondo et al. (1981) measured the ultrasonic acoustic velocities and attenuation in silica glass to 3 GPa. A minimum in the acoustic wave velocities was observed near 2.5 GPa, in good agreement with earlier static compression measurements (Birch and Dow, 1936; Bridgman, 1948). Kondo et al. also found that the ultrasonic acoustic waves were highly attenuated near the pressure of the minimum in compressibility. Ultrasonic measurements were later extended to 6 GPa by Sasakura et al. (1989; Suito et al., 1992) and are in good agreement with earlier measurements (Fig. 8).

Vukcevich (1972) showed that it was possible to rationalize most of the observed anomalous behavior of silica glass in terms of a simple two-state model. The states

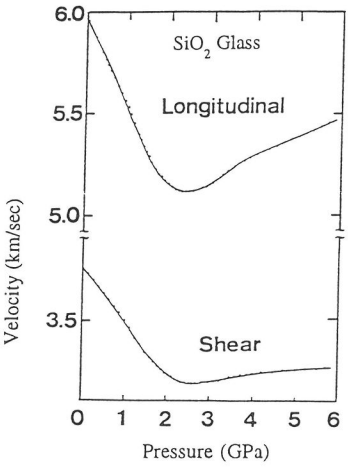

Figure 8 (above). Pressure dependence of ultrasonic acoustic wave velocities in silica glass (Suito et al., 1992).

Figure 9 (right). High-pressure Brillouin scattering data of silica glass.
(a) Pressure dependence of the hypersonic longitudinal, V_p, and shear, V_s, velocities of silica glass. Data from Zha et al. (1994) (filled symbols) and Schroeder et al. (1982) (open symbols).
(b) Comparison of the pressure dependence of the hypersonic bulk sound velocity for silica glass (filled circles; from Zha et al., 1994) with that estimated for quartz, coesite, and stishovite. Bulk sound velocities of the crystalline polymorphs estimated from

$$V_B = \sqrt{K/\rho}$$

using a 3rd-order Birch-Murnaghan equation of state. Equations of state for quartz and coesite from Hemley et al. (1988), for stishovite from Ross et al. (1990).
(c) A comparison of the static (Bridgman, 1948; Meade and Jeanloz, 1987) and shock (Marsh, 1980) compression data for silica glass with that derived from Brillouin data of Zha et al. (1994).

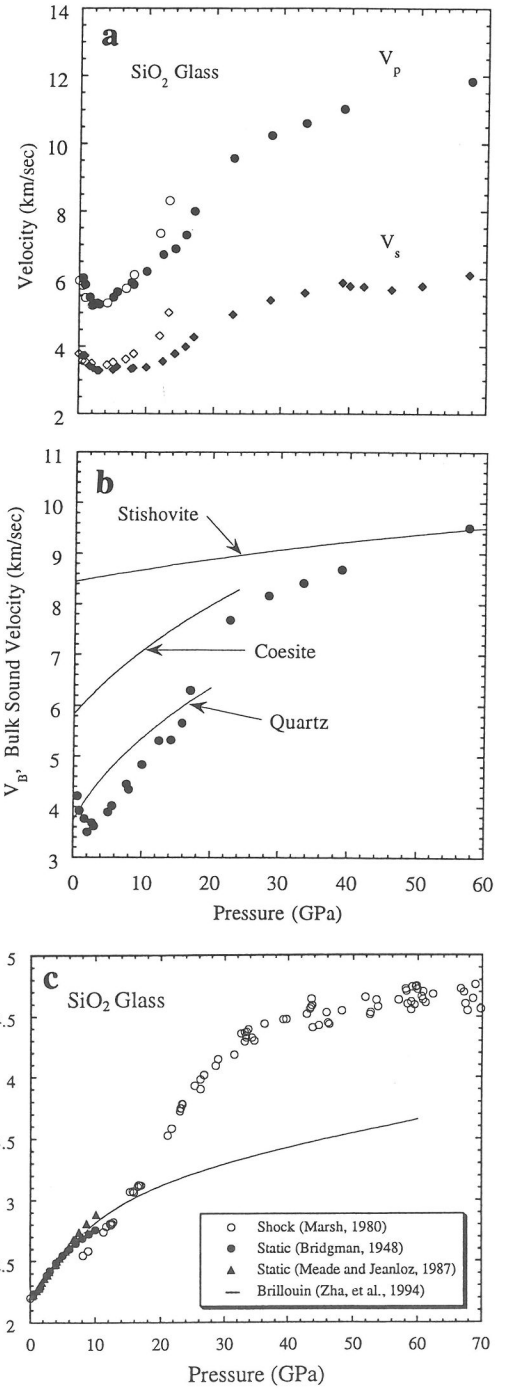

represent two local minima in the silica potential energy surface with distinct intertetrahedral angles and volumes, analogous to that of the α and β states in quartz, tridymite, and cristobalite. Anomalous temperature and pressure-dependent behavior in silica glass arises from a change in the distribution of these states. In this model, the primary contribution to the increase in compressibility of silica glass with pressure arises from the negative volume change associated with the transition between these two states. At pressures above 3 GPa, this reaction is nearly saturated and the compressibility behaves as that of a normal solid.

The elastic properties of silica glass have been investigated to much higher pressures using Brillouin scattering. Grimsditch (1984, 1986) and Polian and Grimsditch (1993) measured the Brillouin scattering spectrum of silica glass up to 25 GPa in a diamond anvil cell. Because of the backscattering geometry used in their studies, index of refraction corrections are needed in order to extract the acoustic wave velocities from the Brillouin data. These corrections were applied in the latest work of Polian and Grimsditch (1993). Schroeder et al. (1982) and Zha et al. (1994) also employed Brillouin scattering, using an equal angle scattering geometry to eliminate the index of refraction correction, to directly obtain the acoustic velocities of silica glass to 13 and 57 GPa, respectively.

At pressures up to about 6 GPa, the ultrasonic and Brillouin scattering data are generally in accord, although, the shear velocities obtained by Schroeder et al. (1982) appear high above 3 GPa, in comparison with the ultrasonic and other Brillouin scattering measurements. At pressures above 6 GPa, the velocities obtained by Schroeder et al. increase much more rapidly with pressure than those obtained from the other Brillouin experiments. The velocity data from Zha et al. (1994) and Polian and Grimsditch (1993) are in good agreement with each other over the entire range of comparison.

One of the most significant aspects of the high-pressure behavior of the acoustic velocities in silica glass is the marked increase in the pressure dependence of both the longitudinal and transverse acoustic velocities which occurs near 15 GPa (see Fig. 9a). This strong pressure dependence saturates near 30 GPa, above which the increase in the velocities is more gradual on up to 57 GPa. The rapid increase in the acoustic velocities above 15 GPa is consistent with the formation of dense, highly rigid domains composed of high-coordinated silicon species. We further suggest that the saturation of the strong pressure dependence of the acoustic velocities, which occurs near 30 GPa, is an indication of a near-complete conversion of tetrahedral silicon sites to either five- or six-coordinated silicon. Some tetrahedral species, however, remain resistant to conversion even at these pressures, perhaps those bound in the smaller siloxane ring structures. The more gradual increase in velocities above 30 GPa, up to 57 GPa, indicates that the completion of the coordination transformation, to all six-coordinated silicon, occurs more gradually.

These arguments can be further validated by a comparison of the bulk sound speed, V_B, ($V_B^2 = V_P^2 - \frac{4}{3}V_S^2$) of silica glass, derived from the Brillouin scattering measurements, with those estimated for stishovite and metastable quartz and coesite (Fig. 9b). The metastable compression limits for quartz and coesite occur at about 21 and 26 GPa, respectively (Hemley et al., 1988; Kingma et al., 1993a), so any extrapolation above these limits is not meaningful. At 22 GPa, the bulk sound velocity of silica glass is similar to that of metastable coesite at this same pressure. With increasing pressure, the sound velocity gradually tends toward that of stishovite. It is interesting to note that there is not much difference between the bulk sound velocities of coesite and stishovite at high pressures. This coincidence is a result of the tradeoff between rigidity and density in

determining the sound velocity ($V_B = \sqrt{K/\rho}$, where K is the adiabatic bulk modulus and ρ is the density).

Further insights into the deformational behavior of silica glass has been obtained from both static and dynamic compression measurements of the equation of state. Static compression measurements on the room temperature equation of state of silica glass have been made to about 10 GPa by Bridgman (1948) and by Meade and Jeanloz (1987) (Fig. 9c). Above 6 GPa there is a growing discrepancy between the compression results of these two studies, the origin of which is difficult to evaluate. In Meade and Jeanloz's experiments, the compression measurements were made on samples in a diamond anvil cell employing a novel optical method for measuring linear strains. In these experiments the sample was immersed in a liquid medium which remained completely hydrostatic to 10 GPa. Bridgman carried out his compression experiments in a modified piston-cylinder type apparatus using a liquid pentane/isopentane pressure medium which is known to remain hydrostatic to 7 GPa. In his experiments, the pressure and volume were derived from piston force and displacement measurements.

In the absence of strong viscoelastic (or anelastic) effects, the acoustic wave velocities can also be used to estimate the equation of state (see chapter by Dingwell in this volume). Estimates of the equation of state obtained in this manner are based on the premise that the structural response of the glass which occurs over the timescale of the static compression measurements (~10^4 sec) will also occur over hypersonic timescales (10^{-11} sec). Although some viscoelastic behavior is observed in the acoustic velocities at MHz (Kondo et al., 1981) and GHz (Rau, 1995) frequences for silica glass near 2-3 GPa, the relaxing part of the acoustic moduli is not large in this pressure region in comparison to the overall pressure dependencies of the static moduli. In Figure 9c, we compare the static compression data of Bridgman (1948) and Meade and Jeanloz (1987) to estimates based on the ultrasonic and Brillouin scattering measurements. All of the compressional curves are in reasonable agreement up to about 6 GPa. The equation of state estimate derived from Schroeder et al.'s (1982) Brillouin scattering measurements remains in very good agreement with the static compression data of Meade and Jeanloz to 10 GPa. The Brillouin scattering results of Polian and Grimsditch (1983) and Zha et al (1994) show an increasing deviation with the static compression data of Meade and Jeanloz above about 7 GPa. However, these latter Brillouin scattering studies are more in line with Bridgman's original compression data.

Shock compression investigations have been made on silica glass both in the elastic regime (Barker and Hollenback, 1970) and to pressures in excess of 100 GPa (Wackerle, 1962; Anan'in et al., 1974; Marsh, 1980; Sugiura et al., 1981; Lyzenga and Ahrens, 1983; Chhabildas and Grady, 1984; Schmitt and Ahrens, 1989; McQueen, 1992). However, in comparing the properties of shocked silica glass with those obtained from static measurements, it is important to emphasize that the state of silica under dynamic and static compressions is quite different. The behavior of silica glass under shock compression is complex and the interpretation of the shock wave data has been controversial. Early shock recovery experiments (Anan'in et al., 1974) found that silica glass undergoes heterogeneous deformation between 10 and 30 GPa, very similar to that of quartz. These observations are consistent with the high radiative temperature measurements found for shocked silica glass between 10 and 30 GPa (Schmitt and Ahrens, 1989) and indicate that localized hot spots occur within the sample in this shock regime that are nearly 2000 K hotter than the bulk. Shock heating estimates, based on a homogeneous continuum, predict a temperature rise of less than 10 K up to 26 GPa, increasing to 495 K at 30 GPa (Wackerle, 1962). At higher shock pressures, between 30

and 70 GPa, the deformation is largely homogeneous. Lyzenga and Ahrens (1983) have estimated, on the basis of their own thermal emission studies, that the temperature of shocked silica glass at 50 GPa is nearly 4500 K. They suggest that, under these conditions, the silica exists as superheated crystalline stishovite and interpret the sudden decrease in thermal emission at 70 GPa to indicate the metastable melting of this phase.

Figure 9c includes a plot of the shock Hugoniot data for silica glass obtained by Marsh (1980). For comparison, the static compressional data for silica glass, together with the high-pressure equations of state of quartz, coesite, and stishovite, are also included in this figure. The dynamic and static compression data are in general agreement in the elastic regime below 10 GPa. Above 15 GPa the shock Hugoniot strongly deviates from that of the equation of state derived from the hypersonic acoustic velocities. The density of the glass sample under shock becomes greater than that of quartz and coesite above 15 GPa and approaches that of stishovite above 30 GPa. The decoupling of the Hugoniot and hypersonic equation of state above 15 GPa, indicates that there is a significant structural rearrangement that occurs under shock at these conditions that is essentially frozen at hypersonic timescales. This is likely due to both the higher temperature and the longer characteristic timescale of the shock experiment. The characteristic timescale in the dynamic compression experiments can be estimated by the shock rise time and is several orders of magnitude longer than that for the Brillouin experiments (Rigden et al., 1988).

Germania. Germania (GeO_2) is a useful chemical and structural analog for silica and exhibits a number of the same structural motifs and anomalous physical properties as SiO_2 (Ringwood, 1978). Most useful is the fact that many of the inferred structural deformation modes in silica glass also occur in germania glass but at much lower pressures. In addition, the pressure-induced coordination changes occurring in germania glass have been well characterized using EXAFS (Itie et al., 1989) and Raman spectroscopy (Durben and Wolf, 1991; Smith and Wolf, to be published). At ambient pressure germania glass exhibits a tetrahedral framework structure similar to that of silica. One important difference, however, is that the germania network possesses a much greater degree of intermediate range order compared to silica. In germania, the average intertetrahedral angle is only about 133° at room pressure and the width of the angle distribution is much smaller (~10°) than that found in silica (Leadbetter and Wright, 1972; Sayers et al., 1972; Desa and Wright, 1988). The structure of germania glass at ambient pressure has been likened to that of the silica glass structure at about 8 GPa (Hemley et al., 1986) based on a comparison of the Raman spectra.

High pressure X-ray absorption (XANES and EXAFS) (Itie et al., 1989) studies on germania glass indicate that germanium undergoes a four-fold to six-fold coordination change between about 5 and 10 GPa (see Fig. 10a). The relatively low pressure of this coordination change in GeO_2 has made this system particularly amenable to experimental inquiries aimed at understanding the nature of the structural transition and the manner in which this structural change is manifested in the physical and spectroscopic properties.

Durben and Wolf (1991) and Smith and Wolf (1995, to be published) have made extensive investigations of the changes in the Raman spectrum of germania through the pressure-induced coordination change in germania glass (Fig. 11). Perhaps the most noticeable change exhibited in these spectra is the dramatic reduction in the absolute intensity of the main symmetric bending mode near 500 cm^{-1} beginning just above 4 GPa. This pressure only slightly precedes that inferred from the X-ray absorption data for the onset of germanium coordination change (Itie et al., 1989) (although the onset pressures may be consistent within resolution of the X-ray experiment).

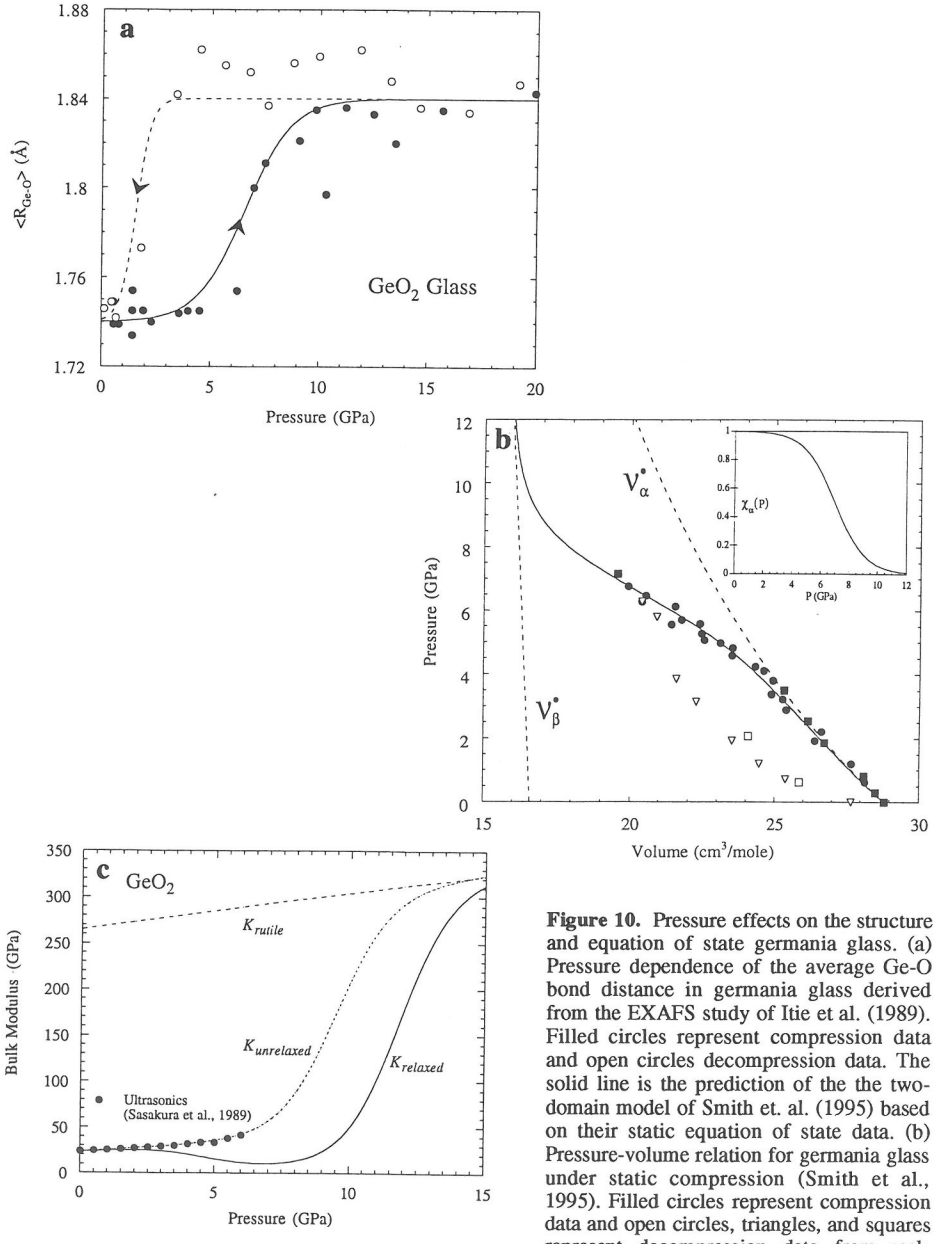

Figure 10. Pressure effects on the structure and equation of state germania glass. (a) Pressure dependence of the average Ge-O bond distance in germania glass derived from the EXAFS study of Itie et al. (1989). Filled circles represent compression data and open circles decompression data. The solid line is the prediction of the the two-domain model of Smith et. al. (1995) based on their static equation of state data. (b) Pressure-volume relation for germania glass under static compression (Smith et al., 1995). Filled circles represent compression data and open circles, triangles, and squares represent decompression data from peak pressures of 3.5, 6.5, and 7.1 GPa, respectively. Dashed lines are the model equations of state for the pure $^{[4]}$Ge and $^{[6]}$Ge domains, v_α and v_β. Solid line is a fit of the compression data to the two-domain equation of state model. The inset is a plot of the pressure dependence of the mole fraction of $^{[4]}$Ge, χ_α. (c) Pressure dependence of the bulk modulus of germania glass. Solid circles are ultrasonic data from Suito et al. (1992). Solid line is the bulk modulus derived from the static compression data of Smith et al. (1995). Dotted line is the high-frequency (unrelaxed) bulk modulus predicted from the two-domain model of Smith et al. (1995). Dashed line is the pressure-dependent bulk moduli of the crystalline rutile phase of germania extrapolated from the equation of state parameters of Hazen and Finger (1981).

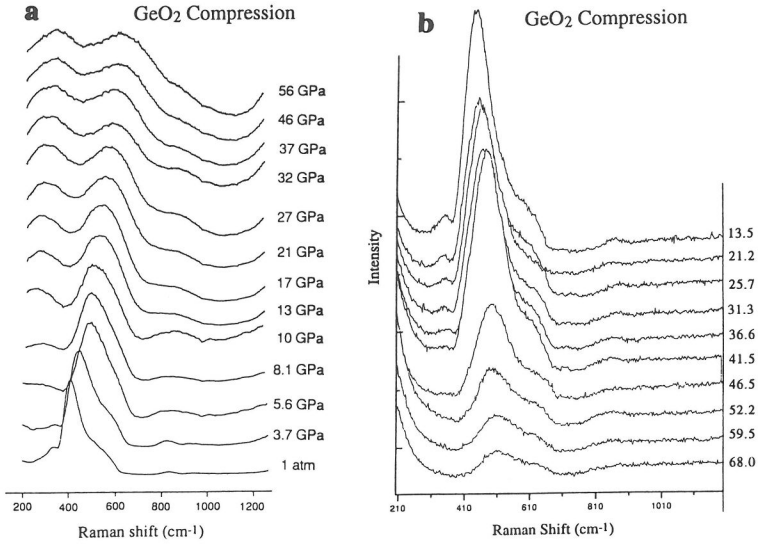

Figure 11. Pressure dependence of the Raman spectrum of germania glass. (a) Relative Raman intensities between ambient and 56 GPa (Durben and Wolf, 1991). (b) Absolute Raman intensities between ambient and 7 GPa (Smith and Wolf, to be published).

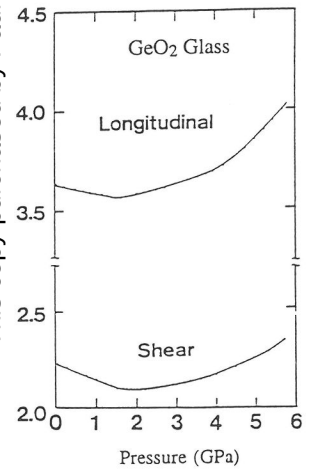

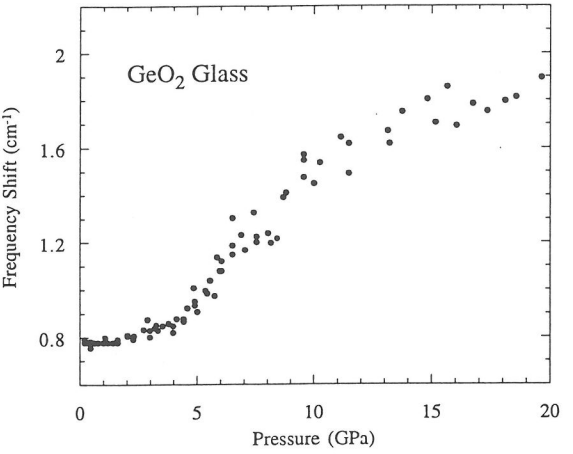

Figure 12. Pressure dependence of the the ultrasonic acoustic wave velocities in germania glass (Suito et al., 1992).

Figure 13. Pressure dependence of the Brillouin frequency shift (backscattering geometry) of the longitudinal acoustic mode in germania glass (Grimsditch et al., 1988).

The pressure-dependent acoustic wave velocities in germania glass have been obtained from both ultrasonic (Fig. 12) (Suito et al., 1992) and Brillouin scattering (Schroeder et al., 1990; Wolf et al., 1992) measurements up to about 6 GPa. Brillouin frequency shifts in germania glass (without index of refraction corrections) have been obtained up to 20 GPa (Fig. 13) (Grimsditch et al., 1988). All of the data reveal the onset

of a rapid increase in both the acoustic velocities and Brillouin frequency shifts near 4 GPa (this is most pronounced for the longitudinal waves), similar to that which occurs in silica glass near 15 GPa. Acoustic wave attenuation studies (Wolf et al., 1992) reveal that at room temperature the inferred germanium coordination change above 4 GPa occurs over much longer timescales than that sampled by waves propagating at hypersonic frequencies (i.e., $\tau_c \gg 10^{-11}$ sec). This observation validates the inference that acoustic wave velocities of silicates derived from Brillouin measurements at room temperature sample a frozen coordination configuration. Hence, equations of state directly derived from the acoustic velocities will decouple (be less compressible than) from the equations of state derived from a static compression measurement in the pressure region where these coordination transformations occur.

Very recently, Smith et al. (1995) have measured the equation of state of germania glass under static compression up to 7 GPa (Fig. 10b). The data indicate a marked increase in the static compressibility of the glass that also begins near 4 GPa. Up to 4 GPa the compressional behavior of germania glass is completely reversible in a hydrostatic medium. At higher pressures, a residual densification is always observed, even when the sample is maintained under completely hydrostatic conditions.

Smith et al. (1995) were able to quantitatively fit their equation of state data to a simple two-domain model in which the glass is assumed to be made up of a mixture of low and high density domains. The structural interpretation of this model is that the low density domains are composed of tetrahedral germanium while the high density domains are rutile-like with germanium in six-fold coordination. Within this *ansatz*, the pressure dependence of the mole fraction of tetrahedral germanium could be extracted from the static equation of state data and was used to predict the pressure dependences of the average Ge-O bond length and compressibility of germanium glass. The behavior of the average Ge-O bond length with pressure predicted with this model was in quantitative agreement with the X-ray results of Itie et al. (1989, 1990) (see Fig. 10a).

In the two-domain model, the static compressibility is given by the volume-averaged compressibilities of the low and high density domains, together with a term representing the volume change associated with the coordination change (Vukcevich, 1972). Employing the earlier observation that high-frequency acoustic waves do not access this compression mechanism, Smith et al. (1995) were able to quantitatively reproduce the pressure-dependent behavior of the bulk sound velocity of germania glass obtained from the ultrasonic measurements of Suito et al. (1992) (Fig. 10c).

The consistency of the two-domain model for the description of the high-pressure properties of germania glass does not eliminate the possibility for the existence of five-coordinated Ge species at high pressures. More complex models (with additional parameters) could certainly be found which will also provide a consistent interpretation of the data. For silica, molecular dynamics simulations on the glass and melt predict that a distribution of four-, five-, and six-coordinated Si species occur at high pressures (Angell et al., 1982, 1983, 1987; Rustad et al., 1991). Moreover, experimental investigations of the more "depolymerized" aluminosilicate systems, which we discuss below, have unequivocally established that five-coordinated silicon and aluminum species do occur at high pressures in the glass and liquid states. However, the existence of $^{[5]}Ge$ species in GeO_2 has not been established from spectroscopic studies on either in situ or quench samples. Furthermore, G. Calas (personal communication to PM) has indicated that the XANES data of Itie et al. (1989, 1990) would be most consistent with only $^{[4]}Ge$ and $^{[6]}Ge$ species.

The extensive in situ structural data on germania glass provides an unusual opportunity to develop semi-quantitative "calibrations" of vibrational spectral bands. Smith and Wolf (to be published) have recently made a detailed analysis of the pressure-dependent absolute Raman band intensities of germania glass. The Raman data show (Fig. 11b) that between 4 and 7 GPa there is a near 85% loss in the total intensity of the main symmetric tetrahedral stretching mode. This intensity reduction can be qualitatively interpreted by a model in which approximately half of the $^{[4]}$Ge species are converted to high-coordinated ($^{[5]}$Ge or $^{[6]}$Ge) species, effectivley eliminating nearly all Q^4-Q^4 linkages (which are associated with the main symmetric stretching band). This would result in an average Ge coordination of about 4.5 to 5.0, depending on whether five- or six-coordinated germanium is formed and assuming a random spatial distribution. By comparison, the results of Itie et al. (1989, 1990) suggest that at 7 GPa the average coordination is also in this same range (on the basis of bond length inferences). This general consistency between the Raman absolute intensity data and the XANES data suggest that absolute Raman intensity data may be a useful marker for inferring coordination changes in network glasses and melts.

"Charge-balanced" aluminosilicates. Spectroscopic investigations of the ambient structure of aluminosilicate glasses with compositions along the "charge-balanced" SiO_2–M^+AlO_2 or SiO_2–$M^{2+}Al_2O_4$ joins (M^+ = alkali metal; M^{2+} = alkaline earth) generally indicate that Al enters the framework structure in tetrahedral coordination substituting for Si as a "network former." At ambient pressure the structures of glasses along these joins are well described in terms of fully polymerized networks of tetrahedral silicon and aluminum (Taylor and Brown, 1979a,b; Taylor et al., 1980; Engelhardt and Michel, 1987; Oestrike et al., 1987), in similarity to the crystalline structures they form at ambient pressure. A possible exception to this generalization has been suggested from NMR data on ambient glasses very near the charge-balanced SiO_2-$MgAl_2O_4$ join which are inconsistent with the presence of small amounts of $^{[5]}$Al and $^{[6]}$Al species (McMillan and Kirkpatrick, 1992).

Waff (1975) was the first to suggest that aluminum and other tetrahedral network cations in aluminosilicate melts would undergo transformations to six-coordinated species at high pressures. The basis for his speculation was from analogy with the well-documented transformations of this type in the crystalline state of these same systems. He further suggested that these coordination transformations would take place over relatively narrow pressure ranges producing dramatic changes in melt properties. Kushiro (1976) and Velde and Kushiro (1978) later rationalized their observations of the anomalous pressure dependence of viscosity in a number of highly polymerized aluminosilicate liquids in terms of Waff's original ideas. In part, this rationalization was based on their interpretation of infrared absorption data and wavelength shifts in the aluminum K_α and K_β X-ray absorption lines of jadeite ($NaAlSi_2O_6$) composition glasses quenched from high-pressure melts (Velde and Kushiro, 1978). From this data they concluded that in melts of this composition aluminum converts to six-coordination at pressures below 3 GPa.

The spectral interpretations of Velde and Kushiro were later criticized by Sharma et al. (1979) who could find no evidence for an aluminum coordination change in Raman spectroscopic studies of similar glasses. This negative result was borne out in a number of subsequent Raman (McMillan and Graham, 1980; Mysen et al., 1982, 1985; Seifert et al., 1982) and X-ray (Hochella and Brown, 1985) studies on jadeite ($NaAlSi_2O_6$), albite ($NaAlSi_3O_8$), and other fully polymerized aluminosilicate glasses that were quenched from melts as high as 4 GPa.

Later, Ohtani et al. (1985) reported observation of spectral lines indicative of six-coordinated aluminum in the ^{27}Al MAS NMR spectra of albite glasses quenched from 6 and 8 GPa melts. This claim was again questioned, however, by Stebbins and Sykes (1990), who were not able reproduce the results of Ohtani et al. in their own ^{27}Al MAS NMR studies of high-pressure albite composition melts. In their study, spectrally well-defined $^{[5]}Al$ or $^{[6]}Al$ bands were not present in NMR spectra of melt glasses quenched from pressures as high as 10 GPa (Fig. 14a). These authors suggested that the well resolved peak at -16 ppm present in the spectra of Ohtani et al. may be due to contamination or the presence of poorly crystalline jadeite nuclei. The spectra of Stebbins and Sykes did, however, exhibit a small feature on the high-field side of the main $^{[4]}Al$ resonance, which could indicate the presence of small quantities (< 5%) of $^{[5]}Al$ and $^{[6]}Al$ sites in the high-pressure glass. Moreover, these features were found to be independent of the magnetic field strength and so are not likely to originate from quadrupole broadened, highly distorted tetrahedral sites. Furthermore, Stebbins and Sykes concluded that ~50%

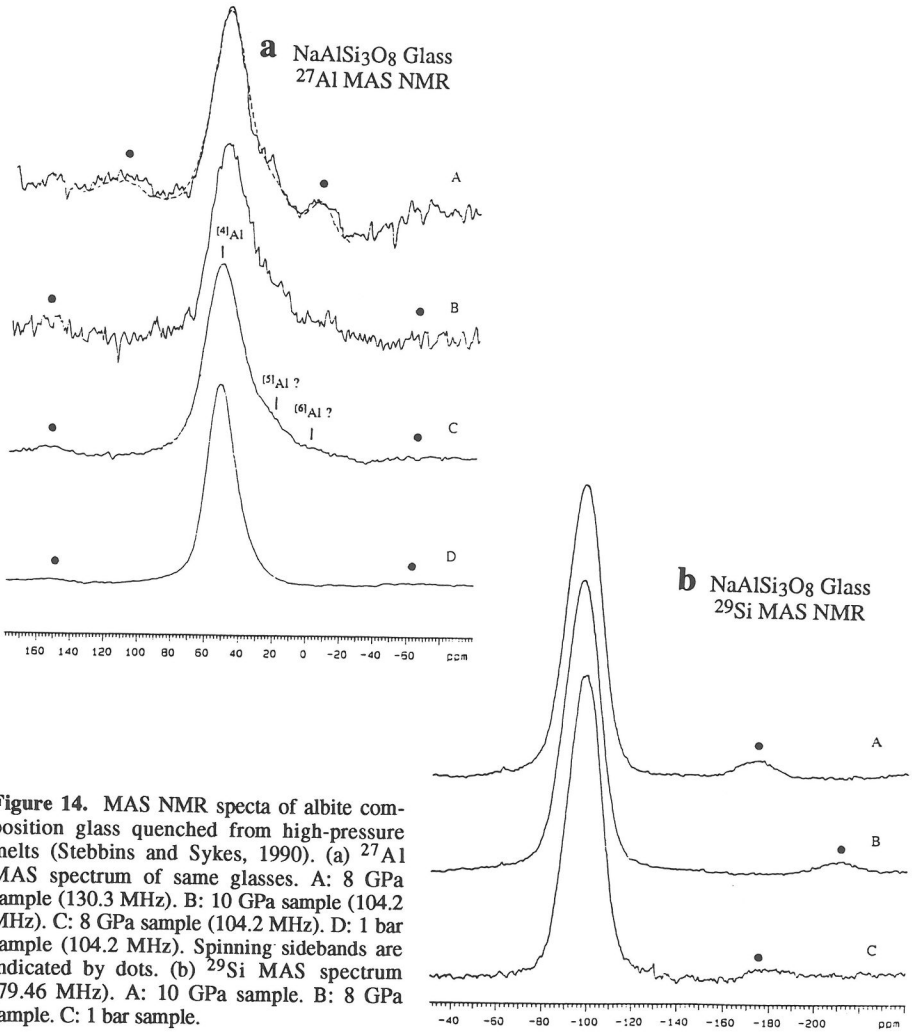

Figure 14. MAS NMR specta of albite composition glass quenched from high-pressure melts (Stebbins and Sykes, 1990). (a) ^{27}Al MAS spectrum of same glasses. A: 8 GPa sample (130.3 MHz). B: 10 GPa sample (104.2 MHz). C: 8 GPa sample (104.2 MHz). D: 1 bar sample (104.2 MHz). Spinning sidebands are indicated by dots. (b) ^{29}Si MAS spectrum (79.46 MHz). A: 10 GPa sample. B: 8 GPa sample. C: 1 bar sample.

of the total ^{27}Al signal intensity could not be accounted for in their spectral bands. They suggested that the loss of signal in the NMR spectrum of these high-pressure glasses is an indication of the presence of highly distorted Al polyhedra with large quadrupolar coupling constants. Very similar ^{27}Al NMR spectroscopic results were also obtained in a more recent study on orthoclase ($KAlSi_3O_8$) composition glasses quenched from high-pressure melts (Sykes et al., 1993).

For silicon, the resolving power of ^{29}Si MAS NMR for different coordination species is much greater than for ^{27}Al which has a quadrupolar lineshape. In the Stebbins and Sykes (1990) study, no evidence was found for the presence of five- or six-coordinated Si species in the high-pressure albite glasses above the detection limit of 0.5% (see Fig. 14b).

Unambiguous evidence for the existence of high-coordinated Al and Si species in aluminosilicate composition glasses along the charge-balanced joins has been difficult to establish from studies of quenched samples at ambient pressure. This can be contrasted to the results from some recent studies on fully-polymerized aluminate melts. Daniel et al. (1995) have inferred, from an in situ Raman study, that the aluminum in $CaAl_2O_4$ glass increases in coordination above 11 GPa. Very recently, this was confirmed by Yarger et al. (1995) who found NMR evidence for the retention of high-coordinated Al species in $CaAl_2O_4$ glasses quenched from high pressures. In their study, well resolved features occur in the ^{27}Al MAS NMR spectra of glasses quenched from high pressure that are consistent with relatively high abundances (tens of %) of $^{[5]}Al$ and $^{[6]}Al$ species.

Contrary to ambient studies on fully polymerized aluminosilicate composition glasses quenched from high-pressure melts, in situ spectroscopic studies on silica and germania glasses (discussed in the previous sections) provide compelling evidence that high-coordinated species are formed in fully polymerized silicate and related systems at high pressures, even though these species are not retained on decompression (Hemley et al., 1986; Williams and Jeanloz, 1988; Itie et al., 1990; Durben and Wolf, 1991). Similar results in an aluminosilicate system were found by Williams and Jeanloz (1988). In their study, the infrared absorbance spectrum of anorthite ($CaAl_2Si_2O_8$) composition glass was measured as a function of pressure to 31 GPa (see Fig. 15). In general the spectral changes observed for anorthite glass are similar to that observed for silica glass, but occur at lower pressures. The infrared data suggest that the tetrahedral coordination change in anorthite glass commences between 3 and 11 GPa. By 22 GPa the high frequency spectral bands associated with tetrahedral species are essentially gone.

The spectral interpretations of Williams and Jeanloz (1988) are remarkably consistent with molecular dynamic simulations on jadeite ($NaAlSi_2O_6$) melts by Angell et al (Angell et al., 1982, 1983, 1987). In these simulations it was found that the tetrahedral network cations (Si^{4+}, Al^{3+}) undergo coordination changes over a wide range in pressure (at least at simulation temperatures, 4000 to 6000 K). Furthermore, the coordination changes for Al^{3+} take place at considerably lower pressures than for Si^{4+}. In jadeite, the average coordination of Al^{3+} is 5 at about 10 GPa. However, for Si^{4+} cations, this average coordination state is not realized until pressures of about 20 GPa.

One of the more interesting results of the experimental and theoretical investigations on the fully polymerized silicate and germanate systems, has been the diversity in character that the coordination transformations can display in the amorphous state. It appears that these coordination changes can, in some systems, resemble first-order transformation (i.e., GeO_2) with relatively sharp changes in properties and significant hysteresis, while in silica and the few other fully polymerized aluminosilicates

that have been studied, the transformations appear to occur with minimal hysteresis over a much larger pressure range. These generalities must be modified, however, in describing the high-pressure behavior of the more "depolymerized" aluminosilicates. As we discuss below, additional coordination change mechanisms are expressed that can display extreme hysteresis, resulting in the retention of high-coordinated species in the decompressed samples.

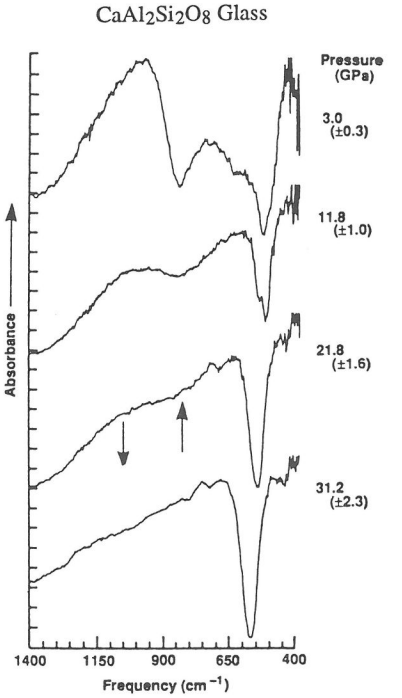

Figure 15. Pressure dependence of the infrared absorbance of anorthite glass (Williams and Jeanloz, 1988). [Used with permission of the American Association of the Advancement of Science, from Williams and Jeanloz (*Science*, 1988, Fig. 1, p. 903.]

Depolymerized silicate systems

Alkali and alkaline earth oxides are known to act as depolymerizing agents on the silicate tetrahedral network structure. This action results from the chemical disruption of the strong Si-O-Si linkages and formation of much weaker and less directional $Si\text{-}O^{-}\text{--}M^{+}$ and $Si\text{-}O^{-}\text{--}M^{2+}$ interactions (Brawer and White, 1975; Hess, 1977; Murdoch et al., 1985; Dupree et al., 1986; Schneider et al., 1987). The degree of disruption of the tetrahedral framework is strongly evident by its effect on the viscosity and thermodynamic properties of melts in these systems (Bockris and Lowe, 1954; Charles, 1967; Bottinga and Weill, 1972; Mysen et al., 1980; Urbain et al., 1982; Hochella and Brown, 1984; Richet, 1984; Stebbins et al., 1984; Richet and Bottinga, 1985).

In describing the structure of "depolymerized" aluminosilicate networks, it is convenient to distinguish between two different chemical environments of the oxygen atoms. Oxygen atoms that are contained within the strong T-O-T (T = Si or Al) linkages are typically referred to as *bridging* oxygens or *BOs* while those directly bonded to only one silicon atom are called *nonbridging* oxygens or *NBOs*. It is also useful to distinguish silicate tetrahedral units in terms of the number of NBOs they contain. In this description, the increasing depolymerization of the silicate framework is expressed by the successive appearance of tetrahedral silicate units with 1, 2, 3, and 4 NBOs. These tetrahedral units are often labeled as Q^n species, where n ($0 \leq n \leq 4$) indicates the number of BOs in that unit (Engelhardt et al., 1975). In amorphous SiO_2, all of the oxygen atoms are bridging and hence each silicon tetrahedral unit is a Q^4 species. In alkali and alkaline earth aluminosilicates, the glass and melt structures exhibit a distribution of Q^n species, where the abundances of lower n value species proportionally increases with increasing alkali or alkaline earth oxide concentrations. The presence and compositional dependence of these different structural species has been extensively documented using Raman scattering (Brawer and White, 1975; Sharma et al., 1978; Mysen et al., 1980, 1982; Virgo et al., 1980; Furukawa et al., 1981; Matson et al., 1983; McMillan, 1984b; Mysen, 1988, 1990) and NMR spectroscopy (Murdoch et al., 1985; Dupree et al., 1986; Schneider et al.,

1987; Kirkpatrick, 1988; Stebbins, 1988; Stebbins et al., 1992) (see also the chapter in this volume by McMillan and Wolf).

Binary alkali silicates. Spectroscopic measurements on glasses quenched from high-pressure melts have been used to investigate the effect of pressure on the equilibrium tetrahedral species distributions in several high silica binary alkali silicates (Dickinson and Scarfe, 1985; Stebbins and McMillan, 1989; Xue et al., 1989, 1991; Dickinson et al., 1990). These studies have generally concluded that increasing pressure results in a greater distribution of Q species in these melts. The observed changes in the tetrahedral species distribution have been discussed in terms of pressure shifts in the equilibrium for disproportionation reactions of the type

$$2\,Q^3 \leftrightarrow Q^2 + Q^4 \quad (1)$$

$$2\,Q^2 \leftrightarrow Q^3 + Q^1 \quad (2)$$

Xue et al. (1989, 1991) used ^{29}Si MAS NMR, Raman and infrared spectroscopies in an attempt to quantify the pressure dependence of the species distributions in potassium tetrasilicate ($K_2Si_4O_9$) and sodium disilicate ($Na_2Si_2O_5$) and tetrasilicate ($Na_2Si_4O_9$) composition glasses that were quenched from melts at pressures up to 12 GPa. Below about 4 to 5 GPa the quenched glasses displayed only minor changes in their vibrational and NMR spectra. However, at higher pressures, significant changes were observed in the NMR, Raman and infrared reflectance spectra of all of the quenched glasses (Fig. 14). By modeling the ^{29}Si MAS NMR spectra, Xue et al were able to estimate the pressure-induced changes in the tetrahedral speciation abundances in these glasses. In general, the abundances of the Q^3 species decreased and the Q^2 and Q^4 species increased with increasing pressure. For example, in sodium disilicate melts, essentially no resolvable change in the species distribution was found in glasses quenched from 5 GPa compared to that of a normal ambient sample. However, for the same composition glass quenched from 8 GPa, the relative abundance of Q^3 species decreased from about an ambient value of 84% to a value of 72%, while the Q^4 and Q^2 species abundances increased from 8% to 16% and from ~0 to 3%, respectively.

It is interesting that the changes inferred in the tetrahedral species distribution of alkali silicate glasses quenched from high-pressure melts are qualitatively similar to those observed to occur with increasing temperature at ambient pressure (Seifert et al., 1981; Stebbins, 1987; Liu et al., 1988; Stebbins, 1988; Mysen, 1990). It is generally assumed that the structure of a glass represents the structure of the liquid at the glass transition temperature, T_g (Gibbs and DiMarzio, 1958) (see also chapters in this volume by Richet and Bottinga, and Dingwell). Thus, it might be expected that if T_g increases with pressure in these systems, then the inferred pressure-dependent structural changes might instead result from a temperature effect. It is known that the viscosity of high-silica alkali silicates decreases with increasing pressure. Thus, the glass transition temperature in these high silica systems will also likely decrease with increasing pressure. This conclusion of the relation between the pressure dependences of viscosity and T_g is supported by low pressure (< 0.7 GPa) T_g measurements on silicate melts (Rosenhauer et al., 1979). On the basis of these arguments, Xue et al. (1991) concluded that their observed changes in the tetrahedral speciation distribution would likely underestimate the true pressure effects.

Dickinson et al. (1990) have suggested that the increase in the distribution of tetrahedral species in alkali silicate melts with pressure could significantly contribute to the observed decrease in viscosity of these systems with increasing pressure. Their argument is based on the Adam-Gibbs (1965) configurational entropy theory of

relaxation processes and the expectation that an increase in the speciation distribution would result in an increase in the configurational entropy and a decrease in size of polymeric flow units (see chapter by Richet and Bottinga). Dickinson et al. (1990) further speculated that the increase in the Q^3 disproportionation with pressure could be the primary compression mechanism of alkali silicate melts at low pressures.

Much more significant than the observation of the effect of pressure on the tetrahedral speciation distribution was Xue et al.'s (1989) report of spectral evidence for the existence of $^{[6]}Si$ species (~ 1.5% abundance) in a sodium disilicate glass quenched from 8 GPa and 1500 °C. The ^{29}Si MAS NMR data presented by these authors was the first clear evidence for the existence of $^{[6]}Si$ species in a silicate or aluminosilicate melt; although, $^{[6]}Si$ species were previously known to occur in phosphosilicate glasses prepared at ambient pressure (Dupree et al., 1987, 1988).

Stebbins and McMillan (1989) reported evidence for the existence of both five- and six-coordinated silicon species (0.4% and 0.2% abundances, respectively) in a potassium disilicate glass quenched from 1.9 GPa and 1200°C. This was the first report for the existence of a $^{[5]}Si$ species in a silicate, a species postulated years before by Angell et al. (1982) to play a key role in the viscous flow mechanism of silicate liquids. The presence of very small amounts of $^{[5]}Si$ species even in ambient pressure alkali silicate melts was later documented by Stebbins (1991) for potassium tetrasilicate. It was found that the abundance of $^{[5]}Si$ increased with increasing fictive temperature, ranging from 0.06% in slow quenched melts to 0.10% in fast quenched samples. Although the observation of five-coordinated silicon in a silicate is novel, this species does occur, typically as a distorted trigonal bipyramidal structure, in organic molecules (Marsmann, 1981; Coleman, 1983; Tandura et al., 1986) and has also been matrix stabilized in a SiF_5^- complex (Ault, 1979).

Although the abundances of $^{[5]}Si$ and $^{[6]}Si$ species in silicate glasses reported in these early studies were extremely low, the study by Xue et al. (1991) demonstrated that much higher fractions of five- and six-coordinated silicon could be retained in alkali silicate glasses quenched from higher pressures (see Fig. 16). Maximum abundances of about 8.5% $^{[5]}Si$ and 6.3% $^{[6]}Si$ were recorded in a sodium tetrasilicate sample quenched from a melt at 12 GPa. Xue et al. also found a marked compositional dependence to the fractional abundances of the $^{[4]}Si$, $^{[5]}Si$, and $^{[6]}Si$ species at all pressures (see also Stebbins and McMillan, 1993 and chapter in this volume by Stebbins).

One of the most significant trends supported by Xue et al.'s data is that the proportion of high-coordinated species ($^{[5]}Si + {}^{[6]}Si$) is greatest near the tetrasilicate composition and decreases strongly both toward SiO_2 and toward higher alkali concentrations (Fig. 17). As these authors have discussed, this observation is consistent with observations made in the alkali germanate system at ambient pressure. Spectroscopic analyses suggest that alkali germanate glasses formed at ambient pressure contain both four- and six-coordinated germanium species (Ueno et al., 1983). The abundance of high-coordinated germanium is strongly sensitive to the alkali concentration and is maximized near the tetrasilicate composition (Ueno et al., 1983). Studies on the alkali germanate system further suggest that the high-coordinated germanium species are formed through a consumption of the non-bridging oxygens rather than by an attack from bridging oxygens. A similar explanation has been made to rationalize the compositional dependence of boron coordination species in alkali borate glasses at atmospheric pressure (Bray and O'Keefe, 1963; Jellison et al., 1978) and is also consistent with trends observed for the composition dependence of silicon speciation in alkali silicophosphate glasses at 1 bar (Dupree et al., 1987).

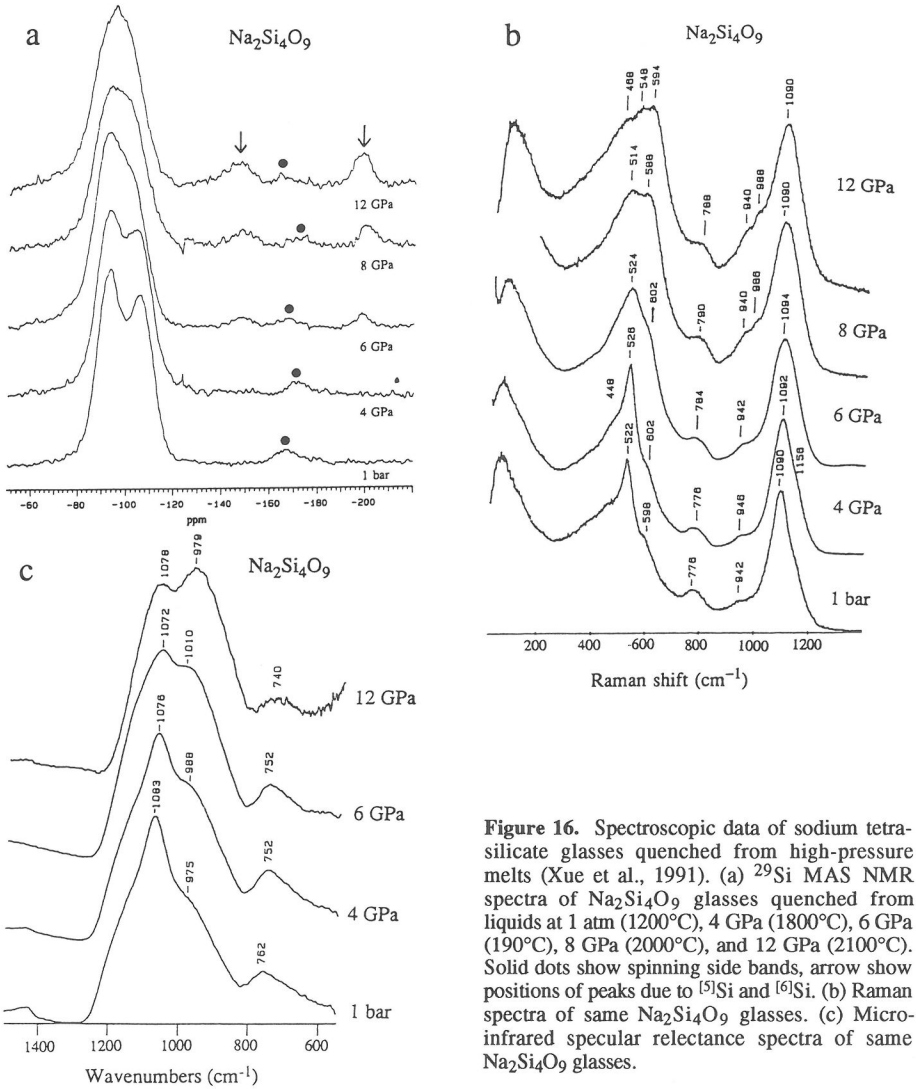

Figure 16. Spectroscopic data of sodium tetrasilicate glasses quenched from high-pressure melts (Xue et al., 1991). (a) ^{29}Si MAS NMR spectra of $Na_2Si_4O_9$ glasses quenched from liquids at 1 atm (1200°C), 4 GPa (1800°C), 6 GPa (190°C), 8 GPa (2000°C), and 12 GPa (2100°C). Solid dots show spinning side bands, arrow show positions of peaks due to $^{[5]}Si$ and $^{[6]}Si$. (b) Raman spectra of same $Na_2Si_4O_9$ glasses. (c) Micro-infrared specular relectance spectra of same $Na_2Si_4O_9$ glasses.

Xue et al. (1991) and Wolf et al. (1990) have suggested that the formation of high-coordinated silicon species in alkali silicate melts at low pressures also occurs through a consumption of non-bridging oxygens via mechanisms of the type

$$Q^3 + Q^4 \rightarrow {}^{[5]}Si + Q^{4*} \quad (3)$$

or

$$2Q^3 + Q^4 \rightarrow {}^{[6]}Si + 2Q^{4*}. \quad (4)$$

where Q^{4*} is a SiO_4 species that has three $^{[4]}Si$ neighbors and one $^{[5]}Si$ or $^{[6]}Si$ neighbor (see Fig. 18). The greater reactivity of the non bridging oxygens to formation of high-coordinated Si species over that of the bridging oxygens is also consistent with the known crystalline transformation of $K_2Si_4O_9$ near 2.5 GPa to a wadeite-structured phase (Kinomura et al., 1975; Kanzaki et al., 1989). In this phase, 1/4 of the silicon atoms occur in octahedral sites and the remaining 3/4 occur in tetrahedral sites in a fully polymerized network with no non-bridging oxygens.

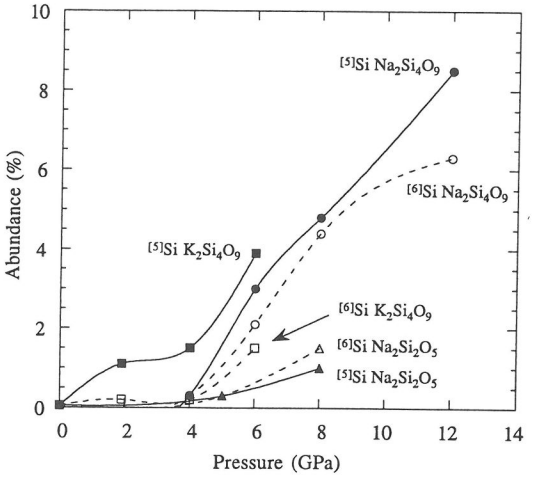

Figure 17. Abundances of [5]Si and [6]Si species for alkali silicate glasses quenched from high-pressure liquids estimated from ^{29}Si MAS NMR spectra. Data from (Xue et al., 1991) and (Stebbins and McMillan, 1989).

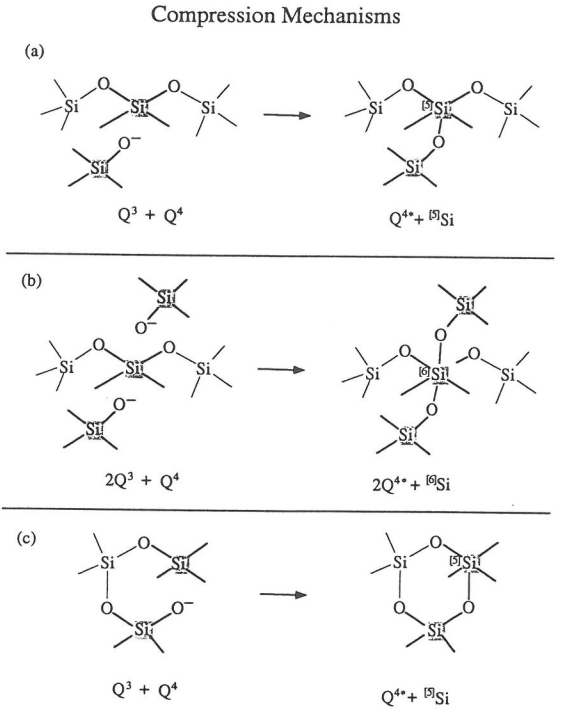

Figure 18. Compression mechanisms proposed by Wolf et al. (1990) and Xue et al. (1991) for the formation of high-coordinate Si species through the reaction non-bridging oxygen atoms. (a) Formation of [5]Si species. (b) Formation of [6]Si species. (c) Formation of small ring structures with high-coordinated Si.

Raman scattering, like NMR spectroscopy, has also proven to be useful for investigating the degree of polymerization in silicate networks. One important advantage of Raman scattering is that in situ studies can now be routinely made on extremely small samples contained at high pressures (and high temperatures) in the diamond anvil optical

cell. Unlike NMR however, the Raman intensity of any particular mode is not in itself quantitative. (The Raman intensity depends on the modulation amplitude of the sample polarization that accompanies the mode atomic displacements. Since these displacement patterns can, in general, change with pressure, temperature, or composition, the scattering cross section can also change.) Nevertheless, with sufficient cross referencing with other probes, Raman scattering provides a useful qualitative, and sometimes semiquantitative, description of pressure or temperature induced changes in the short and medium range structure of glasses and melts.

With increasing alkali or alkaline earth content, the increasing depolymerization of the silica tetrahedral network is characterized in the Raman spectrum by the successive appearance of strong, highly polarized modes at frequencies near 1100 cm^{-1}, 950 cm^{-1}, 900 cm^{-1}, and 850 cm^{-1} which have been assigned to highly localized symmetric Si-O stretching vibrations of Q^3, Q^2, Q^1 and Q^0 species, respectively (Brawer and White, 1975; Sharma et al., 1978; Mysen et al., 1980, 1982; Virgo et al., 1980; Furukawa et al., 1981; Matson et al., 1983; McMillan, 1984b; Mysen, 1988, 1990). Antisymmetric stretching vibrations of the fully polymerized Q^4 units also appear in the frequency region between 1000 and 1250 cm^{-1} but are considerably weaker than the symmetric stretching vibrations of the depolymerized units. At the tetrasilicate and disilicate compositions, there are on average 0.5 and 1.0 NBOs per SiO_4 tetrahedron, respectively. For alkali tetrasilicate glasses the Raman spectrum in the high frequency region consists of a strong asymmetric band near 1100 cm^{-1}, corresponding to vibrations of Q^3 units, and a weaker band near 950 cm^{-1}, more evident for the higher field strength cations, corresponding to Q^2 vibrations (see Fig. 16b). For the disilicate glasses, both the Q^2 and Q^3 vibrational bands are considerably stronger, indicative of the greater depolymerization of the network.

The interpretation of the Raman spectra of alkali silicate glasses in the frequency range below 700 cm^{-1} is less clear. At ambient pressure, the Raman spectra of high silica alkali silicate glasses in this frequency range is characterized by two relatively sharp, polarized bands near 600 cm^{-1} and 520 cm^{-1} with weaker, diffuse scattering at lower frequencies. The diffuse scattering below 500 cm^{-1} is generally assigned to bending deformations associated with fully polymerized regions within the glass structure. Matson et al. (1983) have suggested that the 600 cm^{-1} band in alkali silicates has a similar origin to the 606 cm^{-1} defect band of vitreous silica and have assigned it to a symmetric oxygen breathing motion from three-membered siloxane rings vibrationally decoupled from the glass network. The weak dependence of the position of this band both on the nature of the alkali cation and on temperature is consistent with this interpretation. Furthermore, the retention of this band to higher alkali contents indicates that depolymerized tetrahedral species can be incorporated in tri-siloxane ring structures. The 520 cm^{-1} band has been assigned to delocalized symmetric bending deformations of structural units that contain both Q^3 and Q^4 species (Matson et al., 1983). This assignment is partly based on the observation that the intensities of the 520 cm^{-1} band and 1100 cm^{-1} are highly correlated with changes in alkali content (Verweij and Konijnendijk, 1976; Verweij, 1979; Mysen et al., 1980; Furukawa et al., 1981).

Wolf et al. (1990) and Durben (1993) used Raman scattering to investigate the in situ high-pressure behavior of binary alkali tetrasilicate and disilicate glasses under room temperature compression. The in situ Raman spectra of the tetrasilicate and disilicate glasses clearly reveal a reduction in intensities of both the 1100 cm^{-1} and 520 cm^{-1} bands with increasing pressure (see Figs. 19 and 20). For all of the tetrasilicate glasses studied, the 520 cm^{-1} band shows a marked reduction in intensity beginning at about 3 GPa. In

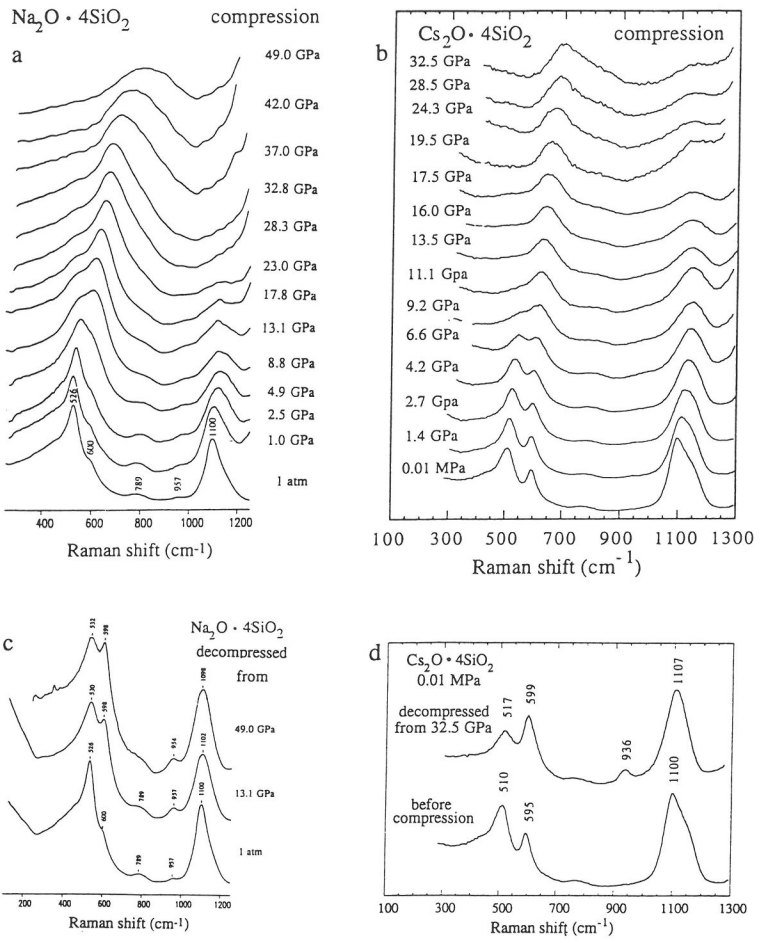

Figure 19. Pressure dependence of the Raman spectra of sodium and cesium tetrasilicate glasses (Wolf et al., 1990; Durben, 1993). (a) In: situ Raman spectrum of $Na_2Si_4O_9$ glass. (b) In situ Raman spectrum of $Cs_2Si_4O_9$ glass. (c) Comparison of the ambient Raman spectra of $Na_2Si_4O_9$ glasses pressure-cycled to 49 and 13 GPa with the spectrum of an unpressurized sample. (d) Comparison of the ambient Raman spectrum of $Cs_2Si_4O_9$ glass pressure-cycled to 32.5 GPa with the spectrum of an unpressurized sample.

sodium and potassium tetrasilicate glasses, the disappearance of the 520 cm^{-1} band near 16 and 23 GPa, respectively, closely coincides with the disappearance of the 1100 cm^{-1} band. However, for Cs tetrasilicate glass, the 520 cm^{-1} band disappears at about 11 GPa while the 1100 cm^{-1} band, although weak, can still be resolved to at least 32 GPa.

For all of the disilicate glasses studied, the 520 cm^{-1} band disappears at a much lower pressure (~ 5 GPa) than that found for the tetrasilicate glasses. Moreover, although the Q^2 and Q^3 bands near 950 cm^{-1} and 1100 cm^{-1} show a gradual reduction in their absolute intensities (not apparent in the scaled spectra shown in Figures 19 and 20) with increasing pressure, scattering in this frequency envelope persists to the highest pressures of the experiments. In this spectral region, the ratio of the relative band intensity, Q^2:Q^3,

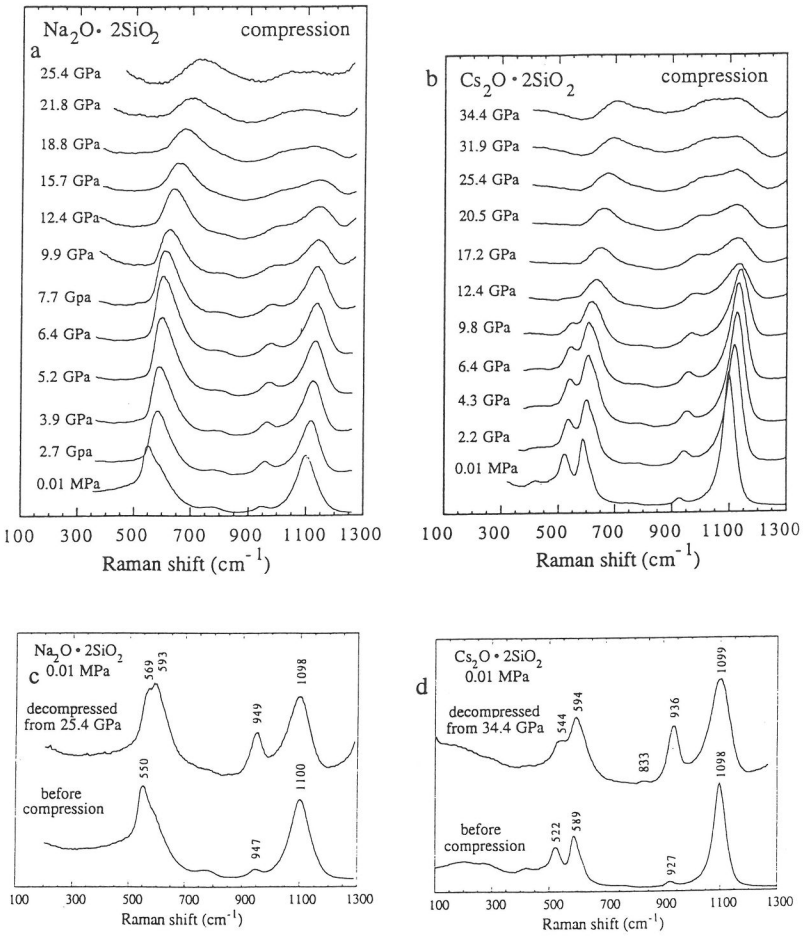

Figure 20. Pressure dependence of the Raman spectra of sodium and cesium disilicate glasses (Durben, 1993). (a) In situ Raman spectrum of $Na_2Si_2O_7$ glass. (b) In situ Raman spectrum of $Cs_2Si_2O_7$ glass. (c) Comparison of the ambient Raman spectrum of $Na_2Si_2O_7$ glasses pressure-cycled to 25.4 GPa with the spectrum of an unpressurized sample. (d) Comparison of the ambient Raman spectrum of $Cs_2Si_2O_7$ glass pressure-cycled to 34.4 GPa with the spectrum of an unpressurized sample.

appears to increase with pressure. In addition, there is also a buildup of relative scattering intensity between the 950 cm^{-1} and 1100 cm^{-1} bands resulting in a loss in resolution of these bands above 10 GPa.

Common to both the tetrasilicate and disilicate glasses, there is a gradual broadening and shift of the 600 cm^{-1} band to higher frequencies which begins near ambient pressure and continues to the highest pressures of these experiments. For the tetrasilicate glasses, the 600 cm^{-1} band is shifted to about 680 cm^{-1} near 28 GPa, independent of the nature of the alkali cation. Data at higher pressures from Wolf et al. (1990) on sodium tetrasilicate glass show that above 28 GPa the pressure dependence of the width and position of this band markedly increases. At 49 GPa, only a single band centered near 820 cm^{-1}, with a band width at half height of nearly 300 cm^{-1}, can be

resolved in the Raman spectrum of sodium tetrasilicate glass. For the disilicate glasses, the pressure shift of the 600 cm^{-1} band is greater and exhibits a more significant alkali effect. Near 20 GPa, the 600 cm^{-1} band is shifted to about 700 cm^{-1} for sodium disilicate glass but appears at about 680 cm^{-1} and 660 cm^{-1} for the potassium and cesium disilicate glasses, respectively, at the same pressure.

The pressure-induced changes in the in situ Raman spectra of the tetrasilicate and disilicate glasses can be interpreted in terms of two distinct silicon coordination change reactions which operate over different, but possibly overlapping, pressure intervals (Wolf et al., 1990; Durben, 1993). At low pressure, the loss in the 520 cm^{-1} band and the reduction in intensity of the 1100 cm^{-1} band in both the tetrasilicate and disilicate glasses are consistent with the mechanisms (described above in Eqns. 3 and 4) where high-coordinated Si species are formed through the reaction of non-bridging oxygen atoms associated with Q^3 species. At much higher pressures, as discussed more fully below, the marked increase in the frequency shift and width of the 600 cm^{-1} band are consistent with the formation of high-coordinated Si species through the reaction of bridging oxygen atoms with neighboring silicon atoms. The differing energetics of these two mechanisms can be rationalized by an inspection of the cation arrangement around the oxygen anion The higher pressure mechanism, involving bridging oxygens, requires the energetically costly step of forming $^{[3]}O$ species where oxygen is bonded to three silicon atoms. However, the lower pressure mechanism involves non-bridging oxygens and the formation of $^{[2]}O$ species where oxygen is bonded to only two silicons.

The detailed interpretation of the pressure-induced changes in the Raman spectra of the tetrasilicate glasses is more straightforward than that of the disilicate glasses. For the tetrasilicate glasses, the reaction of the non-bridging oxygen atoms associated with Q^3 species to form high-coordinated Si species shows a significant alkali effect. In $K_2Si_4O_9$ glass the consumption of non-bridging oxygen atoms to form high-coordinated Si species largely occurs in the pressure range between 3 and 16 GPa. For $Na_2Si_4O_9$ glass the pressure range extends to about 23 GPa and for $Cs_2Si_4O_9$ glass to at least 30 GPa. This alkali effect, inferred from the in situ Raman measurements, is consistent with that found in the NMR studies of alkali tetrasilicate glasses quenched both from high-pressure and ambient pressure melts (Xue et al., 1991; Stebbins and McMillan, 1993). In the NMR studies, the abundance of $^{[5]}Si$ retained in the quenched glasses is greatest for potassium silicate (Stebbins and McMillan, 1993).

For the sodium and potassium tetrasilicate glasses, the 520 cm^{-1} and 1100 cm^{-1} bands display a nearly simultaneous decrease in intensity with pressure, and disappear at about the same pressure for each glass. The concomitant intensity reduction of these bands generally supports their assignment to vibrations involving Q^3 units in the glass structure. However, for cesium tetrasilicate glass and, more significantly for all of the disilicate glasses studied, the 1100 cm^{-1} band persists to higher pressures than that at which the 520 cm^{-1} band disappears. These observations suggest that the 1100 cm^{-1} band results from a localized vibration of all the Q^3 species whereas the 520 cm^{-1} band results from only a subset of medium ranged structural units that contain Q^3 species. One possible interpretation for this observation is that the 520 cm^{-1} band arises from symmetric bending vibrations of Q^3-O-Q^4 linkages. Linkages involving two Q^3 species may, instead, contribute to the band envelope at higher frequencies, and would be more dominant in the disilicate and lower silica glasses. In this interpretation, regions that contain isolated non-bridging oxygens (i.e., structural regions related to the 520 cm^{-1} band) would generally be expected to be involved in the formation of high-coordinated Si species more easily (at lower pressures) than regions where non-bridging oxygen and

alkali metal atoms are clustered, especially for the larger alkali metal ions. The increased steric restrictions imposed by the cations in the clustered regions would substantially reduce the efficiency of the Si coordination transformation.

The increase in relative intensity of the 600 cm^{-1} band in the tetrasilicate and disilicate glasses with pressure is reminiscent of the behavior observed for vitreous silica and germania. In silica glass, the relative intensity of the 606 cm^{-1} "defect" mode increases most significantly at pressures above 15 GPa (Hemley et al., 1986). Similarly, the relative intensity of the related 520 cm^{-1} "defect" band in germania glass increases above 4 GPa (Durben and Wolf, 1991). We have speculated above that these spectral changes are related to the formation of three-ring structures through high-coordinated species in these fully polymerized networks. The in situ Raman data on the alkali silicate glasses is consistent with the interpretation that related structural changes may be taking place in these glasses as well, but beginning at lower pressures. Under the interpretation that vibrations associated with three-membered rings strongly contribute to the scattering intensity of the 600 cm^{-1} band in alkali silicate glasses, then the increase in intensity of this band at low pressures suggests a relatively easy pathway for the formation of three-membered rings in silicates containing non-bridging oxygens. Wolf et al. (1990) proposed a mechanism for the formation of small ring structures in alkali silicate glasses (Fig. 18). In this reaction a non-bridging oxygen associated with a tetrahedral Q^3 species binds to a Q^4 species in the same chain to form $^{[5]}$Si and $^{[2]}$O species and a three-membered ring. In vitreous silica, since all of the oxygen atoms are *bridging* the formation of a small ring requires either the formation of an $^{[3]}$O species and $^{[5]}$Si species, or Si-O bond breaking and rearrangement of the tetrahedral network. The available pathways for three-ring formation in fully polymerized systems would be expected to have a higher activation energy than that for depolymerized systems since, in the latter, neither high-coordinated $^{[3]}$O species are formed nor are any Si-O bonds broken.

Wolf et al. (1990) suggested that scattering associated with bending vibrations of Q^{4*}–$^{[5]}$Si and Q^{4*}–$^{[6]}$Si linkages may also contribute to the observed increase in the relative intensity and broadening of the 600 cm^{-1} band in alkali silicate glasses with increasing pressure. Raman spectra of the high-pressure $MgSiO_3$ garnet and $K_2Si_4O_9$ wadeite phases provide some support for this interpretation. Both of these phases, which contain corner-shared linkages between SiO_4 and SiO_6 polyhedra, have modes in their Raman spectra near 600 cm^{-1}.

As discussed above, the Raman data indicate that there are essentially no non-bridging oxygens in sodium and potassium tetrasilicate glass above 20 GPa. If we assume that only the non-bridging oxygens are incorporated in higher coordinated silicon species, this would imply an average Si coordination of 4.5, similar to that of the high-pressure wadeite phase of $K_2Si_4O_9$. Any further transformation of the remaining tetrahedral silicon atoms in the tetrasilicate glass to high-coordinated states requires the involvement of bridging oxygens and the formation of $^{[3]}$O species. Wolf et al. (1990) suggested that the marked increase in the frequency shift and broadening of the 600 cm^{-1} band in sodium tetrasilicate glass above about 28 GPa is an indication of the formation of high-coordinated Si species through reactions involving non-bridging oxygen atoms. It is difficult to establish the onset pressure of this higher pressure reaction mechanism since the formation of high-coordinated species via non-bridging oxygens also results in a shift and broadening of the 600 cm^{-1} band.

An interesting comparison can be made between the high-pressure Raman spectra of the alkali silicate glasses with that of silica glass. At about 27 GPa, the Raman spectra

of silica glass shows a broad weak feature centered at about 620 cm^{-1} with a spectral width of about 200 cm^{-1} at half height (see Fig. 5a). At about this same pressure, the in situ diffraction measurements of silica glass by Meade et al. (1992) suggest an average Si coordination of about 5. Hemley et al. (1986) report that at higher pressures the main Raman band of silica glass further broadens and becomes indistinct, perhaps reflecting the complete reaction of all remaining tetrahedral Si to high-coordinated species. In the tetrasilicate glasses the main Raman band is centered near 680 cm^{-1} GPa at 28 GPa. Above 28 GPa, this band markedly broadens and weakens, and displays a stronger shift to high frequencies without disappearing.

In all of the disilicate glasses, residual intensity persists in the 800 to 1200 cm^{-1} region to the highest pressures obtained in these experiments. Moreover, the spectral intensity in this region is considerably greater for the cesium disilicate glass than for sodium disilicate. These observations suggest that tetrahedral species can persist to much higher pressures in more depolymerized glasses than in the highly polymerized systems. Thus, whereas NBOs can easily react to form high-coordinated Si species in highly polymerized silicates, this reaction pathway becomes progressively less favored with increasing depolymerization. The shift in the energetics of this reaction likely arises from the increasing steric restrictions imposed by the increasing concentration of alkali metals.

Additional important inferences can be made from the in situ Raman data regarding the pressure dependence of the Q^n speciation distribution in alkali silicate glasses. For the disilicate glasses, the Raman data indicate that the relative intensity ratio of the Q^2:Q^3 bands increases strongly with increasing pressure in these systems. This observation, by itself, is consistent with earlier conclusions, based on ambient pressure studies of glasses quenched from high-pressure melts, that there is an increase in the Q^n speciation distribution in alkali silicate glasses with increasing pressure (Dickinson and Scarfe, 1985; Xue et al., 1989, 1991; Dickinson et al., 1990; Mysen, 1990). In the earlier studies the changes in the Q^n speciation distribution were discussed in terms of pressure shifts in tetrahedral speciation reactions. However, the in situ Raman measurements suggest that the pressure-induced formation of high-coordinated Si species may play a more significant role in altering the Q^n speciation distribution in alkali silicate liquids. In particular, the Raman data indicate that the non-bridging oxygens associated with the Q^3 species display a much greater reactivity to formation of high-coordinated Si species in comparison to those associated with the Q^2 species. These inferences are further supported by the in situ Raman data on the tetrasilicate glasses. In these systems there appears to be no significant increase in the relative intensity of the Q^2 band with increasing pressure, but only a gradual reduction in the intensity of the Q^3 band.

The greater reactivity of the Q^3 species compared to the that of Q^2 species (and presumably Q^1 and Q^0 species) is also consistent with the conjecture that increased cation clustering decreases the efficiency of the reaction of non-bridging oxygens to form high-coordinated species. The increase in abundance of high-coordinated Si species observed by Xue et al. (1991) in sodium tetrasilicate composition glasses quenched from high-pressure melts compared to that found in the sodium disilicate systems further supports this idea. It would thus be expected, that Si coordination changes would be much more difficult in the highly depolymerized metasilicate systems despite the increase in the concentration of non-bridging oxygens.

The Q^n speciation reactions inferred from studies on quenched glasses were based on the assumption that structural relaxations do not occur in the glass on decompression to ambient pressure. The in situ Raman measurements on the alkali tetrasilicate and

disilicate glasses clearly demonstrate that significant local structural changes do occur along the decompression route (Wolf et al., 1990; Durben, 1993). Examples of this behavior can be seen in comparing the high-pressure Raman spectra of the tetrasilicate and disilicate glasses with that of the initial starting materials and the pressure-cycled samples (Figs. 17 and 18). On decompression of sodium tetrasilicate glass, the 1100 cm^{-1} band is essentially absent until about 5 GPa. It is only below 1.3 GPa that this band, and the 520 cm^{-1} band, recover a significant fraction of their original intensities.

There are important differences in the Raman spectra of the normal uncompressed glasses in comparison with glasses that have been pressure-cycled (Figs. 19c,d and 20c,d). In particular, the pressure-cycled glasses display an increase in the relative intensities of the Q^2 band near 950 cm^{-1} and the "defect" band near 600 cm^{-1}. The enhanced intensity of the 600 cm^{-1} band indicates that a greater fraction of three-membered siloxane ring structures is retained in the pressure cycled samples. As discussed above, a similar enhancement of the intensity of the defect band of silica and germania glass is also observed under pressure cycling.

Wolf et al. (1990) have proposed that much of the increase in the Q^2 species abundance observed in decompressed alkali silicate samples could result from non-equilibrium reactions that take place along the decompression route. They propose that these highly depolymerized species are formed on the reversion of the high-coordinated silica species to tetrahedral coordination via reaction pathways that differ from those which occur under compression. An example of these differing reaction pathways is illustrated in Figures 21a,b. Under compression, the reaction of Q^4 and Q^3 species can

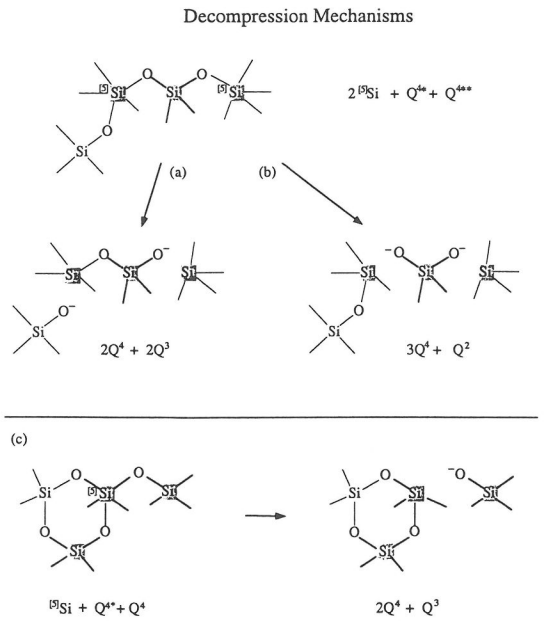

Figure 21. Decompression reversion mechanisms of high-coordinated Si species proposed by Wolf et al. (1990). (a) Formation of Q^4 and Q^3 species. (b) Formation of Q^2 and Q^4 species. (c) Formation of a three-membered siloxane ring.

result in the formation of Si tetrahedral species, labeled Q^{4**}, which are linked to two $^{[5]}$Si species. Under pressure release, the $^{[5]}$Si species can revert via two alternate pathways:

$$2\ ^{[5]}Si + Q^{4*} + Q^{4**} \rightarrow 2\ Q^4 + 2\ Q^3 \quad (5)$$

or

$$2\ ^{[5]}Si + Q^{4*} + Q^{4**} \rightarrow 3\ Q^4 + Q^2. \quad (6)$$

In one reaction the Q^{4**} species reverts to a Q^3 species whereas in the other reaction it reverts to a Q^2 species. In either mechanism, atomic diffusion is not required and the resultant distribution of tetrahedral species depends only on which particular Si–O bonds break under decompression. Alternate reaction pathways can also occur for the reversion of $^{[6]}$Si species.

Finally, it is important to point out that differences may occur in the decompression pathways of glasses that were thermally equilibrated at high pressures above T_g compared to that of glasses which are pressure-cycled at room temperature. Significant structural differences are evident in comparing the Raman spectra of room temperature pressure-cycled glasses with that of glasses at 1 bar that were quenched from high-pressure melts. Compare, for example, the 1 bar Raman spectrum of a sodium tetrasilicate glass sample obtained from a melt at 12 GPa (Xue et al., 1991) with those of the room temperature glass sample cycled to a peak pressure of 13 GPa (Figs. 14 and 17). This underscores the general belief that pressure-induced structural changes that occur in glasses below T_g are likely to occur at much lower pressures in samples that are simultaneously annealed at high temperatures. Furthermore, it may also be that high-pressure samples that are also annealed at high temperatures may be less susceptible to local structural relaxations on decompression to ambient pressure. These questions also indicate the importance of obtaining in situ spectroscopic measurements on silicate liquids under simultaneous high-pressure/high-temperature conditions.

Alkali aluminosilicate systems. Mysen et al. (1990) have used Raman spectroscopy to investigate pressure-induced structural changes in depolymerized alkali aluminosilicate melts. These studies were limited to a peak pressure of 3 GPa and were made on glass samples at 1 bar that were quenched from melts at high pressure. Small changes in the tetrahedral Q^n speciation distribution in these systems were inferred from the Raman spectra. These authors attempted to make a quantitative analysis of the speciation distribution by deconvoluting the Raman band envelope in the 800 cm^{-1} to 1200 cm^{-1} frequency region and calibrating the Raman band cross sections with available NMR data. Through this analysis, Mysen et al. obtained estimates for the equilibrium constant of the Q^3 disproportionation reaction (given in Eqn. 1) for a variety of depolymerized alkali aluminosilicate systems as a function of pressure. They concluded that the Q^3 disproportionation reaction shifts in the direction of increasing disproportionation both with increasing pressure and with increasing Al/(Al+Si) ratio. Although the general conclusion that disproportionation increases with pressure is consistent with Xue et al.'s (1991) interpretations, Mysen et al. find that for high silica aluminosilicates (Al/(Al+Si) = 0.05) the most significant pressure effects occur at low pressure (<1 GPa) whereas Xue et al. (1991) found no significant change in disproportionation below 5 GPa for alumina-free alkali silicate melts.

Yarger et al. (1995) have recently investigated the pressure-dependent structural properties of a slightly depolymerized alkali aluminosilicate melt intermediate along the albite-sodium tetrasilicate join (Al/(Al+Si) = 0.125 with an average of 0.25 NBOs per network cation). [The degree of depolymerization and silica content of this system are much closer to basaltic or andesitic magmas than either albite or sodium tetrasilicate.] In their study, glass samples quenched from melts up to 12 GPa were characterized by

vibrational spectroscopy and MAS NMR on ^{29}Si, ^{27}Al, and ^{23}Na nuclei. One very interesting result from this study was that, in contrast to the behavior observed for the depolymerized alkali silicates with the same silica content, no spectral evidence (< 1.0% detection limit) was found for the presence of high-coordinated Si species in these quenched samples to at least 12 GPa (Fig. 22a). Instead, a broad distribution of Al coordination species, including $^{[4]}Al$, $^{[5]}Al$, and $^{[6]}Al$, were inferred from the ^{27}Al MAS spectra of all the high-pressure samples (Fig. 22b). In the normal glass quenched from an ambient pressure melt, the ^{27}Al MAS spectrum shows a single resonance that indicates that essentially all of the aluminum atoms are in four-coordinated sites. With increasing pressure, the average Al coordination gradually increases with the appearance of peaks for five- and six-coordinated aluminum. The concentration of $^{[5]}Al$ reaches a maximum value of about 28% at 8 GPa, and then decreases at higher quench pressures. The concentration of $^{[6]}Al$ continues to increase with increasing pressure, reaching a value of 48% at 12 GPa. The average Al coordination at 12 GPa is about 5.1. No substantial changes are found in the ^{23}Na MAS NMR spectra with increasing pressure (see Fig. 22c).

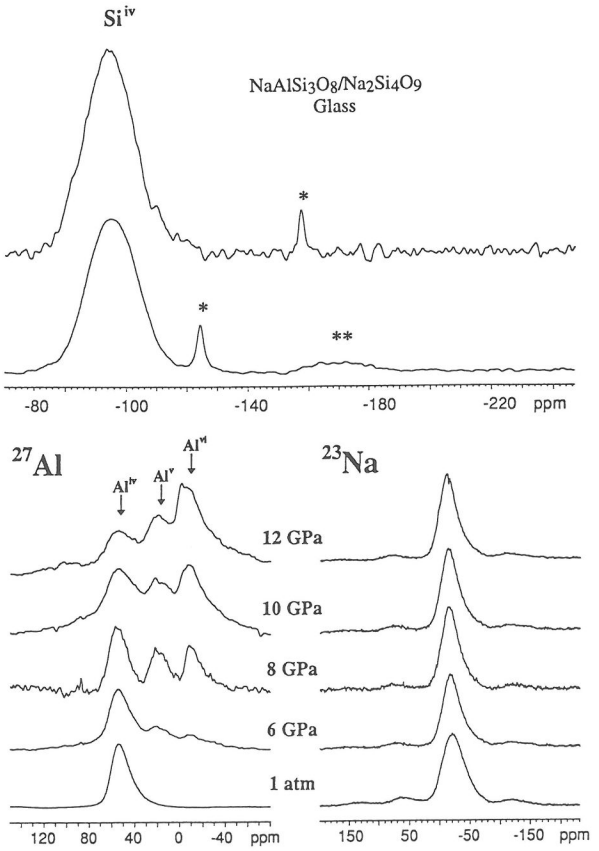

Figure 22. MAS NMR spectra of Ab_{50}/NTS_{50} glass quenched from high-pressure melts at temperatures between 1900 and 2200°C (Yarger et al., 1995). (a) ^{29}Si MAS NMR spectrum of Ab/NTS glass quenched from 10 GPa (top spectrum) and 0.1 MPa (bottom spectrum). Samples were enriched in ^{29}Si (92%). Spinning sidebands from the Si_3N_4 rotor (*) and the $^{[4]}Si$ resonance (**) are also indicated. (b) ^{27}Al MAS NMR spectrum of Ab/NTS glasses quenched from high pressures. Resonances for $^{[4]}Al$, $^{[5]}Al$, and $^{[6]}Al$ are indicated. (c) ^{23}Na MAS NMR spectrum of Ab/NTS glasses quenched from high pressures.

Raman spectra of the pressure-quenched Ab_{50}/NTS_{50} glass samples (Fig. 23a) show a strong increase in the intensity of the 600 cm^{-1} band and a marked weakening of the 1100 cm^{-1} band (Yarger et al., to be published). These effects become enhanced with increasing peak pressure. As in the alkali tetrasilicate glasses, there is also enhanced scattering intensity in the 950 cm^{-1} region and a buildup of intensity in the region between the 950 cm^{-1} Q^2 and 1100 cm^{-1} Q^3 bands with increasing pressure.

Yarger et al. (to be published) also measured the in situ Raman spectrum of the same albite-sodium tetrasilicate glass as a function of pressure (Fig. 23b). As in the high-silica alkali silicate glasses, the Raman spectrum of this glass shows a concerted loss of the 520 cm^{-1} and 1100 cm^{-1} bands with increasing pressure. Over this same pressure interval, the 600 cm^{-1} band broadens and displays a marked increase in both its absolute and relative intensities. At 12.5 GPa, the 520 cm^{-1} and 1100 cm^{-1} bands have nearly disappeared.

The results of Yarger et al. (1995) support the early suggestion by Waff (1975) that network aluminum atoms are much more susceptible to the formation of high-coordinated species under pressure than silicon. As discussed above, earlier studies on fully polymerized aluminosilicate systems (no NBOs) have found no definitive evidence for the retention of high-coordinated Al or Si species in decompressed samples. It is interesting, however, that in such a weakly depolymerized alkali aluminosilicate melt (0.25 NBOs per network cation), that such a large fraction of high-coordinated Al species can be retained in the decompressed sample. In the melt composition studied by Yarger et al., if all of the NBOs were bound up in the formation of high-coordinated Al species, then a maximum aluminum coordination of six could be obtained. Thus, the energetically costly reaction mechanism involving bridging oxygens is not required to account for the pressure-dependent coordination trends observed in this low alumina (Al/(Al+Si) = 0.125) system. If the coordination change does take place via reaction pathways involving NBOs, these results further suggest that the NBOs in this sodium aluminosilicate system reside on the silicon atoms with at least one aluminum atom present in the surrounding cosphere.

The in situ Raman scattering results of Yarger et al. suggest that at 12.5 GPa, nearly all of the NBOs have been consumed in the formation of high-coordinated Al or Si species. Furthermore, there is no evidence in the in situ Raman spectra that bridging oxygens become involved in the formation of high-coordinated species up to 12.5 GPa at room temperature. The in situ Raman spectra of the pressure-cycled sample shows that a large fraction of the high-coordinated Al species revert to tetrahedral coordination on decompression. Further ^{27}Al MAS NMR measurements by Yarger et al. (to be published) show that far fewer high-coordinated Al species are actually retained in decompressed samples that are pressure cycled without heating than in samples that were heated above T_g at the same pressure. For example, in a glass sample pressure-cycled at room temperature to 12 GPa, a quantitative analysis of the MAS NMR spectra shows that only 5% $^{[5]}Al$ and 6% $^{[6]}Al$ species are recovered compared to 17% and 48%, respectively, for a glass sample quenched obtained from a melt at the same peak pressure. In addition, the increased relative intensity of the 600 cm^{-1} band in the room temperature pressure-cycled sample (Fig. 23c) is consistent with the previous suggestion that three-membered tetrahedral siloxane-type rings are formed on the reversion of high-coordinated species under decompression (see Fig. 21c) (Wolf et al., 1990). Also similar to the alkali silicate glasses is the inference from the in situ Raman data that a significant fraction of Q^2 species are formed through a reversion of high-coordinated species along the decompression path.

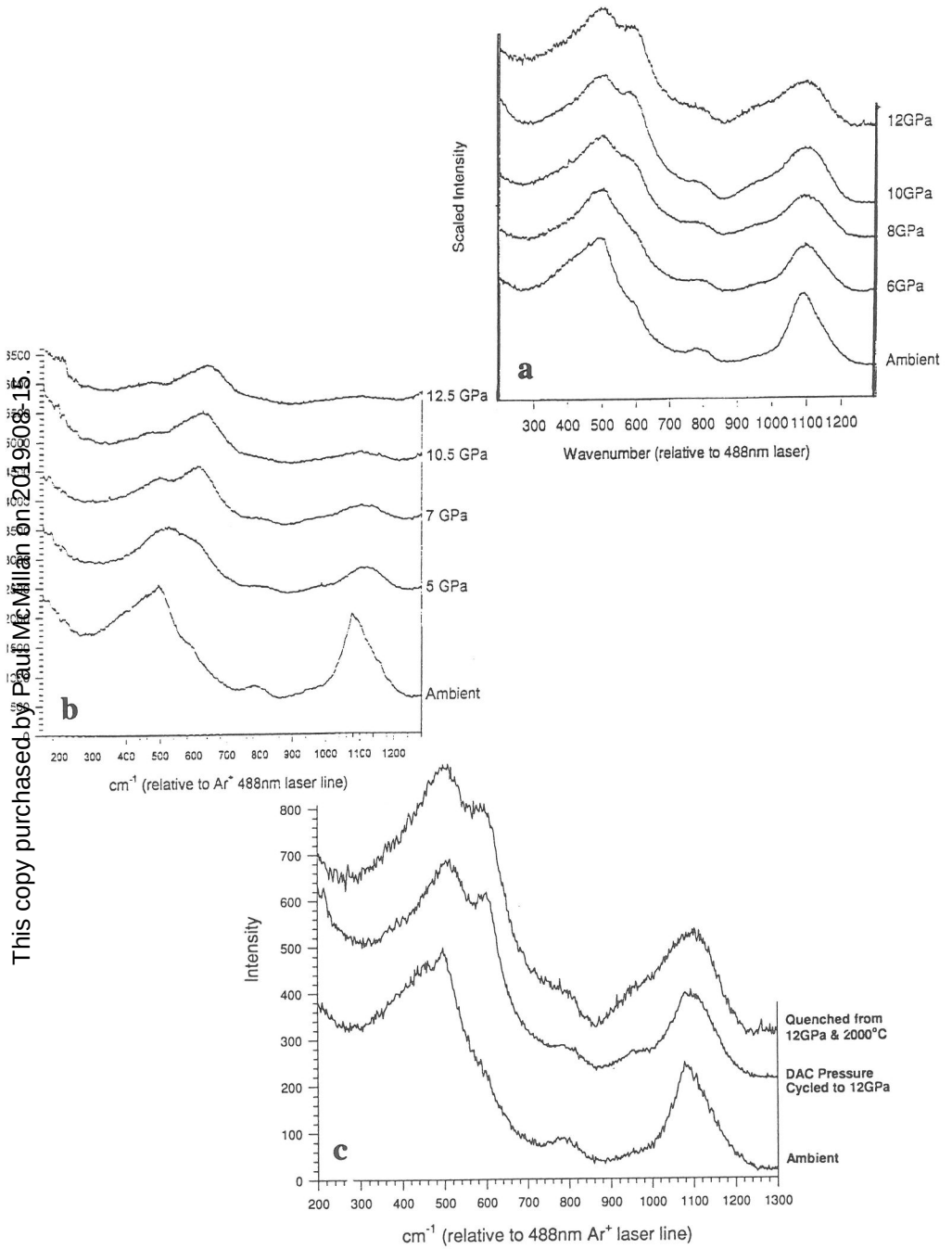

Figure 23. Raman spectra of high-pressure Ab_{50}/NTS_{50} glasses (Yarger et al., to be published). (a) Ambient Raman spectra of glasses quenched from high-pressure melts. (b) *In situ* Raman spectrum of glass obtained as a function of pressure. (c) Comparison of the Raman spectra of glasses quenched from 12 GPa and 2000°C, pressure-cycled at room temperature to 12 GPa, and quenched from a melt at 0.1 Mpa.

A final important observation can be made in comparing the 1 bar Raman spectra of the room temperature pressure-cycled sample with that of the high-pressure melt quench, both obtained from a peak pressure of about 12 GPa (Fig. 23c). The Raman spectrum of the high-pressure thermally annealed sample displays an enhanced scattering intensity in the region between the Q^2 and Q^3 high frequency stretching bands (i.e., 950 to 1100 cm^{-1}) compared to that of the room temperature pressure-cycled sample. Alkali silicate glass samples quenched from melts at high pressures also show an enhanced Raman scattering intensity in the spectral region between 950 cm^{-1} and 1100 cm^{-1} which is not observed to the same extent in glass samples that are pressure-cycled below T_g (Dickinson et al., 1990; Xue et al., 1991) (see Fig. 16b). Dickinson et al. (1990) have suggested that scattering in this same region may arise from vibrational modes related to high-coordinated Si (or Al) species. Further work on cross-calibrating the Raman spectrum with NMR data is necessary to more fully interpret these spectral changes.

Alkaline earth metasilicates. In alkaline earth silicates, the structural distinction between "network former" and "network modifier" cations is not as precise as in the alkali silicates (Navrotsky et al., 1982, 1985; McMillan, 1984a). Analysis of X-ray diffraction data on $MgSiO_3$ glass indicates that the Mg ion is surrounded by four oxygen atoms at a distance of 2.08 Å with two additional oxygens at 2.50 Å (Yin et al., 1983). Molecular dynamic simulations generally find that the Mg^{2+} ion coordination is ill defined in alkaline earth silicate melts at low pressures, and occurs in both tetrahedral and octahedral coordinations (Matsui and Kawamura, 1980, 1984; Matsui et al., 1982; Angell et al., 1987; Kubicki and Lasaga, 1991). In contrast Ca^{2+} and the larger, more basic alkaline earth cations primarily exist in octahedral sites. EXAFS and neutron scattering experiments on $CaSiO_3$ glass indicate that Ca has a well-defined octahedral coordination (Eckersley et al., 1988a,b).

Williams and Jeanloz (1988) investigated the pressure-induced structural changes in diopside ($CaMgSi_2O_6$) composition glass in situ to pressures above 30 GPa using infrared absorption spectroscopy. The high-pressure spectral changes observed for diopside glass closely parallel the behavior they found for silica glass (Fig. 24). In the diopside glass spectra above 20 GPa, there is a noticeable reduction in intensity of the high frequency tetrahedral stretching band near 1000 cm^{-1} relative to absorption in the 600-900 cm^{-1} region. By 37 GPa, only a broad, featureless absorption band is observed over the entire spectral range from 700 to 1200 cm^{-1}, very similar to that observed for silica glass at the same pressure. On decompression, the pressure-induced spectral changes of diopside glass are largely reversible, again reminiscent of the behavior of silica glass. Williams and Jeanloz concluded that the changes in the infrared absorption spectra of diopside glass are a result of a pressure-induced Si coordination change. This coordination transformation takes place over a large pressure range and, even at 37 GPa, there is probably a significant distribution of Si over the different coordination states.

The spectral interpretations of Williams and Jeanloz (1988) are generally consistent with molecular dynamic simulations on diopside ($CaMgSi_2O_6$) melts by Angell et al. (1987). In these simulations it was found that tetrahedral Si^{4+} and Mg^{2+} cations increase coordination over a wide range in pressure, and that at 20 GPa the average coordination state of both the Si^{4+} and Mg^{2+} cations is about five.

Kubicki et al. (1992) used both infrared and Raman vibrational spectroscopies to study in situ the pressure-induced structural changes in $MgSiO_3$ (enstatite), $CaMgSi_2O_6$, (diopside), and $CaSiO_3$ (wollastonite) composition glasses to pressures up to 45 GPa. The in situ infrared absorption and Raman spectra of these glasses are shown in Figure 25. All

of the glasses display a gradual decrease with pressure in their IR absorbance between 900 cm^{-1} and 1250 cm^{-1} with a simultaneous increase in absorbance in the 600 cm^{-1} to 900 cm^{-1} region. These spectral changes appear to occur at lower pressures in enstatite glass than for either the diopside or wollastonite glasses. At 24 GPa, the infrared absorption spectra of $MgSiO_3$ glass shows a relatively flat absorption between 700 and 1200 cm^{-1}, and is similar to that of silica glass at about 38 GPa (see Fig. 5b). At 35 GPa, the absorption of $CaSiO_3$ glass becomes very broad in this same spectral region, however a distinct band in the 1100 cm^{-1} region can still be resolved at this pressure.

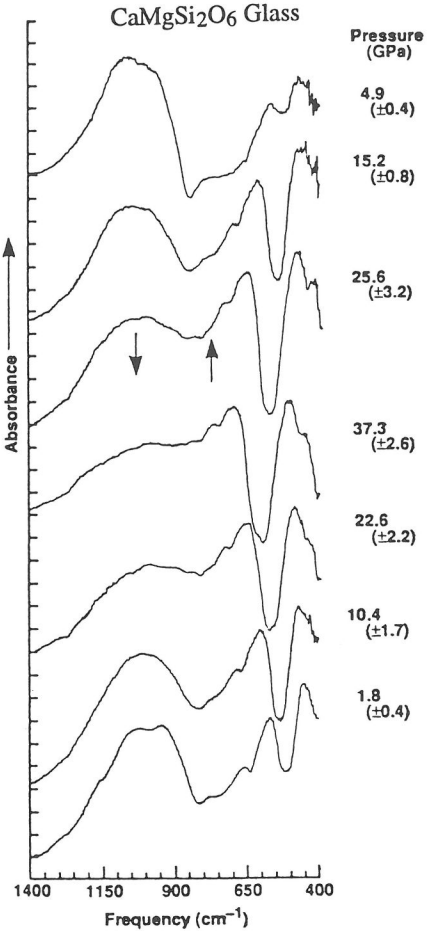

Figure 24. In situ infrared absorbance spectrum of diopside composition glass on increasing and decreasing pressure, top to bottom (Williams and Jeanloz, 1988). [Used by permission of the editor of *Science*, from Williams and Jeanloz (1988), Fig. 1, p. 903.]

At ambient pressure the Raman spectra of the $MgSiO_3$-$CaSiO_3$ glasses show two relatively strong bands centered near 630 cm^{-1} and 1000 cm^{-1}. The broad band envelope at high frequency can be deconvoluted into four bands at about 850 cm^{-1}, 900 cm^{-1}, 950 cm^{-1}, and 1100 cm^{-1} which, as in the alkali silicates correspond to symmetric Si-O stretching vibrations in Q^0, Q^1, Q^2 and Q^3 species, respectively. The band near 650 cm^{-1} probably corresponds to symmetric bending deformations of Si-O-Si linkages in the highly depolymerized network.

With increasing pressure there is a marked positive frequency shift and broadening of the 630 cm^{-1} Raman band. This band weakens and disappears in all three samples near 20 GPa. Simultaneous to these changes, there is a gradual reduction in intensity and loss of resolution in the high frequency band envelope between 800 and 1150 cm^{-1}. However, even at the highest pressures of the Raman measurements, 35 to 45 GPa, some residual scattering intensity persists in this spectral region.

The infrared absorbance data for the $CaSiO_3$-$MgSiO_3$ glasses are consistent with the interpretation that there is a gradual increase in the Si and Mg coordinations with increasing pressure. The interpretation of the Raman data is less clear. The reduction in intensity of the Raman bands in the 800 cm^{-1} to 1150 cm^{-1} region with increasing pressure, more marked for $MgSiO_3$ glass, suggests that NBOs are consumed in forming high-coordinated species. However, the decrease in intensity in this spectral region is not as dramatic as in the alkali tetrasilicate and disilicate glasses, and occurs over a broader pressure range. This observation is in line with the trend inferred from data on alkali

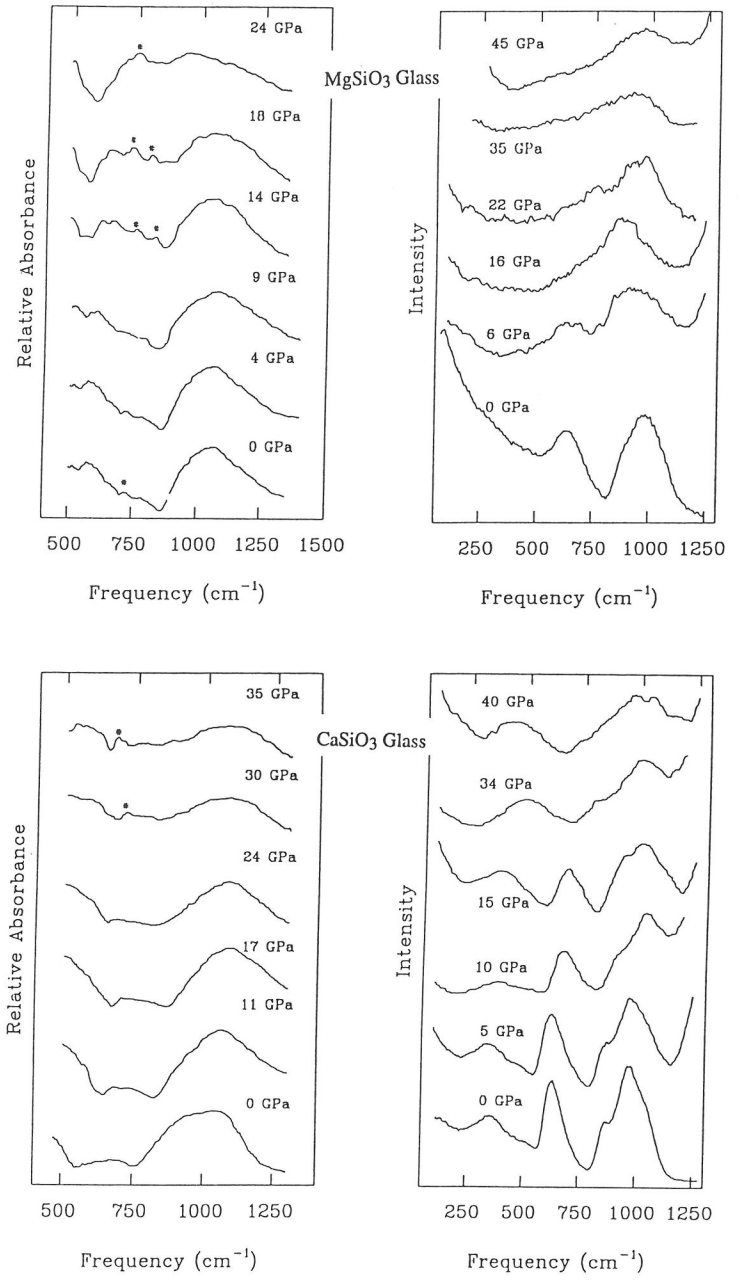

Figure 25. Pressure dependence of the vibrational spectra of alkaline earth metasilicate glasses (Kubicki et al., 1992). (a) Infrared absorbance spectrum of $MgSiO_3$ glass. (b) Infrared absorbance spectrum of $CaSiO_3$ glass. (c) Raman spectrum of $MgSiO_3$ glass. (d) Raman spectrum of $CaSiO_3$ glass.

silicate glasses that the activation energy for the formation of high-coordinated species through NBOs increases with increasing depolymerization of the tetrahedral network. The onset of the coordination transformations in the metasilicate glasses is difficult to establish from the data. However, there is a distinct reduction in intensity in both the 630 cm^{-1} and 1000 cm^{-1} Raman band envelopes of $MgSiO_3$ glass even in the 6 GPa spectrum and suggests that coordination transformations could begin in $MgSiO_3$ glass at pressures as low as 6 GPa. A similar degree of change in the Raman spectrum of $CaSiO_3$ glass does not occur until about 15 (± 3) GPa.

Kubicki et al. (1992) concluded that the residual Raman intensity observed in the 800 cm^{-1} to 1100 cm^{-1} region for the metasilicate glasses indicates that tetrahedral species with NBOs are retained in the glass structures to at least 45 GPa. However, this conclusion must be considered tentative since, as discussed above, high-pressure Raman studies on depolymerized alkali silicate and aluminosilicate glasses suggest that scattering in this spectral region may also arise from vibrational modes of structural units incorporating high-coordinated network species (Dickinson et al., 1990; Xue et al., 1991; Yarger et al., to be published). In addition, if ordered regions containing edge-shared SiO_6 octahedra are present in the glass structure at this pressure (formed via the reaction on bridging oxygens), then Raman active vibrational modes could occur in this frequency region. At 45 GPa, the A_{1g} Raman mode of stishovite occurs at about 900 cm^{-1}, and the much weaker E_g and B_{2g} modes occur near 680 cm^{-1} and 1120 cm^{-1}, respectively (Kingma et al., 1995).

The experimental high-pressure studies on $MgSiO_3$ glass can be compared to several molecular dynamic simulations on this same system. Kubicki and Lasaga (1991; see also Kubicki et al., 1992) carried out MD simulations on $MgSiO_3$ glass at 300 K using potentials derived from molecular orbital theory and electron-gas calculations. In these simulations, the transformation of Si^{4+} to octahedral coordination occurred over an extremely broad range in pressure, and at much higher (estimated) pressures than that suggested by the in situ spectroscopic measurements. In the simulation experiments, only about 8% of the Si^{4+} ions are in high-coordinated ($^{[5]}Si + {}^{[6]}Si$) sites at 30 GPa; whereas between 60 GPa and 90 GPa the abundance of high-coordinated Si species changes more significantly, from 27% to 65%. The Mg^{2+} coordination change occurs at much lower pressures. By 30 GPa, essentially all of the Mg^{2+} ions in the simulation runs occur in high-coordinated sites. A precise comparison with the simulation results of Kubicki et al. is complicated by the fact that the simulation pressures were not directly obtained but, instead, were estimated from the simulation densities and an extrapolation of the equation of state of $MgSiO_3$ glass (based on the ambient experimental compressibility). A perhaps more meaningful comparison is that the most pronounced change in the Si coordination in the simulations occurs over the same density range as that which occurs in the solid state on the transformation from tetrahedral to octahedral Si near 25 GPa (Ito and Matsui, 1977, 1978; Yagi et al., 1978). Qualitatively similar results are also found in the MD simulation experiments by Matsui and Kawamura (1980, 1984) and Matsui et al. (1982) on $MgSiO_3$ glass and by Wasserman et al. (1993) on $MgSiO_3$ melts. In these studies, empirical pair potential models were used with parameters derived from fitting to structural data at ambient pressure.

Alkaline earth orthosilicates. A characterization of the ultra-high pressure melt behavior in highly depolymerized silicate systems is crucial for an understanding of mantle melting relations in ultrabasic rock assemblages and the properties of deep-origin ultramafic magmas. However, very little data currently exists on the high-pressure structural changes in orthosilicate or other highly depolymerized composition glasses and

melts. At ambient pressure, the structure of orthosilicate glasses are thought to be very similar to that of their related crystalline phases. In crystalline orthosilicates, the silica tetrahedra are completely depolymerized and the structure is composed entirely of isolated Q^0 tetrahedral species.

Considerable insights into the compressional mechanisms and high-pressure behavior of orthosilicate liquids and glasses has resulted from studies on the high-pressure metastable behavior of crystalline orthosilicates. Fayalite (Fe_2SiO_4) and forsterite (Mg_2SiO_4) are two of the most extensively studied orthosilicate minerals. It is found that near 35 to 40 GPa, fayalite becomes X-ray amorphous under static, room-temperature compression (Richard and Richet, 1990; Williams et al., 1990). Near this same pressure there is significant collapse in the volume along the shock Hugoniot (Mashimo et al., 1980). In situ infrared absorption measurements of fayalite by Williams et al. (1990) indicate that, beginning near 20 to 25 GPa, there is a dramatic and reversible weakening of the high frequency tetrahedral stretching band and an emergence of a strong band between 600 and 800 cm^{-1} (Fig. 26). These authors have interpreted the spectral changes to indicate that silicon undergoes a continuous transition from fourfold toward sixfold coordination in metastable fayalite beginning near 20 GPa and extending to pressures above 46 GPa. Furthermore, they have speculated that the crystal-to-amorphous transition in this system is precipitated by a pressure-induced instability of the tetrahedral silicon coordination.

Shock and static compression experiments suggest that similar behavior occurs in crystalline forsterite, but at much higher pressures. Shock measurements on crystalline

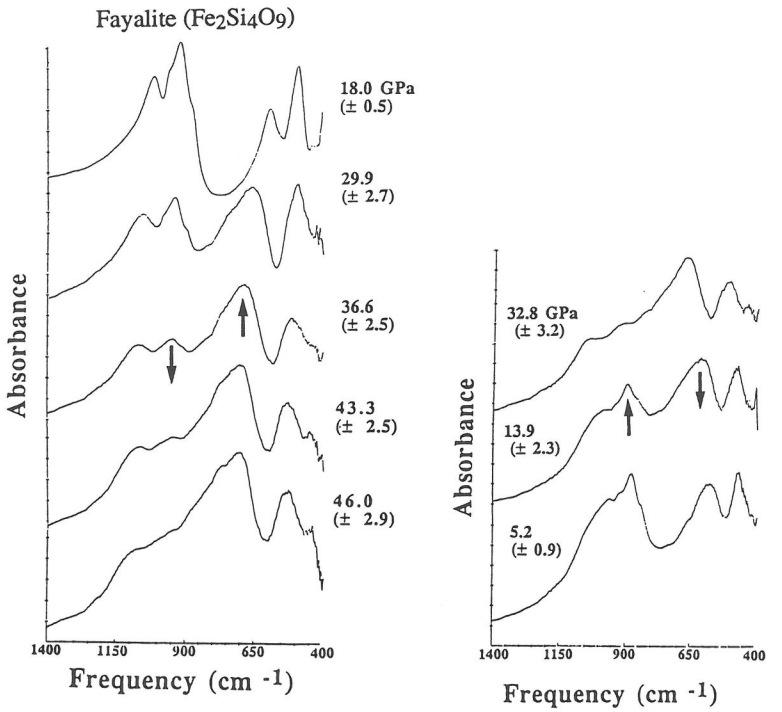

Figure 26. In situ infrared absorbance spectrum of crystalline fayalite (Fe_2SiO_4) (Williams et al., 1990). (a) Increasing pressure. (b) Decreasing pressure.

forsterite indicate a significant volume collapse of the structure occurs along the Hugoniot near 50 GPa (Jackson and Ahrens, 1979; Furnish and Brown, 1986; Brown et al., 1987) and that samples recovered above this pressure show diaplectic glass formation (Jeanloz et al., 1977; Jeanloz, 1980). Experiments (Guyot and Reynard, 1992) suggest that crystalline olivine, $(Mg,Fe)_2SiO_4$, transforms to an amorphous phase under static compression near 70 GPa.

There have been few high-pressure structural studies on orthosilicate liquids and glasses. Williams (1990) made one of the first attempts at investigating the ultra-high pressure structure of an orthosilicate composition melt. In his study, 1-bar infrared absorption spectra were measured of quenched Mg_2SiO_4 glasses which were synthesized by laser fusion at pressures near 50 GPa. The infrared spectrum of these glasses was consistent with a structure that was completely composed of tetrahedral silicon. Williams concluded that if high-coordinated Si species are formed at high pressures in orthosilicate liquids then they are completely unstable under decompression to ambient pressure.

Durben et al. (1993) used Raman spectroscopy to investigate the high-pressure structural properties of Mg_2SiO_4 glass at room temperature as a function of pressure. The in situ Raman spectra they obtained for forsterite glass to 50 GPa are shown in Figure 27. At ambient pressure, the Raman spectrum of the glass is characterized by a single broad asymmetric band centered near 870 cm^{-1} which is assigned to vibrations principally involving symmetric and antisymmetric stretching motions of isolated Q^0 tetrahedral species (Williams et al., 1989; Cooney and Sharma, 1990). The small band at somewhat lower frequencies (near 720 cm^{-1}) has been assigned to stretching vibrations of Si_2O_7 dimers in the structure (Williams et al., 1989; Cooney and Sharma, 1990).

Under initial compression, the frequency of the main tetrahedral stretching band of Mg_2SiO_4 glass increases at a similar rate to the pressure shift of the Q^0 tetrahedral stretching band of crystalline forsterite (Durben et al., 1993). The 720 cm^{-1} "dimer" band has a slightly greater positive frequency shift which is consistent with a tightening of the Si-O-Si angles within these units. The intensity of this band decreases with increasing pressure and cannot be followed to above about 20 GPa. However, it is difficult to distinguish whether this apparent loss in intensity is real or is due to a shift of the dimer band into the broadened manifold of the main Raman band. No other major changes in the spectrum are evident up to 20 GPa, and all frequency shifts are fully reversible over this pressure range. At pressures above 20 GPa there is a gradual but marked increase in the breadth of the main Raman band in forsterite glass, primarily arising from an increase in intensity on the low frequency side of this band between 700 cm^{-1} and 900 cm^{-1}. These changes continue gradually to at least 51 GPa where the main Raman band is centered near 950 cm^{-1}. On decompression, the increased scattering intensity in the 700 to 900 cm^{-1} region is lost and the Si_2O_7 dimer band near 720 cm^{-1} returns.

At ambient pressure, the Raman spectrum of the pressure-cycled glass sample shows some small but significant differences from that of the normal glass sample. For the pressure-cycled glass sample there is a well-defined shoulder near 950 cm^{-1}, which does not appear in the normal glass spectrum, and a small increase in the intensity of the Si_2O_7 dimer band near 720 cm^{-1}.

The pressure-induced changes in the Raman spectrum of Mg_2SiO_4 glass can be related to similar changes that occur in crystalline forsterite at high pressure (Fig. 27) (Durben et al., 1993). In forsterite, two new bands emerge in the Raman spectrum near

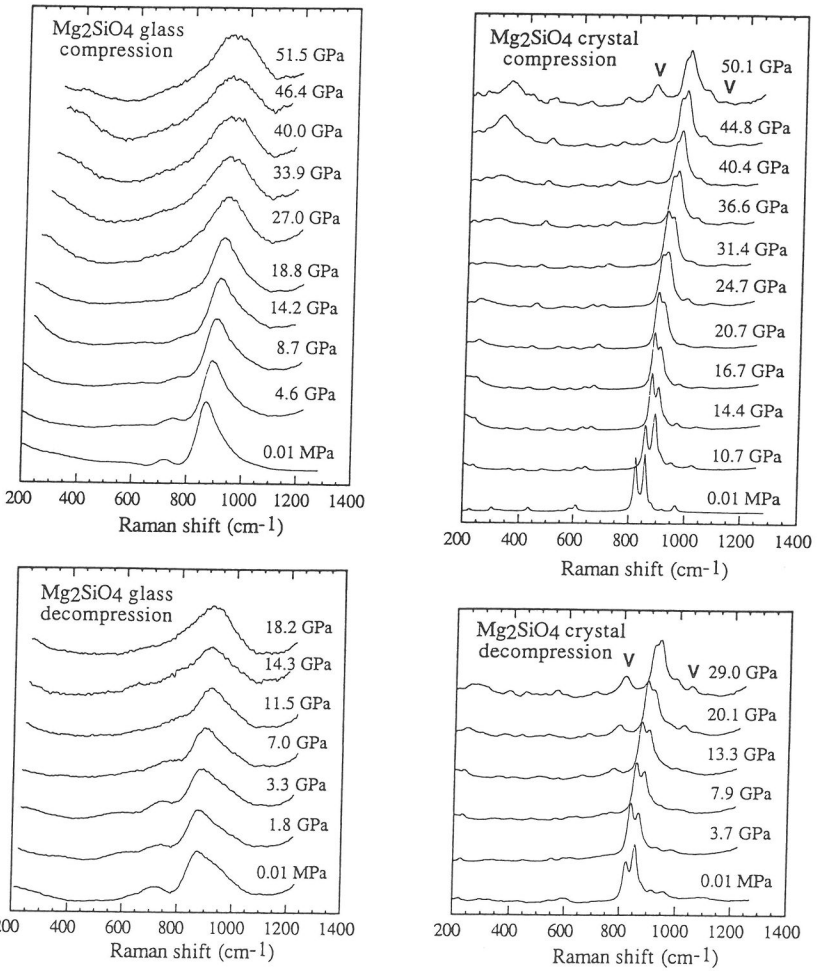

Figure 27. Pressure dependence of the Raman spectra of Mg_2SiO_4 crystal and glass (Durben et al. 1993). (a) Glass Raman spectrum on compression. (b) Crystal Raman spectrum on compression. (c) Glass Raman spectrum on decompression. (d) Crystal Raman spectrum on decompression.

30 GPa: a relatively strong band at 825 cm^{-1} and a weaker band at 1060 cm^{-1}. Both of these bands increase in intensity and shift to higher frequencies with increasing pressure. On decompression the new bands are retained in the Raman spectrum to about 8 GPa, below which they can no longer be resolved. From an extrapolation of the pressure data, estimated values of 750 cm^{-1} and 960 cm^{-1} are obtained for the positions of these bands at ambient pressure. The Raman spectrum of the pressure-cycled crystal sample is very similar to that of uncompressed crystalline forsterite except for a residual broadening of all of the Raman bands and an enhanced scattering intensity on the high frequency side of the main Raman bands.

Durben et al. (1993) have interpreted the spectral changes of both Mg_2SiO_4 glass and crystal to indicate that pressure-induced Si-O-Si linkages begin to form in both of

these materials above about 20 and 30 GPa, respectively. The extrapolated position of the new Raman band in crystalline forsterite at 750 cm^{-1} occurs in a frequency range typical of symmetric bending vibrations of Si-O-Si dimers in β-Mg_2SiO_4 and other pyrosilicate structures (McMillan and Akaogi, 1987). The assignment of the extrapolated 960 cm^{-1} band is more ambiguous but may be related to vibrations of terminal Q^1 species on silica dimers, or possibly Q^2 species on more polymerized silica units. In β-Mg_2SiO_4, a similar band, assigned to the terminal Q^1 vibrations, appears near 918 cm^{-1} (McMillan and Akaogi, 1987). The observation of excess spectral intensity in the Raman spectrum of pressure-cycled forsterite glass in the 750 cm^{-1} and 950 cm^{-1} region suggests that similar silica dimer, or more polymerized, silica species may be retained in the glass structure of the decompressed sample.

Whether these polymerized species involve tetrahedral or higher coordinated silicon can not be distinguished from the spectral data. Formation of $Si_2O_7^{-6}$ dimers would retain four-fold Si coordination. However, this could only occur in the olivine stoichiometry if a Si-O bond were broken leaving one oxygen atom (per dimer) nonbonded to silicon. Formation of $Si_2O_8^{-8}$ dimers would not require Si-O bond breakage and would result in the formation of either one or two five-coordinated silicon species (depending on whether the polyhedra are corner- or edge-shared). The assignment of the 750 cm^{-1} band to vibrations involving higher coordinated silicon polyhedral species is consistent with Williams et al.'s (1990) interpretation of a new band which appears in the same spectral region of the infrared absorption spectrum of crystalline fayalite (Fe_2SiO_4) above 20 GPa.

Durben et al. (1993) have proposed that the formation of dimer defects in metastable forsterite at lower pressures is a prelude to the crystal-amorphous transition. The high-pressure shock and static experiments on forsterite suggest that a more complete polymerization of the silica network, through an extensive formation of high-coordinated silicon species at higher pressures, may be required to produce a significant volume collapse and irreversible disordering of the structure. Because of the inferred similarity in the pressure-dependent structural properties of crystalline and amorphous Mg_2SiO_4, analogous high-pressure polymerization reactions would be expected to occur in the glass in a similar pressure regime.

ACKNOWLEDGMENTS

The authors are indebted to Jeffrey Yarger, Brent Poe, Kenneth Smith, David Rubie, Dan Durben, Mary VerHelst-Voorhees, Isabelle Daniel, and Jason Diefenbacher for allowing us to include in this review some of their most recent data which is not yet in press. This most recent and highly seminal work has greatly increased our general understanding of pressure-effects on aluminosilicate melt structure and properties and has added immensely to the scope of this review. We are also grateful to Jonathan Stebbins, Kathleen Kingma, Andrew Chizmeshya, Don Dingwell and two anonymous reviewers for constructive comments on the manuscript and to A. Chizmeshya for his help in preparing several of the figures. We owe a special thanks to Paul Ribbe, Series Editor, without whom there would be no Short Course series. Our research on silicate melt studies has been supported by grants from the National Science Foundation, Experimental Geochemistry program.

REFERENCES

Adam G, Gibbs JH (1965) On the temperature dependence of cooperative relaxation properties in glass-forming liquids. J Chem Phys 43:139-146

Agee CB, Walker D (1988) Static compression and olivine flotation in ultrabasic silicate liquid. J Geophys Res 93:3437-3449

Agee CB, Walker D (1993) Olivine flotation in mantle melts. Earth Planet Sci Lett 114:315-324

Anan'in AV, Breusov ON, Dremin AN, Pershin SV, Rogacheva AI, Tatsii VF (1974) Action of shock waves on silicon dioxide, II, quartz glass. Combust Explos Shock Waves 10:504-508

Angell CA, Cheeseman PA, Kadiyala R (1987) Diffusivity and thermodynamic properties of diopside and jadeite melts by computer simulation studies. Chem Geol 62:85-95

Angell CA, Cheeseman PA, Tamaddon S (1983) Water-like transport property anomalies in liquid silicates investigated at high T and P by computer simulation techniques. Bull Minéral 1 -2:87-9 9

Angell CA, Cheeseman PA, Tammadon S (1982) Pressure enhancement of ion mobilities in liquid silicates from computer simulation studies to 800 kbar. Science 218:885-887

Arndt J (1983) Densification of glasses of the system TiO_2-SiO_2 by very high static pressures. Phys Chem Glasses 24:104-110

Ault BS (1979) Infrared matrix isolation studies of $M+SiF_5^-$ ion pair and its chlorine-fluorine analogs. Inorg Chem 18:3339-3343

Barker LM, Hollenbach RE (1970) Shock-wave studies of PMMA, fused silica, and sapphire. J Appl Phys 41:4208-4226

Binggeli N, Chelikowsky JR (1992) Elastic instability in α-quartz under pressure. Phys Rev Lett 69:2220-2223

Binggeli N, Keskar NR, Chelikowsky JR (1994) Pressure-induced amorphization, elastic instability, and soft modes in α-quartz. Phys Rev B 49:3075-3081

Birch F, Dow RB (1936) Compressibility of rocks and glasses at high temperatures and pressures. Bulletin of the Geological Society of America 47:1235-1255

Bockris JOM, Lowe DC (1954) Viscosity and the structure of molten silicates. Proceedings of the Royal Society London A 226:423-435

Boslough MB, Rigden SM, Ahrens TJ (1986) Hugoniot equation of state of anorthite glass and lunar anorthosite. Geophys J R Astron Soc Geophys Res Letts 84:455-473

Bottinga Y (1985) On the isothermal compressibility of silicate liquids at high pressure. Earth Planet Sci Lett 74:350-360

Bottinga Y, Weill D (1970) Densities of liquid silicate systems calculated from partial molar volumes of oxide components. Am J Sci 269:169-182

Bottinga Y, Weill DF (1972) The viscosity of magmatic silicate liquids: a model for calculation. Am J Sci 272:438-475

Boyd FR, England JL (1963) Effect of pressure on the melting of diopside, $CaMgSi_2O_6$, and albite, $NaAlSi_3O_8$, in the range up to 50 kilobars. J Geophys Res 68:311-323

Brawer SA (1981) Defects and fluorine diffusion in sodium fluoroberyllate glass: a molecular dynamics study. J Chem Phys 75:3522-3541

Brawer SA, White WB (1975) Raman spectroscopic investigation of the structure of silicate glasses. I. The binary alkali silicates. J Chem Phys 63:2421-2432

Bray PJ, O'Keefe JG (1963) Nuclear magnetic resonance investigations of the structure of alkali borate glasses. Phys Chem Glasses 4:37-46

Bridgman PW (1939) The high pressure behavior of miscellaneous minerals. Am J Sci 237:7-18

Bridgman PW (1948) The compression of 39 substances to 100,000 kg/cm^2. Proc Am Acad Arts Sci 76:55-70

Bridgman PW, Simon J (1953) The effects of very high pressures on glass. J Appl Phys 24:405-413

Brown JM, Furnish MD, McQueen RG (1987) Thermodynamics for $(Mg,Fe)_2SiO_4$ from the Hugoniot. In: Manghnani MH, Syono Y (eds) High Pressure Research in Mineral Physics, p. 373-384, AGU, Washington D. C.

Bruckner R (1970) Properties and structure of vitreous silica. I. J Non-Cryst Solids 5:123-175

Burnham CW (1979) The importance of volatile constituents. In: Yoder HS (ed) The Evolution of Igneous Rocks. Princeton Univ Press, Princeton, p 439-482.

Chaplot SL, Sikka SK (1993) Molecular dynamics simulation of pressure-induced crystalline-to-amorphous transitions in some corner-linked polyhedral compounds. Phys Rev B47: 5710-5714

Charles RJ (1967) Activities in the Li_2O-, Na_2O- and K_2O-SiO_2 solutions. J Am Ceram Soc 50:631-640

Carroll MR, Holloway Jr (eds) (1994) Volatiles in Magmas. Rev Mineral Vol 30, 517 p, Mineralogical Soc America, Washington, DC

Chelikowsky JR, King HE, Jr., Troullier N, Martins JL, Glinnemann J (1990) Structural properties of α-quartz near the amorphous transition. Phys Rev Lett 65:3309-3312

Chhabildas LC, Grady DE (1984) Shock loading behavior of fused quartz. In: Asay JR, Graham RA, Straub GK (eds) Shock Waves in Condensed Matter—1983. p 155-178, Elsevier, New York

Cohen HM, Roy R (1965) Densification of glass at very high pressure. Phys Chem Glasses 6:149-161

Coleman B (1983) Applications of silicon-29 NMR spectroscopy. In: Lazlo P (ed) NMR of Newly Accessible Nuclei, 2:192-228, Academic Press, New York

Couty R, Sabatier G (1978) Contribution a l'étude de l'enthalpie du verre de silice densifie. J Chimie Phys 75:843-848

Daniel I, Gillet Ph, Poe BT, McMillan PF (1995) Raman spectroscopic study of structural changes in calcium aluminate ($CaAl_2O_4$) glass at high pressure and high temperature. Chem Geol, submitted

Davoli I, Paris E, Stizza S, Benfatto M, Fanfoni M, Gargano A, Bianconi A, Seifert F (1992) Structure of densified vitreous silica: silicon and oxygen XANES spectra and multiple scattering calculations. Phys Chem Min 19:171-175

Desa JAE, Wright AC, Sinclair RN (1988) A neutron diffraction investigation of the structure of vitreous germania. J Non-Cryst Solids 99:276-288

Devine RAB, Arndt J (1987) Si-O bond length modification in pressure-densified amorphous SiO_2. Phys Rev B 35:

Devine RAB, Dupree R, Farnan I, Capponi JJ (1987) Pressure-induced bond-angle variation in amorphous SiO_2. Phys Rev B 35:2560-2562

Dickinson JE, Scarfe CM (1985) Pressure induced structural changes in $K_2Si_4O_9$ silicate melt. EOS Trans Am Geophys Union 66:395

Dickinson JE, Scarfe CM, McMillan P (1990) Physical properties and structure of $K_2Si_4O_9$ melt quenched from pressures up to 2.4 GPa. J Geophys Res 95:15675-15681

Dunn T, Scarfe CM (1986) Variation of the chemical diffusivity of oxygen and viscosity of an andesite melt with pressure at constant temperature. Chem Geol 54:203-215

Dupree E, Pettifer RF (1984) Determination of the Si-O-Si- bond angle distribution in vitreous silica by magic angle spinning NMR. Nature 308:523-525

Dupree R, Holland D, Mortuza MG (1987) Six-coordinated silicon in glasses. Nature 328:416

Dupree R, Holland D, Mortuza MG, Collins JA, Lockyer MWG (1988) An MAS study of network-cation coordination in phosphosilicate glasses. J Non-Cryst Solids 106:403-407

Dupree R, Holland D, Williams DS (1986) The structure of binary alkali silicate glasses. J Non-Cryst Solids 81:185-200

Durben DJ (1993) Raman Spectroscopic Studies of the High Pressure Behavior of Network Forming Tetrahedral Oxide Glasses. Ph.D Dissertation, Arizona State University

Durben DJ, McMillan PF, Wolf GH (1993) Raman study of the high-pressure behavior of forsterite (Mg_2SiO_4) crystal and glass. Am Mineral 78:1143-1148

Durben DJ, Wolf GH (1991) Raman spectroscopic study of the pressure-induced coordination change in GeO_2 glass. Phys Rev B 43:2355-2363

Eckersley MC, Gaskell PH, Barnes AC, Chiex P (1988a) The environment of Ca ions in silicate glasses. J Non-Cryst Solids 106:132-136

Eckersley MC, Gaskell PH, Barnes AC, Chiex P (1988b) Structural ordering in a calcium silicate glass. Nature 335:525-527

Engelhardt G, Michel D (1987) High-Resolution Solid-State NMR of Silicates and Zeolites. John Wiley and Sons, New York

Engelhardt G, Zeigan D, Jancke H, Hoebbel D, Weiker W (1975) Zu abhangigkeit der struktur der silicatanionen in wassrigen natriumsilicatlosungen vom Na:Si verhaltnis. Z Anorg Allg Chem 418:17-28

Farber DL, Williams Q (1992) Pressure-induced coordination changes in alkali-germanate melts: an in-situ spectroscopic investigation. Science 256:1427-1430

Fujii T (1981) Ca-Sr chemical diffusion in melt of albite at high temperature and pressure. EOS Trans Am Geophys Union 62:429

Fujii T, Kushiro I (1977) Density, viscosity and compressibility of basaltic liquids at high pressures. Carnegie Inst Washington Yearb 76:419-424

Furnish MD, Brown JM (1986) Shock loading of single-crystal olivine in the 100-200 GPa range. J Geophys Res 91:4723-4729

Furukawa T, Fox KE, White WB (1981) Raman spectroscopic investigation of the structure of silicate glasses. III. Raman intensities and structural units in sodium silicate glasses. J Chem Phys 75:3226-3237

Galeener FL (1988) Current models for amorphous SiO_2. In: Devine RAB (ed) The Physics and Technology of Amorphous SiO_2, p 1-13, Plenum Press, New York

Gibbs JH, DiMarzio EA (1958) Nature of the glass transition and the glassy state. J Chem Phys 28:373-383

Grimsditch M (1984) Polymorphism in amorphous SiO_2. Phys Rev Lett 52:2379-2381
Grimsditch M (1986) Annealing and relaxation in the high-pressure phase of amorphous SiO_2. Phys Rev B 34:4372-4373
Grimsditch M, Bhadra R, Meng Y (1988) Brillouin scattering from amorphous materials at high pressures. Phys Rev B 38:7836-7838
Guyot F, Reynard B (1992) Pressure-induced structural modifications and amorphization in olivine compounds. Chem Geol 96:411-420
Halvorson K, Wolf GH (1990) Pressure-induced amorphization of cristobalite: structural and dynamical relationships of crystal-amorphous transitions and polymorphic glass transitions in silica polymorphs. EOS Trans Am Geophys Union 71:1671
Hazen RM, Finger LW (1981) Bulk moduli and high-pressure crystal structures of rutile-type compounds. J Phys Chem Solids 42:143-151
Hazen RM, Finger LW, Hemley RJ, Mao HK (1989) High-pressure crystal chemistry and amorphization of α-quartz. Solid State Comm 72:507-511
Hemley RJ, Jephcoat AP, Mao HK, Ming LC, Manghnani MH (1988) Pressure-induced amorphization of crystalline silica. Nature 334:52-54
Hemley RJ, Mao HK, Bell PM, Mysen BO (1986) Raman spectroscopy of SiO_2 glass at high pressure. Phys Rev Lett 57:747-750
Hemley RJ, Prewitt CT, Kingma KJ (1994) High-pressure behavior of silica. In: Heaney PJ, Prewitt CT, Gibbs GV (eds) Silica: Physical Behavior, Geochemistry, and Materials Applications. Rev Mineral 29:41-81
Hess PC (1977) Structure of silicate melts. Can Mineral 15:162-178
Hochella MF, Brown GE (1984) Structure and viscosity of rhyolitic composition melts. Geochim Cosmochim Acta 48:2631-2640
Hochella MF, Brown GE (1985) The structures of albite and jadeite composition glasses quenched from high pressure. Geochim Cosmochim Acta 49:1137-1142
Houser B, Alberding N, Ingalls R, Crozier ED (1988) High-pressure study of α-quartz GeO_2 using extended X-ray absorption fine structure. Phys Rev B 37:6513-6516
Hsich S-Y, Montrose CJ, Macedo PB (1971) The annealing dynamics of fused silica. J Non-Cryst Solids 6:37-48
Itie JP, Polian A, Calas G, Petiau J, Fontaine A, Tolentino H (1989) Pressure-induced coordination changes in crystalline and vitreous GeO_2. Phys Rev Lett 63:398-401
Itie JP, Polian A, Calas G, Petiau J, Fontaine A, Tolentino H (1990) Coordination changes in crystalline and vitreous GeO_2. High Press Res 5:717-719
Ito E, Matsui Y (1977) Silicate ilmenites and the post-spinel transformations. In: Manghnani MH, Akimoto S (eds) High-Pressure Research - Applications to Geophysics, p 193-209, Academic Press, New York
Ito E, Matsui Y (1978) Synthesis and crystal-chemical characterization of $MgSiO_3$ perovskite. Earth Planet Sci Lett 38:443-450
Jackson I, Ahrens TJ (1979) Shock-wave compression of single crystal forsterite. J Geophys Res 84:3039-3048
Jeanloz R (1980) Shock effect in olivine and implications for the Hugoniot data. J Geophys Res 85:3163-3176
Jeanloz R, Ahrens TJ, Lally JS, Nord Jr. GL, Christie JM, Heuer AM (1977) Shock produced olivine glass: first observation. Science 197:457-459
Jellison GE, Feller SA, Bray PJ (1978) A re-examination of the fraction of 4-coordinated boron atoms in lithium borate glass system. Phys Chem Glasses 19:52-53
Jorgensen JD (1978) Compression mechanisms in α-quartz structures—SiO_2 and GeO_2. J Appl Phys 49:5473-5478
Kanzaki M, Xue X, Stebbins F (1989) High pressure phase relations in $Na_2Si_2O_5$, $Na_2Si_4O_9$ and $K_2Si_4O_9$ up to 12 GPa. EOS Trans Am Geophys Union 70:1418
Kimmel RM, Uhlmann DR (1969) On the energy spectrum of densified silica glass. Phys Chem Glasses 10:12-17
Kingma KJ, Cohen RE, Hemley RJ, Mao HK (1995) Transformation of stishovite to a denser phase at lower mantle pressures. Nature 374:243-245
Kingma KJ, Hemley RJ, Mao H-K, Veblen DR (1993a) New high-pressure transformation in α-quartz. Phys Rev Lett 70:3927-3930
Kingma KJ, Meade C, Hemley RJ, Mao HK, Veblen DR (1993b) Microstructural observations of α-quartz amorphization. Science 259:666-669
Kinomura N, Kume S, Koizumi M (1975) Synthesis of $K_2SiSi_3O_9$ with silicon in 4- and 6-coordination. Mineral Mag 40:401-404
Kirkpatrick RJ (1988) MAS NMR spectroscopy of minerals and glasses. In: Spectroscopic Methods in Mineralogy and Geology. Hawthorne FC (ed) Rev Mineral 18: 341-404

Kondo KI, Ito S, Sawaoka A (1981) Nonlinear pressure dependence of the elastic moduli of fused quartz up to 3 GPa. J Appl Phys 52:2826-2831

Kress VC, Williams Q, Carmichael ISE (1988) Ultrasonic investigation of melts in the system Na_2O-Al_2O_3-SiO_2. Geochim Cosmochim Acta 52:283-293

Kubicki JD, Hemley RJ, Hofmeister AM (1992) Raman and infrared study of pressure-induced structural changes in $MgSiO_3$, $CaMgSi_2O_6$, and $CaSiO_3$ glasses. Am Mineral 77:258-269

Kubicki JD, Lasaga AC (1988) Molecular dynamics simulations of SiO_2 melt and glass: ionic and covalent models. Am Mineral 73:941-955

Kubicki JD, Lasaga AC (1990) Molecular dynamics and diffusion in silicate melts. In: Ganguly J (ed) Diffusion, atomic ordering, and mass transport: selected problems in geochemistry, p 1-50, Springer-Verlag, New York

Kubicki JD, Lasaga AC (1991) Molecular dynamics simulation of pressure and temperature effects on $MgSiO_3$ and Mg_2SiO_4 melts and glasses. Phys Chem Min 17:661-673

Kushiro I (1976) Changes in viscosity and structure of melts of $NaAlSi_2O_6$ composition at high pressure. J Geophys Res 81:6347-6350

Kushiro I (1977) Phase transformation in silicate melts under upper-mantle conditions. In: Manghnani MH, Akimoto S (eds) High-Pressure Research: Applications in Geophysics, p 25-37, Academic Press,

Kushiro I (1978a) Density and viscosity of hydrous calc-alkalic andesite magma at high pressures. Carnegie Inst Washington Year Book 77:675-678

Kushiro I (1978b) Viscosity and structural change of albite ($NaAlSi_3O_8$) melt at high pressure. Earth Planet Sci Lett 41:87-90

Kushiro I (1980) Viscosity, density, and structures of silicate melts at high pressures, and their petrological applications. In: Hargraves RB (ed) Physics of Magmatic Processes, p 92-120, Princeton University Press, Princeton

Kushiro I (1983) Effect of pressure on the diffusivity of network-forming cations in melts of jadeitic compositions. Geochimica Cosmochimica Acta 47:1415-1422

Kushiro I (1986) Viscosity of partial melts in the upper mantle. J Geophys Res 91:9343-9350

Kushiro I, Yoder HS, Mysen BO (1976) Viscosities of basalt and andesite melts at high pressures. J Geophys Res 81:66351-6356

Lange RL, Carmichael ISE (1990) Thermodynamic properties of silicate liquids with emphasis on density, thermal expansion and compresibility. In: Nicholls J, Russell JK (eds) Modern Methods of Igneous Petrology: Understanding Magmatic Processes. Rev Mod Mineral 24:25-64.

Leadbetter AJ, Wright AC (1972) Diffraction studies of glass structure II. The structure of vitreous germania. J Non-Cryst Solids 7:37-52

Lebedev AA (1921) Proc State Opt Inst Leningr 2:10

Liu SB, Stebbins JF, Schneider E, Pines A (1988) Diffusive motion in alkali silicate melts: an NMR study at high temperature. Geochim Cosmochim Acta 52:527-538

Lyzenga GA, Ahrens TJ (1983) Shock temperatures of SiO_2 and their geophysical implications. J Geophys Res 88:2431-2444

Mackenzie JD (1963a) High-pressure effects on oxide glasses: I, Densification in rigid state. J Am Ceram Soc 46:461-470

Mackenzie JD (1963b) High-pressure effects on oxide glasses: II, Subsequent heat treatment. J Am Ceram Soc 46:470-476

Marsh SP (1980) LASL Shock Hugoniot Data. University of California Press, Berkeley

Manghnani MH, Sato H, Rai CS (1986) Ultrasonic velocity and attenuation measurements on basalt melts to 1500 °C: role of composition and structure in the viscoelastic properties. J Geophys Res 91:9333-9342

Marsmann H (1981) Silicon-29 NMR. In: Diehl P, Fluck E, Kosfeld R (eds) NMR Basic Principles and Progress, 17, p 65-235, Springer-Verlag, Berlin

Mashimo T, Kondo KI, Sawaoka A, Syono Y, Takei H, Ahrens TJ (1980) Electrical conductivity measurement of fayalite under shock compression up to 56 GPa. J Geophys Res 85:1876-1881

Matson DW, Sharma SK, Philpotts JA (1983) The structure of high-silica alkali-silicate glasses: a Raman spectroscopic investigation . J Non-Cryst Solids 58:323-352

Matsui Y, Kawamura K (1980) Instantaneous structure of an $MgSiO_3$ melt simulated by molecular dynamics. Nature 285:648-649

Matsui Y, Kawamura K (1984) Computer simulation of structures of silicate melts and glasses. In: Sunagawa I (ed) Materials Science of the Earth's Interior, p 3-23, Terra Scientific, Tokyo

Matsui Y, Kawamura K, Syono Y (1982) Molecular dynamics calculations applied to silicate systems: Molten and vitreous $MgSiO_3$ and Mg_2SiO_4 under low and high pressures. In: Akimoto S, Manghnani MH (eds) High Pressure Research in Geophysics, p 511-524, Center for Academic Publications, Tokyo

McMillan P (1984a) A Raman spectroscopic study of glasses in the system CaO-MgO-SiO_2. Am Mineral 69:645-659

McMillan P (1984b) Structural studies of silicate glasses and melts--applications and limitations of Raman spectroscopy. Am Mineral 69:622-644
McMillan P, Piriou B, Couty R (1984) A Raman study of pressure-densified vitreous silica. J Chem Phys 81:4234-4236
McMillan PF, Akaogi M (1987) The Raman spectra of β-(modified spinel) and γ-(spinel) Mg_2SiO_4. Am Mineral 72:361-364
McMillan PF, Kirkpatrick RJ (1992) Al coordination in magnesium aluminosilicate glasses. Am Mineral 77:898-900
McMillan PR, Graham CM (1980) The Raman spectra of quenched albite and orthoclase glasses from 1 atm to 40 kb. In: Ford CE (ed) Progress in Experimental Petrology, p 112-115, Eaton Press,
McQueen RG (1992) The velocity of sound behind strong shocks in SiO_2. In: Schmidt SC (ed) Shock Compression of Condensed Matter - 1991, p 75-78, Elsevier, New York
Meade C, Hemley RJ, Mao HK (1992) High-pressure X-ray diffraction of SiO_2 glass. Phys Rev Lett 69:1387-1390
Meade C, Jeanloz R (1987) Frequency-dependent equation of state of fused silica to 10 GPa. Phys Rev B 35:236-244
Miller GH, Stolper EM, Ahrens TJ (1991a) The equation of state of a molten komatiite, 1, shock wave compression to 36 GPa. J Geophys Res 96:11831-11848
Miller GH, Stolper EM, Ahrens TJ (1991b) The equation of state of a molten komatiite, 2, application to komatiite petrogenesis and the Hadean mantle. J Geophys Res 96:11849-11864
Mozzi RL, Warren BE (1969) The structure of vitreous silica. J Appl Cryst 2:164-172
Murdoch JB, Stebbins JF, Carmichael ISE (1985) High-resolution ^{29}Si NMR study of silicate and aluminosilicate glasses: the effect of network-modifying cations. Am Mineral 70:332-343
Mysen B (1990) Effect of pressure, temperature and bulk composition on the structure and species distrubution in depolymerized alkali aluminosilicate melts and quenched melts . J Geophys Res 95:15733-15744
Mysen BO (1988) Structure and Properties of Silicate Melts. Elsevier, Amsterdam
Mysen BO, Virgo D, Scarfe CM (1980) Relations between the anionic structure and viscosity of silicate melts - a Raman spectroscopic study. Am Mineral 65:690-710
Mysen BO, Virgo D, Seifert FA (1982) The structure of silicate melts: implications for chemical and physical properties of natural magma. Rev Geophys Space Phys 20:353-383
Mysen BO, Virgo D, Seifert FA (1985) Relationships between properties and structure of aluminosilicate melts. Am Mineral 70:88-105
Navrotsky A (1994) Thermochemistry of crystalline and amorphous silica. In: Heaney PJ, Prewitt CT, Gibbs GV (eds) Silica: Physical Behavior, Geochemistry, and Materials Applications. Rev Mineral 29:309-329
Navrotsky A, Geisinger KL, McMillan P, Gibbs GV (1985) The tetrahedral framework in glasses and melts - Inferences from molecular orbital calculations and implications for structure, thermodynamics, and physical properties. Phys Chem Min 11:284-298
Navrotsky A, Peraudeau G, McMillan P, Coutures JP (1982) A thermochemical study of glasses and crystals along the joins silica-calcium aluminate and silica-sodium aluminate. Geochim Cosmochim Acta 46:2093-2047
Nisbet EG, Walker D (1982) Komatiites and the structure of the Archaean mantle. Earth Planet Sci Lett 60:105-113
Oestrike R, Yang W-H, Kirkpatrick RJ, Hervig RL, Navrotsky A, Montez B (1987) High-resolution ^{23}Na, ^{27}Al, and ^{29}Si NMR spectroscopy of framework aluminosilicate glasses. Geochim Cosmochim Acta 51:2199-2210
Ohtani E (1983) Melting temperature distribution and fractionation in the lower mantle. Phys Earth Planet Inter 33:12-25
Ohtani E (1984) Generation of komatiite magma and gravitational differentiation in the deep mantle. Earth Planet Sci Lett 67:261-272
Ohtani E, Kato T, Sawamoto H (1986) Melting of a model chondritic mantle to 20 GPa. Nature 322:352-353
Ohtani E, Sawamoto H (1987) Melting experiment on a model chondritic mantle composition at 25 GPa. Geophys Res Letts 14:733-736
Ohtani E, Taulle F, Angell CA (1985) Al^{3+} coordination changes in liquid aluminosilicates under pressure. Nature 314:78-81
Poe BT, Rubie DC, McMillan PF, Diefenbacher J (1994) Oxygen and silicon self diffusion in $Na_2Si_4O_9$ liquid to 15 GPa. EOS Trans Am Geophys Union 75:713
Poe BT, Rubie DC, Yarger J, Diefenbacher J, McMillan PF (1995) Silicon and oxygen self diffusion in $Na_2Si_4O_9$ liquids to 15 GPa and 2500. Nature (submitted)

Polian A, Grimsditch M (1993) Sound velocities and refractive index of densified a-SiO_2 to 25 GPa. Phys Rev B 47:13979-13982

Primak W (1975) The Compacted States of Vitreous Silica. Gordon and Breach, New York

Rau S, Baebler S, Kasper G, Weiss G, Hunklinger S (1995) Brillouin scattering of vitreous silica. Ann Physik 4:91-98

Richard G, Richet P (1990) Room-temperature amorphization of fayalite and high-pressure properties of Fe_2SiO_4 liquid. Geophys Res Letts 17:2093-2096

Richet P (1984) Viscosity and configurational entropy of silicate melts. Geochim Cosmochim Acta 48:471-483

Richet P, Bottinga Y (1985) Heat capacity of aluminum-free liquid silicates. Geochim Cosmochim Acta 49:471-486

Rigden SM, Ahrens TJ, Stolper EM (1984) Densities of liquid silicates at high pressures. Science 226:1071-1074

Rigden SM, Ahrens TJ, Stolper EM (1988) Shock compression of molten silicate: results for a model basaltic composition. J Geophys Res 93:367-382

Rigden SM, Ahrens TJ, Stolper EM (1989) High-pressure equations of state of molten anorthite and diopside. J Geophys Res 94:9508-9522

Ringwood AE (1978) Composition and Petrology of the Earth's Mantle. McGraw and Hill, New York

Rivers ML, Carmichael ISE (1987) Ultrasonic studies of silicate melts. J Geophys Res 92:9247-9270

Rosenhauer M, Scarfe CM, Virgo D (1979) Pressure dependence of the glass transition temperature in glasses of diopside, albite, and sodium trisilicate composition. Carnegie Inst Washington Yearb 78:556-559

Ross NL, Shu J-F, Hazen RM, Gasparik T (1990) High-pressure crystal chemistry of stishovite. Am Mineral 75:739-747

Rubie DC, Ross CR, Carroll MR, Elphick SC (1993) Oxygen self-diffusion in $Na_2Si_4O_9$ liquid up to 10 GPa and estimation of high-pressure melt viscosities. Am Mineral 78:574-582

Rustad JR, Yuen DA, Spera FJ (1991) Molecular dynamics of amorphous silica at very high pressures (135 GPa): Thermodynamics and extraction of structures through analysis of Voronoi polyhedra. Phys Rev B 44:2108-2121

Ryan MP (1987) Neutral buoyancy and the mechanical evolution of magmatic systems. In: Mysen, BO (ed) Magmatic Processes: Physiochemical Principles. Geochem Soc Special Pub 1:259-287

Sasakura T, Suito K, Fujisawa H (1989) Measurement of ultrasonic wave velocities in fused quartz under hydrostatic pressures up to 6.0 GPa. In: Novikov NV, Chistyakov YM (eds) Proceedings of the XIth AIRAPT Int. Conf. on High Pressure Science and Technology, 2, p 60-72, Naukova Dumka, Kiev

Sayers DE, Lytle FW, Stern EA (1972) Structure determination of amorphous Ge, GeO_2, and GeSe by Fourier analysis of extended X-ray absorption fine structure (EXAFS). J Non-Cryst Solids 8-10:401-407

Scarfe CM, Mysen BO, Virgo D (1979) Changes in viscosity and density of sodium disilicate, sodium metasilicate, and diopside composition with pressure. Carnegie Inst Washington Yearb 78:547-551

Scarfe CM, Mysen BO, Virgo D (1987) Pressure dependence of the viscosity of silicate melts. In: Mysen BO (ed) Magmatic Processes: Physicochemical Principles, p 59-68, The Geochemical Society, University Park, PA

Schmitt DR, Ahrens TJ (1989) Shock temperatures in silica glass: implications for modes of shock-induced deformation, phase transformation, and melting with pressure. J Geophys Res 94:5851-5872

Schneider E, Stebbins FJ, Pines A (1987) Speciation and local structure in alkali and alkaline earth silicate glasses: constraints from ^{29}Si NMR spectroscopy. J Non-Cryst Solids 89:371-383

Schroeder J, Bilodeau TG, Zhao X-S (1990) Brillouin and Raman scattering from glasses under high pressure. High Press Res 4:531-533

Schroeder J, Dunn KJ, Bundy F (1982) Brillouin scattering from amorphous silica under hydrostatic pressures up to 133 kbar. In: Blackman CK, Johannison T, Tegner L (eds) High Pressure in Research and Industry, Proceedings of the 8th AIRAPT Conference, p 259-267, Arkitektkopia, Uppsala

Seifert FA, Mysen BO, Virgo D (1981) Structural similarities of glasses and melts relevant to petrological processes. Geochim Cosmochim Acta 45:1879-1884

Seifert FA, Mysen BO, Virgo D (1982) Three-dimensional network structure of quenched melts (glass) in the systems SiO_2-$NaAlO_2$, SiO_2-$CaAl_2O_4$ and SiO_2-$MgAl_2O_4$. Am Mineral 67:696-717

Sharma SK, Virgo D, Mysen BO (1978) Structure of glasses and melts of Na_2O-xSiO_2 (x=1,2,3) composition from Raman spectroscopy. Carnegie Inst Wash Yearb 77:649-652

Sharma SK, Virgo D, Mysen BO (1979) Raman study of the coordination of aluminum in jadeite melts as a function of pressure. Am Mineral 64:779-787

Shimizu N, Kushiro I (1984) Diffusivity of oxygen in jadeite and diopside melts at high pressures. Geochim Cosmochim Acta 48:1295-1303

Smith KH, Shero E, Chizmeshya A, Wolf GH (1995) The equation of state of polyamorphic germania glass: two-domain description of the viscoelastic response. J Chem Phys 102:6851-6857

Sowa H (1988) The oxygen packings of low-quartz and ReO_3 under high pressure. Zeits Kristal 184:257-268

Spera FJ, Bergman SC (1980) Carbon dioxide in igneous petrogenesis: I. Aspects of the dissolution of CO_2 in silicate liquids. Contrib Mineral Petrol 74:55-66

Stebbins J, Sykes D (1990) The structure of $NaAlSi_3O_8$ liquid at high pressure: new constraints from NMR spectroscopy. Am Mineral 75:943-946

Stebbins JF (1987) Identification of multiple structural species in silicate glasses by ^{29}Si NMR. Nature 330:465-467

Stebbins JF (1988) Effects of temperature and composition on silicate glass structure and dynamics: Si-29 NMR results. J Non-Cryst Solids 106:359-369

Stebbins JF (1991) NMR evidence for five-coordinated silicon in a silicate glass at atmospheric pressure. Nature 351:638-639

Stebbins JF, Carmichael ISE, Moret LK (1984) Heat capacities and entropies of silicate liquids and glasses. Contrib Mineral Petrol 86:131-148

Stebbins JF, Farnan I, Xue X (1992) The structure and dynamics of alkali silicate liquids: a view from NMR spectroscopy. Chem Geol 96:371-385

Stebbins JF, McMillan PF (1989) Five- and six-coordinated Si in $K_2Si_4O_9$ glass quenched from 1.9 GPa and 1200°C. Am Mineral 74:965-968

Stebbins JF, McMillan PF (1993) Compositional and temperature effects on five-coordinated silicon in ambient pressure silicate glasses. J Non-Cryst Solids 160:116-125

Stolper E, Holloway JR (1988) Experimental determination of the solubility of carbon dioxide in molten basalt at low pressure. Earth Planet Sci Lett 87:397-408

Stolper E, Walker D, Hager BH, Hays JF (1981) Melt segregation from partially molten source regions: the importance of melt density and source region size. J Geophys Res 86:6261-6271

Sugiura H, Kondo K, Sawaoka A (1981) Dynamic response of fused quartz in the permanent densification region. J Appl Phys 52:3375-3382

Sugiura H, Yamadaya T (1992) Raman scattering in silica glass in the permanent densification region. J Non-Cryst Solids 144:151-158

Suito K, Miyoshi M, Sasakura T, Fujisawa H (1992) Elastic properties of obsidian, vitreous SiO_2, and vitreous GeO_2 under high pressure up to 6 GPa. In: Syono Y, Manghnani MH (eds) High-Pressure Research: Application to Earth and Planetary Sciences, p 219-225, Am. Geophysical Union, Washington D.C.

Susman S, Volin KJ, Liebermann RC, Gwanmesia GD, Wang Y (1990) Structural changes in irreversibly densified fused silica: implications for the chemical resistance of high level nuclear waste glasses. Phys Chem Glasses 31:144-150

Susman S, Volin KJ, Price DL, Grimsditch M, Rino JP, Kalia RK, Vashishta P, Gwanmesia G, Wang Y, Liebermann RC (1991) Intermediate-range order in permanently densified vitreous SiO_2: a neutron-diffraction and molecular-dynamics study. Phys Rev B 43:1194-1197

Suzuki A, Ohtani E, Kato T (1995) Flotation of diamond in mantle melt at high pressure. Science 269:216-218

Sykes D, Poe B, McMillan PF, Luth RW, Sato RK (1993) A spectroscopic investigation of the structure of anhydrous $KAlSi_3O_8$ and $NaAlSi_3O_8$ glasses quenched from high pressure. Geochim Cosmochim Acta 57:3574-3584

Takahashi E (1986) Melting of a dry peridotite KLB-1 up to 14 GPa: implications on the origin of peridotite upper mantle. J Geophys Res 91:9367-9382

Tandura SN, Alekseev NV, Voronkov MG (1986) Molecular and electronic structure of penta- and hexa-coordinate silicon compounds. Topics in Current Chemistry 131:99-186

Taylor M, Brown GE (1979a) Structure of mineral glasses. I. The feldspar glasses, $NaAlSi_3O_8$, $KAlSi_3O_8$, $CaAl_2Si_2O_8$. Geochim Cosmochim Acta 43:61-77

Taylor M, Brown GE (1979b) Structure of mineral glasses. II. The SiO_2-$NaAlSiO_4$ join. Geochim Cosmochim Acta 43:1467-1473

Taylor M, Brown GE, Fenn PM (1980) Structure of mineral glasses. III. $NaAlSi_3O_8$ supercooled liquid at 805°C and the effects of thermal history. Geochim Cosmochim Acta 44:109-119

Tossell JA, Gibbs GV (1978) The use of molecular-orbital calculations on model systems for the prediction of bridging-bond-angle variations in siloxanes, silicates, silicon nitrides and silicon sulphides. Acta Crystallogr A34:463-472

Tse JS, Klug DD (1991) Mechanical instability of α-quartz: a molecular-dynamics study. Phys Rev Lett 67:3559-3562

Tyburczy JA, Waff HS (1983) Electrical conductivity of molten basalt and andesite to 25 kilobars pressure: Geophysical significance and implications for charge transport and melt structure. J Geophys Res 88:2413-2430

Tyburczy JA, Waff HS (1985) High pressure electrical conductivity in molten natural silicates. In: Schock RN (ed) Point Defects in Minerals, 31, p 78-87, American Geophysical Union, Washington, D. C.

Ueno M, Misawa M, Suzuki K (1983) On the change in coordination of Ge atoms in Na_2O-GeO_2 glasses. Physica 120B:347-351

Uhlmann DR (1973) Densification of alkali silicate glasses at high pressure. J Non-Cryst Solids 13:89-99

Urbain G, Bottinga Y, Richet P (1982) Viscosity of liquid silica, silicates and alumino-silicates. Geochim Cosmochim Acta 46:1061-1072

Valenkov N, Porai-Koshits EA (1936) X-ray investigation of the glassy state. Z Krist Kristall Kristallphys Kristallchem 95:195-229

Velde B, Kushiro I (1978) Structure of sodium alumino-silicate melts quenched at high pressure: infrared and aluminum K-radiation data. Earth Planet Sci Lett 40:137-140

Verhelst-Voorhees M, Yarger J, Diefenbacher J, Poe BT, Wolf GH, McMillan PF (1994) ^{29}Si NMR, HREM, and Raman study of pressure-vitrified quartz: new evidence for high-coordinate silicon. EOS Trans Am Geophys Union 75:635

Verweij H (1979) Raman study of the structure of alkaligermanosilicate glasses II. lithium, sodium and potassium digermanosilicate glasses. J Non-Cryst Solids 33:55-69

Verweij H, Konijnendijk WL (1976) Structural units in K_2O-PbO-SiO_2 glasses by Raman spectroscopy. J Am Ceram Soc 59:517-521

Virgo D, Mysen BO, Kushiro I (1980) Anionic constitution of 1-atmosphere silicate melts: implications for the structure of igneous melts. Science 208:1371-1373

Vukcevich MR (1972) A new interpretation of the anamolous properties of vitreous silica. J Non-Cryst Solids 11:25-63

Wackerle J (1962) Shock-wave compression of quartz. J Appl Phys 33:922-937

Waff HS (1975) Pressure-induced coordination changes in magmatic liquids. Geophys Res Letts 2:193-196

Walrafen GE, Hokmabadi MS (1986) Raman structural correlations from stress-modified and bombarded vitreous silica. In: Walrafen GE, Revesz AG (eds) Structure and Bonding in Noncrystaline Solids, p 185-202, Plenum Press, New York

Warren, BE (1933) X-ray diffraction of vitreous silica. Z Krist Kristall Kristallphys Kristallchem 86:349-352

Wasserman EA, Yuen DA, Rustad JR (1993) Molecular dynamics study of the transport properties of perovskite melts under high temperature and pressure conditions. Earth Planet Sci Lett 114:373-384

Watson EB (1979) Calcium diffusion in a simple silicate melt to 30 kbar. Geochim Cosmochim Acta 43:313-322

Williams Q (1990) Molten $(Mg_{0.88}Fe_{0.12})_2SiO_4$ at lower mantle conditions: melting products and structure of quenched glasses. Geophys Res Letts 17:635-638

Williams Q, Hemley RJ, Kruger MB, Jeanloz R (1993) High pressure infrared spectra of a-quartz, coesite, stishovite, and silica glass. J Geophys Res 98:22157-22170

Williams Q, Jeanloz R (1988) Spectroscopic evidence for pressure-induced coordination changes in silicate glasses and melts. Science 239:902-905

Williams Q, Knittle E, Reichlin R, Martin S, Jeanloz R (1990) Structural and electronic properties of Fe_2SiO_4 -fayalite at ultrahigh pressures: amorphization and gap closure. J Geophys Res 95:21549-21564

Wolf GH, Durben DJ, McMillan PF (1990) High pressure Raman spectroscopic study of sodium tetrasilicate ($Na_2Si_4O_9$) glass. J Chem Phys 93:2280-2288

Wolf GH, Wang S, Herbst CA, Durben DJ, Oliver WF, Kang ZC, Halvorson K (1992) Pressure induced collapse of the tetrahedral framework in crystalline and amorphous GeO_2. In: Syono Y, Manghnani MH (eds) High-Pressure Research: Application to Earth and Planetary Sciences, p 503-517, Am. Geophysical Union, Washington D.C.

Woodcock LV, Angell CA, Cheeseman P (1976) Molecular dynamics studies of the vitreous state: simple ionic systems and silica. J Chem Phys 65:1565-1577

Xue X, Stebbins J, Kanzaki M, Poe B, McMillan P (1991) Pressure-induced silicon coordination and tetrahedral structural changes in alkali oxide-silica melts up to 12 GPa: NMR, Raman and infrared spectroscopy. Am Mineral 76:8-26

Xue X, Stebbins JF, Kanzaki M, Tronnes RG (1989) Silicon coordination and speciation changes in a silicate liquid at high pressures. Science 245:962-964

Yagi T, Mao HK, Bell P (1978) Structure and crystal chemistry of perovskite-type $MgSiO_3$. Phys Chem Min 3:97-110

Yarger JL, Poe BT, Diefenbacher J, Smith KH, Wolf GH, McMillan PF (1995) Al^{3+} coordination changes in high pressure aluminosilicate liquids. submitted to Science

Yin CD, Okuno M, Morikawa H, Marumo F (1983) Structure analysis of $MgSiO_3$ glass. J Non-Cryst Solids 55:131-141

Zachariasen WH (1932) The atomic arrangement in glass. J Am Chem Soc 54:3841-3851

Zha CS, Hemley RJ, Mao HK, Duffy TS, Meade C (1994) Acoustic velocities and refractive index of SiO_2 glass to 57.5 GPa by Brillouin scattering. Phys Rev B 50:13105-13112